

REPUBLIC OF IRAQ
MINISTRY OF HIGHRT EDUCATION
AND SCIENTIFIC RESEARCH
UNIVERSITY OF BAGHDAD
COLLEGE OF SCIENCE
DEPARTMENT OF GEOLOGY



MINERALOGY, GEOCHEMISTRY AND SORPTION EFFICIENCY OF PALYGORSKITE OF DIGMA AND AKASHAT FORMATIONS, WESTERN IRAQ

A THESIS
SUBMITTED TO THE COLLOGE OF SCIENCE
UNIVERSITY OF BAGHDAD IN PARTIAL FULFILLMENT OF THE REQUIRMENTS FOR THE DEGREE
OF DOCTOR OF PHILOSOPHY IN GEOLOGY

By
SAAD MUHI TOWFIK
M.Sc. University of Karachi, Pakstan-1989

SUPERVISED BY
Assist. Prof. Dr. Salih Muhammad Awadh

1434 AH

2013 AD



بِسْمِ اللَّهِ الرَّحْمَنِ الرَّحِيمِ

وَقُلِ اعْمَلُوا فَسَيَرَى اللَّهُ عَمَلَكُمْ وَرَسُولُهُ وَالْمُؤْمِنُونَ

صدق الله العظيم

التوبة (الاية 105)

The Supervisor Certification

I certify that this thesis entitled “Mineralogy, Geochemistry and Sorption efficiency of Palygorskite of Digma and Akashat Formations, Western Iraq” has been prepared under my supervision in the Department of Geology, College of Science, University of Baghdad in partial fulfillment of the requirements for the degree of Doctor of Philosophy of Science in Geology (Rock and Minerals).

Signature:

Name : Dr. Salih Muhammad Awadh
Title : Assist. Professor
Address : Department of Geology
College of Science
University of Baghdad
Date : 17 / 6 / 2013

Recommendation of the head of the Department of Geology

In view of the available recommendation, I forward this thesis for the debate by the examining committee.

Signature:

Name : Dr. Ahmad Shehab Al-Banna
Title : Professor
Address : Department of Geology
College of Science
University of Baghdad
Date : / / 2013

Committee Certification

We certify that we have read this thesis entitled “Mineralogy, geochemistry and sorption efficiency of palygorskite of Digma and Akashat Formations, Western Iraq” and as the examination committee examined the student in its content and in our opinion it adequate for award of the degree of Doctor of Philosophy of Science in Geology (Rock and Minerals).

Signature: 
Name: Dr. Dhyia Y. Al-Rawi
Title: Professor
Address: Department of Geology
College of Science
University of Baghdad
Date: 13 / 8 / 2013

(Chairman)

Signature: 
Name: Dr. Nahida A. Al-Qaraghuli
Title: Professor
Address: Department of Geology
College of Science
University of Baghdad
Date: 11 / 8 / 2013

(Member)

Signature: 
Name: Dr. Mohsin M. Ghazal
Title : Assist. Professor
Address: Department of Geology
College of Science
University of Mosul
Date: 12 / 8 / 2013

(Member)

Signature: 
Name: Dr. Ayten Hadi
Title : Assist. Professor
Address: Department of Geology
College of Science
University of Baghdad
Date: 12 / 8 / 2013

(Member)

Signature: 
Name: Dr. Ahmed Kh. Al-Jumaili
Title: Assist. Professor
Address: Department of Applied Geology
College of Science
University of Babylon
Date: 13 / 8 / 2013
(Member)

Signature: 
Name: Dr. Salih Muhammad Awadh
Title: Assist. Professor
Address: Department of Geology
College of Science
University of Baghdad
Date: 15 / 8 / 2013
(Supervisor)

Approved by the deanery of the College of Science

Signature:
Name : Dr. Saleh Mahdi Ali
Title : Professor
Address : Dean of the College of Science
Date : / / 2013

Declaration

This is to certify that the dissertation / thesis titled:

Mineralogy, Geochemistry and Some Technical Applications of Palygorskite of Digma and Akashat Formations, Western Iraq

Submitted by Saad Muhi Towfik

Department: Geology

College: College of Science

Has been written my linguistic supervision its language, in its present form, is quite acceptable.

Name: Prof. Dr. Zuhair D. Al-Phaikh
Address: Science, Univ. Baghdad
Signature: Z.D. Al-Phaikh

DEDICATION

TO

WHAT KEPT ME FOR LIFE

SHAHAD AND TOMY

THE LIGHT OF MY LIFE

AND

THE CANDLE OF HOPE

SAAD

Acknowledgements

With extreme my pleasure, I express my sincere and deep sense of gratitude and obligation to my supervisor guide, Assist. Prof. Dr. Salih Muhammad Awadh, for proposing the subject of current research, his valuable guidance, research training, encouragement and timely suggestions throughout my research period. I shall ever remain grateful to him.

I would like to thank Prof. Dr. Ahmed Sh. Al-Bana, the head of the Department of Geology for providing the necessary facilities for research. I take this opportunity to thank all the staff of the Department of Geology for their goodwill on all occasions.

My thank goes to the staff of the Nanotechnology and Advance Materials Research Center at the University of Technology-Baghdad for their assistance in SEM, the Ibn-Sena Company for FTIR and some chemical analyses, the Iraqi Geological Survey for XRD analyses and The Ministry of Science and Technology for some chemical and physical analyses. Special thank for Dr. Kamal Barzan Al-Hadethi for his many assistances

I am extremely thankful to the staff of the ALS Lab- Group, in Aspain (Sevilla) and in the Republic of Czech (Prague), for doing the chemical analyses by using ICP method.

I extend my special thanks to of postgraduate student (M. Sc. and Ph. D) at the Department of Geology for their readiness to help on various occasions. I would like to apologize to my daughter and my son for the many hours of my time spent on research instead of being with them.

My sincere thanks to Mr. Mohamed a Major in the Iraqi police and a group of military and police officers for their generous assistance and value in providing a security protection while performing field work, I cannot fail to provide sincere thanks to the family of my supervisor for hosting me during the field work period.

Saad

Abstract

Palygorskite-rich sediments in Digma (Maastrichtian) and Akashat (Paleocene) Formations, within the Western Desert of Iraq are studied in terms of mineralogy, geochemistry and some technical applications. The technical applications include the separation of palygorskite from raw sample and conduct set of laboratory experiments that would indicate the ability of palygorskite to absorb and adsorb the heavy metals from the liquid phase. For this reason, targeted sampling approach is used to follow-up and to collect the palygorskite-rich sediments from 17 sites, some samples were collected from each site and tested mineralogically to select the appropriate sample; then finally, one representative sample was chosen from each site.

X-ray diffraction (XRD), scanning electron microscopy (SEM) and infrared (FTIR) techniques have been used together to study the raw samples (palygorskite-rich sediments) and the separated sample (palygorskite).

The current study reveals the association of palygorskite with the siliceous rocks represented by poracellanite, Opal-CT (cristobalite and tridymite), a considerable amount of dolomite and kaolinite with little amount of calcite within marly limestone, and apatite in Digma Formation. While in Akashat Formation, palygorskite is associated mostly with montmorillonite, dolomite, marly limestone and little porcellanite represented by opal-CT (cristobalite and tridymite) and quartz. This facies indicates a shallow marine environment of inner platform.

The present study suggests two models for the genesis of palygorskite; the first one is the reaction of pore water rich in silicic acid with dolomite to form sepiolite, which eventually transforms into palygorskite by taking alumina from the surroundings, and the second is the transformation of smectite to palygorskite in environment rich in Mg.

In terms of geochemistry, the palygorskite-rich sediments and the pure palygorskite that had been separated from the raw sample are analyzed for SiO₂, Al₂O₃, MgO, Fe₂O₃, TiO₂, MnO, Na₂O, CaO, K₂O, P₂O₅, LOI. The content of MgO in the palygorskite-rich sediments varies between 0.61 to 9.38%, where some of MgO comes from dolomite. In pure palygorskite, the high content of MgO (10.2%) with suitable LOI (19.1%) indicates a success of laboratory separation process which was enhanced by SEM. The structural formula of the separated palygorskite and the charge distribution in the octahedral layer, tetrahedral layer and interlayer were calculated.

In term of technical applications, the pure palygorskite (separated from raw sample) is subjected to a set of laboratory experiments to test the efficiency of palygorskite for sorping the heavy metals (Pb, Cd, Ni, Cr, Co, V, Zn, Cu, Fe and Mn) as well as boron (B) in concentration of 10, 25, 50, 75,

100, 125, 150, 175, 200 and 225 ppm for each element. More than 110 laboratory experiments are conducted as patch process at room temperature. The solid (palygorskite) to liquid ratio (initial solution) is determined to be (1gm/100ml), and the equilibrium reaction time is 1h.

TDS and EC decrease with the trend of alkaline pH in the final solutions (after the end of the reaction). The tendency toward the alkaline occurs with the solutions of low concentration rather than the solutions of high concentration due to lack of cations competes the H^+ on the negative site of palygorskite.

The ability of palygorskite sorption (in percentage) increases when thermally activated, up to 93% at 600°C due to the driving of zeolitic water by heating, the surface area and thus the sorptivity is increased too. Whilst, at 800°C sorption decreases to minimum due to the collapse of palygorskite structure.

The palygorskite is expressed as an active receptive of heavy metals, while Ca^{2+} , Mg^{2+} , Al^{3+} and K^+ are desorb ions from the palygorskite into the solution indicating a one-to-one ion exchange mechanism is responsible for the incorporation of cations into the structure of palygorskite. The expulsion of these cations causes a decrease in positive charge on palygorskite which encourages additional cations to adsorb on surface.

The efficiency of palygorskite sorption (%) of heavy metals varies depending on the nature of the metals. Laboratory experiments have identified a lot of relationships, from which the palygorskite sorption (%) for initial solutions of concentration 50 ppm can be ordered as follows:



List of Contents

Subject No.	Subject Name	Page No.
CHAPTER ONE: INTRODUCTION		
1	Introduction	1
1-1	Preface	1
1-2	Location of the study area	1
1-3	The objectives	2
1-4	The previous studies	3
1-5	Geological setting	4
1-5-1	Lithostratigraphy	5
1-5-1-1	Digma Formation	5
1-5-1-2	Akashat Formation	7
1-5-2	Tectonic and Structure	10
1-5-3	Geomorphology	12
CHAPTER TWO: MATERIALS AND METHODS		
2	Materials and Methods	
2-1	Preface	13
2-2	Field work	13
2-3	Laboratory work	19
2-3-1	Sample preparation	19
2-3-2	Mineral identification	20
2-3-2-1	X-ray diffraction technique	20
A	Acetic Acid treatment	20
B	Random powder mount	21
C	Thermal treatment	22
D	Ethylene Glycol vapor treatment	22
2-3-2-2	Separation of palygorskite	23
2-3-2-3	Scanning Electron Microscope (SEM)	25
2-3-2-4	FTIR technique	25
2-3-3	Laboratory experiment	26
2-3-3-1	Preparation of stock solutions	26
2-3-3-2	Laboratory adsorption experiment	27
2-3-4	Chemical analyses	28
2-3-4-1	ICP-AES method	28
2-3-5	Accuracy and precision	28
2-3-5-1	Accuracy	28
2-3-5-2	Precision	29

List of Contents

Subject No.	Subject Name	Page No.
CHAPTER THREE: MINERALOGY		
3	Mineralogy	30
3-1	Preface	30
3-2	Mineralogical study using XRD, SEM and FTIR	30
3-2-1	Mineralogy of raw samples	30
3-2-2	Clay minerals	37
3-2-2-1	Montmorillonite	37
3-2-2-2	Kaolinite	39
3-2-2-3	Palygorskite	42
3-2-3	Non-clay minerals	51
3-2-3-1	Calcite and dolomite	51
3-2-3-2	Quartz, cristobalite and tridymite	52
3-3	Palygorskite separation from clay minerals	53
3-4	Origin of palygorskite	54
3-5	Discussion	55
CHAPTER FOUR: GEOCHEMISTRY AND SORPTION EFFICIENCY		
4	Geochemistry and Sorption Efficiency	57
4-1	Preface	57
4-2	Geochemistry	57
4-2-1	Geochemistry of separated palygorskite	58
4-2-2	Ionic substitutions	60
A	Tetrahedral substitutions	60
B	Octahedral substitutions	61
C	Interlayer substitution	62
4-2-3	Types of Solid Solution	62
4-2-4	Cation Exchange capacity (CEC)	62
4-3	Sorption efficiency of palygorskite	63
4-3-1	Procedure of laboratory experiments	63
4-3-2	Laboratory experiment conditions determination	65
4-3-2-1	Influence of sorbent mass (solid to liquid ratio)	65
4-3-2-2	Influence of the equilibrium reaction time	66
4-3-3	Sorption experiments	67
4-3-3-1	Lead (Pb)	67
4-3-3-2	Cadmium (Cd)	69

Subject No.	Subject Name	Page No.
4-3-3-3	Nickel (Ni)	71
4-3-3-4	Chromium (Cr)	73
4-3-3-5	Cobalt (Co)	75
4-3-3-6	Vanadium (V)	76
4-3-3-7	Zinc (Zn)	78
4-3-3-8	Copper (Cu)	80
4-3-3-9	Iron (Fe)	82
4-3-3-10	Manganese (Mn)	84
4-3-3-11	Boron (B)	86
4-4	Sorption efficiency	87
4-4-1	Cation exchange capacity (CEC) relationship with pH	88
4-4-2	Effect of concentration	88
4-4-3	Effect of pH	90
4-4-4	Effect of ionic potential	92
4-4-5	Effect of calcinations	93
4-5	Discussion	94
	CHAPTER FIVE: CONCLUSIONS AND RECOMMENDATIONS	
5	Conclusions and Recommendations	97
5-1	Conclusions	97
5-2	Recommendations	99
	REFERENCES	100
	APPENDICES	111

List of Tables

Table No.	Title of Table	Page No.
2-1	Coordinates of samples and field and laboratory description	15
2-2	Standard solutions used for preparation stock solutions	27
2-3	Accuracy and precision results of the standard sample compared with their globally results	28
3-1	Assignments of the bands appearing in the FTIR spectrum of natural kaolinite	41
3-2	XRD data of palygorskite under condition of Cu K α λ 1.54056 $^{\circ}$ A	44
3-3	Characteristics of IR bands associated with quartz	53
4-1	Chemical analyses of the whole samples collected from Digma and Akashat Formations	58
4-2	Chemical results of whole palygorskite-rich sediments and separated palygorskite compared with palygorskite from world	60
4-3	Cations and charge distribution of separated palygorskite	61
4-4	Specifications of the standard solutions used for preparing the stock solutions that are used for laboratory experiments of palygorskite sorption	64
4-5	Results of sorption (%) on different masses of palygorskite	66
4-6	Results of sorption (%) of 100 ppm Pb (100 ml) onto 1 gm palygorskite with time	67
4-7	Results of laboratory experiments of lead (Pb) sorption on palygorskite in ten solutions of various concentrations	68
4-8	Results of laboratory experiments of cadmium (Cd) sorption on palygorskite in ten solutions of various concentrations	70
4-9	Results of laboratory experiments of Nickle (Ni) sorption on palygorskite in ten solutions of various concentrations	72
4-10	Results of laboratory experiments of chromiun (Cr) sorption on palygorskite in ten solutions of various concentrations	74
4-11	Results of laboratory experiments of cobalt (Co) sorption on palygorskite in ten solutions of various concentrations	75

List of Tables

Table No.	Title of Table	Page No.
4-12	Results of laboratory experiments of vanadium (V) sorption on palygorskite in ten solutions of various concentrations	77
4-13	Results of laboratory experiments of zinc (Zn) sorption on palygorskite in ten solutions of various concentrations	79
4-14	Results of laboratory experiments of copper (Cu) sorption on palygorskite in ten solutions of various concentrations	81
4-15	Results of laboratory experiments of iron (Fe) sorption on palygorskite in ten solutions of various concentrations	83
4-16	Results of laboratory experiments of manganese (Mn) sorption on palygorskite in ten solutions of various concentrations	85
4-17	Results of laboratory experiments of boron (B) sorption on palygorskite in ten solutions of various concentrations	86
4-18	Results of final Pb solution of 175 ppm	92
4-19	Ionic potential of elements	92
4-20	Sorption (%) of 100 ppm Pb onto 1 gm of activated palygorskite	93
Ap-1	Table Ap-1: Certification of analyses issued by ALS group-Czech Republic	111
Ap-2	Structure formula and charge equivalent of the separated palygorskite from raw sample no 12D	112

List of Figures

Figure No.	Title of Figure	Page No.
1-1	Geological map shows the study area	2
2-1	Location map shows the study area and the sampling sites	14
2-2	Porcelanite (opal-CT) facies (0.8-1m) of yellowish white color having conchoidal fracture	16
2-3	Phosphatic rocks (14m thick with carbonate rock overburden of 3.5m) at the main working face of Akashat mine, Akashat Formation	16
2-4	View of Safra bed of Digma Formation which forms from claystone with dolomite. The samples 3DS, 4DS and 5DS collected from this site.	17
2-5	kaolinite-palygorskite claystone interbedded with opal-CT in Digma Formation; Sample 8D was collected from this section	17
2-6	Palygorskite-rich clay with porcelanite (opal-CT) and siliceous deposits in Digma Formation, sample 10DN	18
2-7	Palygorskite-rich calystone with dolomite a part of Digma Formation; sample 12D	18
2-8	Traifawi section (2m thickness) illustrates claystone with dolomite. At the ground, quarried bentonite of yellow color exists with papery texture	19
2-9	Separated palygorskite from whole sample centrifugally	24
2-10	Wet and dry samples of separated palygorskite	24
2-11	Studying the palygorskite mineralogy using SEM at the Nanotechnology and Advance Materials Research Center at the University of Technology with device type of VIGA TESCAN II SBH MS12	25
3-1	Figure 3-1: X- ray diffractogram illustrates mineral composition in sample no.1D	31
3-2	XRD Diffractograph illustrates the mineralogical composition in sample no.3DS	32
3-3	X- ray diffractogram illustrates the mineralogical composition in sample no.4DS	32
3-4	X- ray diffractogram illustrates the mineralogical composition in sample no.5DS	33
3-5	X- ray diffractogram illustrates the mineralogical composition in sample no.6D	33

List of Figures

Figure No.	Title of Figure	Page No.
3-6	X- ray diffractogram illustrates the mineralogical composition in sample no.8D	34
3-7	X- ray diffractogram illustrates the mineralogical composition in sample no.9DN	34
3-8	X- ray diffractogram illustrates the mineralogical composition in sample no.10DN	35
3-9	X- ray diffractogram illustrates the mineralogical composition in sample no.11DN	35
3-10	X- ray diffractogram illustrates the mineralogical composition in sample no.13A	36
3-11	X- ray diffractogram illustrates the mineralogical composition in sample no.16AT	36
3-12	X- ray diffractogram illustates the mineralogical composition in sample no.17AT	37
3-13	Montmorillonite structure	38
3-14	Scanning Electron Microscope image of montmorillonite. Sample No. 12D	38
3-15	Scanning Electron Microscope image of smectite changing to palygorskite. Sample No 12D	39
3-16	Scanning Electron Microscope image of pseudo-hexagonal shape of face to face pattern, Sample No. 8D	40
3-17	FTIR spectra of natural kaolinite	40
3-18	FTIR spectra of kaolinite-rich sediments. Sample No.6D	41
3-19	Schematic structure of palygorskite	42
3-20	Scanning Electron Microscope image of palygorskite derived from smectite. Sample No 12D	43
3-21	Scanning Electron Microscope image of palygorskite. Sample No 12D	43
3-22	X-ray diffractogram of sample No.7D	45
3-23	X-ray diffractogram of sample No.8D	45
3-24	X-ray diffractogram of sample No.12D	46
3-25	X-ray diffractogram of sample No.8D	46
3-26	X-ray diffractogram of separated palygorskite from sample No.12D which was heated to different temperatures	47
3-27	FTIR spectra of pure palygorskite separated from sample No.12D	49

List of Figures

Figure No.	Title of Figure	Page No.
3-28	FTIR spectra of typical pure palygorskite	49
3-29	FTIR spectra of palygorskite-rich sediments, sample No.5DS	50
3-30	FTIR spectra of palygorskite-rich sediments, sample No.13A	50
3-31	FTIR spectra of palygorskite-rich sediments, sample No.16AT	51
3-32	FTIR spectra of calcite	52
4-1	Effect of palygorskite mass on adsorption % of Pb at different concentration (100 and 200 ppm) and at 25°C	66
4-2	Equilibrium time of sorption (%) of 100 ppm Pb onto palygorskite	67
4-3	The effect of Pb adsorption on palygorskite	68
4-4	The effect of Cd adsorption on palygorskite	70
4-5	The effect of Ni adsorption on palygorskite	72
4-6	The effect of Cr adsorption on palygorskite	74
4-7	The effect of Co adsorption on palygorskite	76
4-8	The effect of V adsorption on palygorskite	78
4-9	The effect of Zn adsorption on palygorskite	79
4-10	The effect of Zn adsorption on palygorskite	81
4-11	The effect of Fe adsorption on palygorskite	83
4-12	The effect of Mn adsorption on palygorskite	85
4-13	The effect of B adsorption on palygorskite	87
4-14	The range of sorption (%) for metals on palygorskite	89
4-15	Negative relationship between the concentration of initial metals and sorption (%) on palygorskite	89
4-16	Distribution features of the metal sorption (%) on palygorskite	90
4-17	The influence of heating on palygorskite sorption	94

Chapter One

Introduction

1- Introduction

1-1 Preface

Palygorskite $(\text{Mg,Al})_2\text{Si}_4\text{O}_{10}(\text{OH}) \cdot 4(\text{H}_2\text{O})$ is a rare fibrous clay which is also known as attapulgite or fuller's earth. Palygorskite and attapulgite are two names of one minerals; the former is earlier and was used for a leather-like Mg-Al hydrosilicate from Ural (Namecz, 1981). The name attapulgite was introduced by Bradley (1940) for the same mineral from attapulgis, Georgia (USA). Other names for the same mineral include pilolite and Lassallite, which are not in use now (Al-Bassam, 2000).

Palygorskite is a phyllosilicate with a 2:1 layer having periodic inversions of the tetrahedral sheet after every two silicate "chains" to form "ribbons". The octahedral sheet is thus discontinuous and a channel-like structure forms (Giustetto and Chiari 2004; Post and Heaney 2008) owing to octahedral cation substitutions involving Mg, Al, and Fe (Suárez et al. 2007).

The palygorskite may be recovered from the dispersion and dried in such a manner to produce a finely sized powder from ore, without the need for any grinding or milling operation. The dried palygorskite has a little moisture content of 2-3%. Palygorskite plays important roles in many industries ranging from agricultural, wine clarification, medical, cosmetic applications and as an additive to drilling mud (Grim, 1962). Most of the palygorskite are formed less than 25 million years ago in the terrestrial and lagoonal environment (Galan and Castello, 1984; Pletsch, 2003).

1-2 Location of the study area

This study was carried on palygorskite-rich sediments exposed within Digma and Akashat Formations in the Western Desert of Iraq (Figure 1). These formations belong to the Masstrachtian and Paleocene age. Other formations exposed in the study area are Ga'ara, Mulussa, Zor Horan, Ms'ad, Hartha, Digma, Akashat and Ratga Formations. The study area includes a wide area extending from the northern part of the Ga'ara depression and Akashat on the north to the Tarifawi at the south along the exposure of Akashat and Digma Formations.

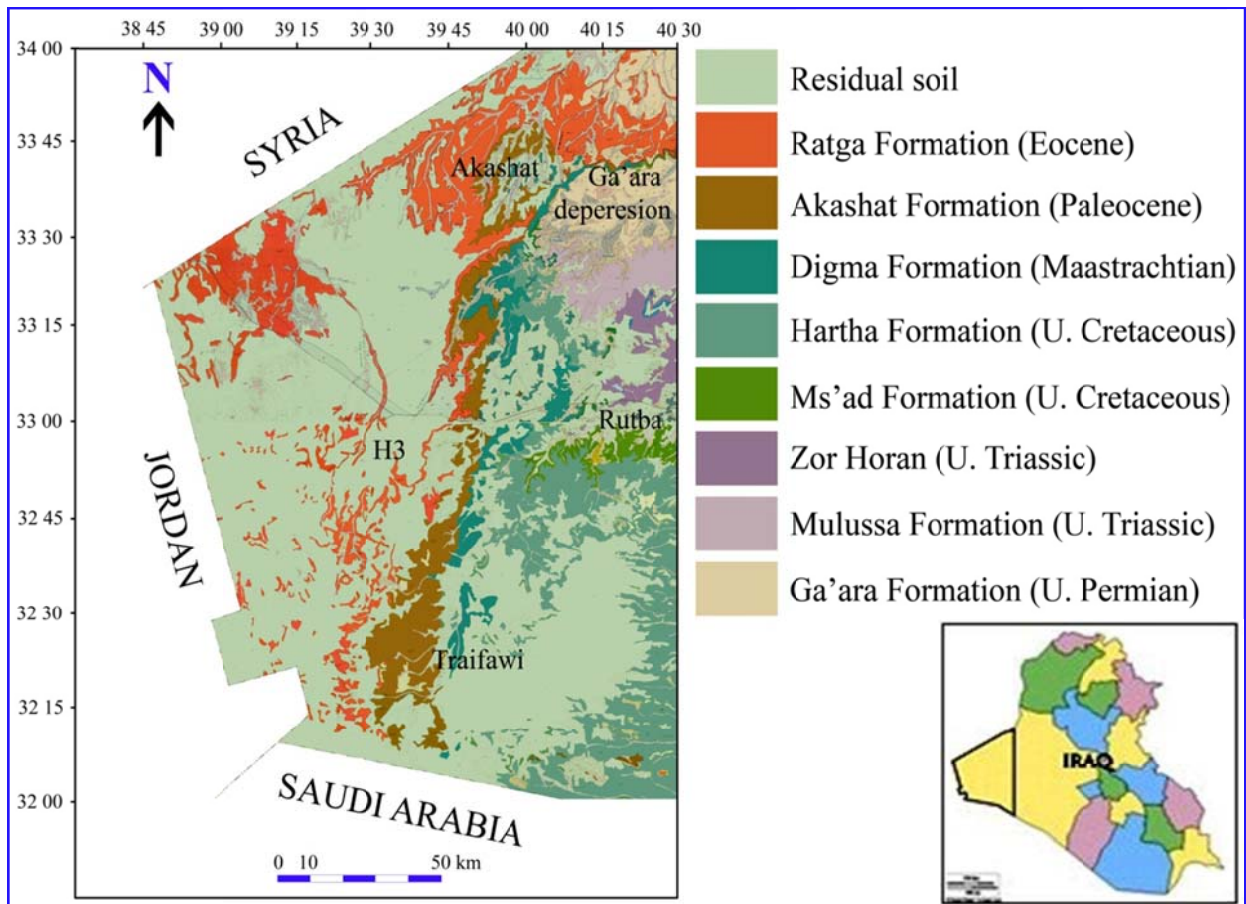


Figure 1-1: Geological map shows the study area, (Modified from Geoserv, 2009).

1-3 The objectives

This study aims to achieve the following objectives:

1. Studying the mineralogy and geochemistry of palygorskite within Digma and Akashat Formations in the Western Desert of Iraq.
2. Concluding the genesis of palygorskite and its importance as a paleo-environment indicator.
3. Reporting the experimental results on adsorption of Pb, Cd, Ni, Co, Cr, V, Zn, Cu, Mn, Fe, and B) on palygorskite at different conditions and identify the factors (concentration, mass and time) which affect the adsorption of these metals onto palygorskite.
4. Assessing the sorption efficiency of palygorskite as clarifying agent to absorb and adsorb the heavy metals (Pb, Cd, Ni, Co, Cr, V, Zn, Cu, Mn, Fe) as well as B.

1-4 The previous studies

The palygorskite has been studied thoroughly in many places in Iraq. Distribution of Iraqi palygorskite in space and time is summarized by Al-Bassam (2000) as localities in the Safra bed of Digma Formation, Traifawi Member, Dwaima Member, Gercus Formation, Nfayil Formation, Injana Formation (Late Miocene Pliocene) Fissure-and Fracture-fill in Injana (post Miocene) and Dibdibba Formations (Pliocene). Palygorskite is found in all environments between the shore and shelf margin.

Tamer-Aga and Aljanabi (1997) studied the Tayarat Formation (Upper Cretaceous) in well KH-6, Ansab within the Western Desert of Iraq; they stated that the clay mineral distribution and abundance is controlled by the environment and the palygorskite is Polygenic. Aswad et al., 1997 mentioned that the Safra bed (Masstrichtian) in Ga'ara-Akashat area is almost always associated with montmorillonite. They noticed that palygorskite is strongly associated with dolomite and there is negative correlation between palygorskite content and montmorillonite content; also they found that Na is the main exchangeable cation and it appears to have formed in-situ, mostly from the transformation of montmorillonite.

Zahra Formation (Late Pliocene-Pleistocene) is exposed as discontinuous belt extending in the Western Desert from Wadi Hauran in the north to the Iraqi-Saudi border in the south. Tamer-Aga et al. (1997) classified the origin of palygorskite into three categories: detrital characterized by short fiber, transformational characterized by platy grains; and neoformalional which is characterized by longer fiber forming tree-like texture. The palygorskite was formed by transformation of low-potassium smectites (montmorillonite).

Palygorskite of Traifawi (Early Paleocene) is believed to have originated by transformation of semictite (Aba-Hussain, 1986; Al-Bassam et al., 1990 and Qassim, 1993).

Dannoun and Al-Dabbagh (1988) studied the origin and chemistry of palygorskite-bearing rocks in the Gercus Formation (Middle Eocene) from north Iraq. They found that palygorskite is probably unstable in aqueous environment in this area.

Al-Bassam, et al. (2000) determined a new occurrence of palygorskite located about 100 km west of Ramadi, within Nfayil Formation (Middle Miocene).

Al-Baidari (1997) used Iraqi palygorskite in pottery. She tested palygorskite- rich mudstone collected from Injana Formation at Najaf area in

the production of pottery, and concluded that the investigated mudstone are suitable for pottery but mixing of various mudstone type is required to obtain the proper mineralogical ingredients and grain size.

Al-Bassam et al. (1997) used Iraqi palygorskite (Digma and Injana Formations) in the dehydration hydraulic oil of electrical power stations.

Anton et al. (1997) used the Iraqi palygorskite (attapulgitite) in oil well drilling, the laboratory results were carried out by drilling an oil well in the Northern field using the palygorskite clay of the Safra Beds in the preparation of the drilling fluid. The results were successful and the clay behavior was up to the required specification.

Al-Ajeel, et al. (1997) used the Iraqi palygorskite- rich clays in decolorizing sun-flower oil. This application is used in the General Company of vegetable oils.

Aswad et al. (1997) studied the crystallochemical and thermodynamic characterization of Nineva palygorskite as microporous absorbent. He concluded that the average enthalpy of absorption is estimated to be 12 Kcal/mol ranging from 10.388 to 16.408 Kcal/mol.

Kadum (2009) Stated that the suggested origin for the palygorskite of the Gercus Formation is formed by transformation of preexisting materials and suggested two types of this transformation. First, was by transformation of montmorillonite with high content of Mg and trace elements. The second, by direct alteration of the basic rocks (may be serpentinite).

1-5 Geological setting

The landscape of the Western Desert of Iraq is not complex, but is characterized by a variety of forms; the study area is hilly and semi flat area. The lithology and hardness of rocks have played a role in the development of different landforms. For example, the hard rocks give the desert a plateau form. Interbedded rocks of variable hardnesses have accelerated the dissection of the plateau into steps or minor plateaus. The soluble rocks have led to forming karst units and features. Finally, the soft rocks contributed in the development of eolian units.

The Western Desert of Iraq is featured by variety of suites of geological formations from Paleozoic (Pre-Carboniferous) to Cenozoic. The area covered by the study involves the ages of Cretaceous to Late Paleocene. Geological setting explains the lithostratigraphy, tectonic and structure and geomorphology of the study area. They can be described as follows:

1-5-1 Lithostratigraphy

The exposed rocks in the Western Desert are of both marine and continental origins. They are represented by limestone, dolomitic limestone, dolomite, sandy limestone, clayey limestone marl, sandstone, and claystone, with rare gypsum and phosphorite.

1-5-1-1 Digma Formation

The presence of the Digma Formation (Maastrichtian) in the Iraqi Western Desert was mentioned for the first time by Sattran and Mansour (1975) in Buday (1980). However, it is worth to mention that the mapped succession of Digma Formation by Buday and Hak (1980) and which was renamed as "Samhat Formation" by Jassim et al., (1984) is not the same succession considered by GEOSURV as the Digma Formation. The upper part of the so called Jeed Formation by Jassim et al. (1984) is identified as "Safra Beds" by Al-Bassam et al. (1990). It is adopted by GEOSURV as the Digma Formation (Sissakian, 2000); Whereas, the lower part of the so called "Samhat Formation" is considered as Marbat Beds and the upper part as Tayarat Formation; moreover, the lower part of the so called "Jeed".

Al-Bassam et al., (1990) mapped the Digma formation as "Safra Beds" for the first time in the Western Desert as an integral part or unit in Digma Formation which represents the sixth sedimentary cycle of the Cretaceous Period. A supplementary type section is proposed by Al-Bassam et al., (1990) at Er Radhuma (Al-Safra), about 10 km southeast of Akashat mine. The original type locality is in oil well Anah 1 (Bellen et al., 1959); it is defined by the coordinates of Longitude $41^{\circ} 15' 48''$ E and Latitude $34^{\circ} 20' 24''$ N.

The Digma Formation is exposed along the northern rim of Ga`ara Depression, from Marbat Al-Hasan hill and extends westwards, then extends along the western rim, farther southwards crossing the Highway No.1 and extends to the Iraqi – Saudi Arabian borders (Figure-1).

In Traifawi vicinity, it extends eastward for about 60 km and northwards to about 35 Km, moreover towards southeast to Muger Al-Na`am vicinity. The subsurface extension of the Digma Formation is clear. It extends northwards from exposed areas to Khlesia passing through Anah trough, and west and eastwards along sides of the Rutbah Uplift.

Buday and Hak (1980) described it as basal conglomerate, sandstone, siltstone, marlstone and organic limestone, beside yellow and green marlstone, thinly bedded calcareous claystone and calcareous siltstone are

present in the northern and northwestern parts of the Ga`ara Depression. Al-Bassam et al., (1990) described the Digma Formation as "Safra Beds" as white to creamy limestone, dolostone with phosphorite horizon and green to ocher papery shale, with the oyster shell horizon. Hassan (1998) described it, in the Ga`ara vicinity as consisting of white, creamy dolomicrite, within phosphorite horizon, overlain by green papery shale and topped by phosphorite horizon consists of oyster rich limestone alternative with marl horizons. Southwards the fossiliferous limestone increases in thickness and passes laterally to shelly limestone, with chert nodules and geodes in the middle and upper parts of this unit. Al-Haza'a (2001) divided it into three parts: The lower part consists of dolostone with phosphorite horizon and porcellanite, in the base. The middle part consists of ocher marl, occasionally with oysters, whereas the upper part consists of oyster rich limestone (lopha bed) which alternates with dolostone. Southwards the upper shelly part increases in thickness and passes to bivalves-rich limestone. Formation is considered, by GEOSURV, as the upper part of the Tayarat Formation.

The following thickness was recorded by different authors. In the supplementary type section, it is 23 m and 15 m in the northern rim of Ga`ara depression (Al-Bassam et al., 1990). It ranges between 12 to 20 m to west of Ga`ara depression and increases to more than 40 m (Al-Haza'a, 2001).

The age of formation has been correlated and determined by fossils. The following fossils were recorded by different authors: Bellen et al., (1959) *Corax pristadontus* AGASSIZ, *Lammina* c.f. *appendiculata* AGASSIZ, *Globotruncana stuarti* (DE LAPPARENT), *Glt. lapparenti bulloides* VOLGER, *Glt. Lapparenti*, *Globuggerina cretacea* DE ORBIGNY, *Gumbelina globulosa* (EHRENBERG), *Vaginulina plummerae* (CUSHMAN). Al-Bassam et al., (1990) recorded *Rugogleobigerina macrocephala* BRCNNIMA, *Ruge. Bronnimanni* EL-NAGGAR, *Pseudotextularia elegans* RZEHAK, *Heterohlix striata* (EHRENBERG), *H. glbosa* (EHRENBERG) and *Guembelitra cretacea* CUSHMAN. Hassan (1998) recorded mainly oysters (*Lopha* and *Ostrea*). Maastrichtian (Bellen et al., 1959 and Hassan, 1998), Early Maastrichtian (Buday and Hak, 1980) and Late Maastrichtian (Al-Bassam et al., 1990 and Al-Haz`za, 2001).

Digma Formation has been deposited in shallow environment. Many authors have been suggested that it has littoral neritic condition (Buday, 1980), shallow marine (Hassan, 1998), shallow water (mostly back reef and

lagoon), in the east and deep water, in the west of the exposure area (Al-Haza'a, 2001).

In term of contact, the Digma Formation is unconformably underlain by Ms`ad Formation (Buday and Hak, 1980). It is conformably underlain by the Tayarat Formation (Na`ja Beds), the contact is based at the top of a shelly limestone and first appearance of white siliceous micrite, with phosphorite horizon. In a very small part of the exposure area, east of MarbatAl-Hasan hill, it is underlain by "Marbat Beds" and is based at the top of last clastic horizon (Al-Bassam et al., 1990). Hassan (1998) mentioned that, it is underlain conformably by the Tayarat Formation and it is based at the top of silicified limestone and first appearance of a yellow marl or pale grey dolomicrite, with phosphorite horizon. Al-Haza'a, 2001 refer to that, it is underlain unconformably by the Ga`ara Formation, along the northern rim of the Ga`ara Depression, and marked by sandy, pebbly, phosphatic limestone or conglomerate, above the cross bedded sandstone of the Ga`ara Formation.

1-5-1-2 Akashat Formation

The Akashat Formation (Early - Late Paleocene) is recently added to the stratigraphic column of Iraq. Formerly, the succession was considered as Umm Er Radhuma Formation. The difference in lithological composition, facial development and Paleo-geographical distribution between Akashat and Umm Er Radhuma Formations were recognized by Bellen et al., (1959); Al-Naqib (1960) and Powers et al. (1967) called it as Hibr Formation, Buday (1980) and Buday and Hak (1980) called it as phosphatic facies of Umm Er Radhuma Formation, Jassim et al. (1984) called it as Akashat Formation and Al-Bassam and Karim (1997) announced it officially as Akashat Formation. It is worth to mention that GEOSURV was using the name of Akashat Formation instead of Umm Er Radhuma Formation since 1990.

The type locality of the Akashat Formation is located by Al-Bassam et al. (1990) in wadi Samhat, along the western rim of Ga'ara Depression, which is located 7 Km to the south of Akashat phosphate mines. It is defined by the following geographic coordinates: of Longitude 39° 50' 06" E and Latitude 33° 37' 30" N.

The Akashat Formation is exposed, only in the western and middle parts of the Iraqi Western Desert. It crops out in Qasir Al-Halqoom, along the northern rim of Ga'ara Depression, extends westwards (along the rim) till Akashat, then southwards to the Iraqi - Saudi Arabian borders, crossing Jabal

Al-Hirri, in a form of narrow strip 2-10 km till the Highway No.1, then it becomes 10- 30km wide. The subsurface extension of Akashat Formation is almost uniform, it extends north and westwards. It is struck in oil wells Akkas 1, Risha 1 (in Jordan). Towards north, it passes to Aaliji Formation and towards east and northeast; it is replaced by Umm Er Radhuma Formation, east and northeast of Rutbah Uplift. According to Al-Mubarak and Amin (1983) the lower part of Akashat Formation is included within the Hartha Formation by Buday and Hak (1980).

The Akashat Formation, in the type locality consists of an alternation of grey phosphorites and limestones (Al-Bassam et al., 1990); it consists of phosphatic conglomerate or breccia, followed by oyster bed (biolitite), overlain by a sequence of calcareous siltstone, with layers of silty limestone and calcareous mudstone, locally phosphatic. Another fossiliferous limestone or Coquina bed occurs; followed by calcareous siltstone, with interbeds of limestone and chalky limestone, with abundant chert nodules, rare geodes and lenses of phosphorites, capped by violet, papery shale (Buday and Hak, 1980). The Akashat Formation is divided into three members by Al-Bassam et al. (1990):

A: Traifawi Member consists of an alternation of lime mudstone, shale and phosphorite. The cycle, which is repeated 2-3 times, consists of coarse grained phosphorite, green shale or marl, followed by creamy siliceous lime mudstone, usually with small chert nodules. South of Highway No.1, yellowish, quartzitic sandstone occurs in the middle part.

B: Hirri Member consists of an alternation of phosphorite, shelly limestone and lime mudstone. The cycle is repeated 2-3 times. In Akashat - Ga'ara area, the upper part of Hirri Member consists of shelly (cardita) limestone, which reaches in thickness to 10 m.

C: Dwaima Member consists of an alternation of grey phosphate, gray and pink, fissile, siliceous marl and phosphates, crystallized limestone, with shark teeth.

The thickness of the Akashat Formation, in the type locality is 27 m (Al-Bassam et al., 1990). It is 25-35 m along the northern rim of the Ga'ara Depression (Buday and Hak, 1980). It is 23- 30 m (Jassim et al., 1984), about 15 m in Tel Samhat, 25 - 30 m in Akashat, 54 m in Traifawi and increases

gradually towards north and west of the exposed areas (Al-Bassam et al., 1990).

The first paleontological study of the Akashat Formation was from subsurface sections, around Akashat. The following fossils were recognized by different authors: Karim and Ctyroky (1981); Karim and Jassim (1985) and Karim in Al-Bassam et al. (1990); *Globigerina daubjergens*, *Globorotalia compressa* (PLUMMER), *Glt. Pseudobulloides* (PLUMMER), *Glt. Trinidodensis* BOLY, *Glt. Imitata* SUBBOTINA, *Glt. Vncinata* BOLY, *Globigerina haynesi* EL-NAGGAR, *G. triloculinoides* (PLUMMER), *Chilogucmbelina midawyensi* (CUHMAN), *Guembelitra cretacea*(CUHMAN), Benthonic fauna asociación age: *Gabonella sp.*, *Lenticulina turbinata* PLUMMER, *Valvulinaria ravni* REUSS and *Anomalinoides midwayensis* BROTZEN. The following fauna are recorded by Karim in Al-Bassam et al. (1990) from the Middle Paleocene: *Globokotalia angulata*, *Glt. Psendobulloides* PLUMMER, *Glt. Quadrata* WHITE, *Glt. Haynesi* EL-NAGGAR, *Glt. Triloculinoides* PLUMMER, *Lenticulina midwayensis* TENDAM, *Valvulinaria ravni* RUSS. They (op. cit) recorded the following fauna from the Late Paleocene: *Globorrotalia velascensis*, *Globorotalia acuta* TOUIMIN, *Glt. Aequa* CUSHMAN and RENZ, *Glt. Esnaensis* (LEROY), *Glt. Irrerata* LOEBLICH and TAPPAN, *Glt. Woodi* EL-NAGGAR, *Glt. Occulosa* LOEBLICH and TAPPAN. The recorded benthonic fauna are, *Frondioularia peshphatica* (REUSS) *Vaginulopsis midwayensis* (Fox and ROSO), *Lenticulina midwayensis* (KUSHMAN and PONION). All these fauna are indicative of Danian age (Al-Bassam et al., 1997).

The age of Akashat Formation has been determined depending on the fossils. Jassim et al., (1984) claimed late Early Paleocene age for the Akashat Formation. Later on Al-Bassam et al., (1990) confirmed that the age of Akashat Formation ranges from Early - Late Paleocene depending on the formation biozones.

Akashat Formation is deeper and cooler shelf environment relative to that of Late Cretaceous (Al-Bassam and Karim, 1997). The middle Paleocene was more transgressive started in the early stages by central-shelf shoal facies to a deeper outer shelf peloidal phosphorite facies (Al-Bassam and Karim, 1997). The Dwaima Member indicates inner shelf, central shelf, and outer shelf to shelf edges, under subtidal and warm conditions The Late Paleocene

cycle come to end by the development of inner shelf – shoal intertidal coprolitic shelly limestone (Al-Bassam et al., 1990).

The Akashat Formation is mainly underlain by Cretaceous rocks. In the northern rim of Ga'ara Depression, it also was considered to be underlain unconformably by the Ga'ara Formation. Its contact was based on the top of last sandstone or conglomerate bed

Jassim et al., (1984) and Al-Bassam et al., (1990) however recognized Marbat Beds instead of the Ga'ara Formation, the contact is unconformable. It is underlain unconformably by Mulussa Formation in the eastern rim of Ga'ara Depression and the Digma Formation in the northern and western rims (Buday and Hak, 1980). It is underlain by Safra Beds (Digma Formation). south of the Ga`ara Depression. The contact is based on the last appearance of *loftusia* and *lopha* bearing limestone, or first appearance of ocher, siliceous lime mudstone or shale (Al-Bassam et al., 1990).

1-5-2 Tectonic and Structure

The Western Desert is a gently sloping plain with a gradient of 5 m/km, towards east and northeast. The dip of the strata is almost horizontal, reaches 1 - 2 degrees. In the western part, around Ga`ara Depression, the beds dip in all directions, while the east and middle parts the beds dip gently northeastwards. The gentle plain reflects the structural position of the Western Desert within the Stable Shelf (Buday and Jassim, 1984).

Rutba Uplift has played a great role in the historical geomorphology of the Western Desert. According to Buday (1980) and Buday and Jassim (1987) the crest of the uplift had remained as a dry land during the Late Cretaceous. Since that time the gradual rise of the uplift has caused an increase of the dry land over the whole Western Desert, in the form of major plateaus. At the same time the plateaus were dissected into many blocks. The common structural features in the Western Desert are faults, joints, folds, grabens and ring structures.

Qasir et al., (1992) determined four sets of faults are ascertained in the Western Desert by means of interpretation of Landsat images on basis of drainage, cliffs, distribution of mesas and orientation of depressions. The fault systems are N-S, NW-SE, E-W and NE-SW. The faults are related to very old Orogenies, Kibiran, Hijaz and Najid, which have been rejuvenated during Late Mesozoic and Tertiary by the Alpine Orogeny. Buday (1980) and Buday and Haq (1980) thought that the faults are to be dissected through the

basement and the overlying Paleozoic, Mesozoic and Tertiary sedimentary cover. The relation between drainage and faults is very visible on Landsat images and topographic maps. Most of the major valleys start on the plateau around Rutba vicinity and extend towards north, northeast and east. In each drainage basin of the main valleys, the valleys change their trends at variable angles, between (45-90), these changes coincide with the directions of fault systems. In addition to that the axes of the meanders that have developed along the courses of the valleys coincide with the trend of faults and joints. A third visible example is represented by the cliffs developed in Umm Er Radhuma Formation along N-S and E-W faults. Wadi Swab and Wadi Ratga, the west of the study area drain the northwestern part of the Western Desert toward Syria border, reflect clear relation between their trend and faults. The lower reaches of the wadies are in N-S direction and reflect their development along weak zone of the same trend. The tributaries of both wadies are also parallel to each other and are controlled by long joints of NW-SE and NE-SW directions. The western tributaries of Wadi Swab are toward NE direction, while the eastern tributaries of Wadi Ratga are toward NW direction. The upper reach of Wadi Swab is dissected by sets of NW-SE joints, resulted in formation of parallel tributaries and rectangular change of the Wadi course. The plateau on Hartha Formation is cut into well oriented mesas due parallel NW-SE trending joints. Al-Mubarak and Amin (1983) and Qaser et al. (1992 and 1993) have identified many faults of the same above mentioned directions, they missed many other faults, which might not be visible due to low displacement or not observed along their traverses, during geological mapping. (Al-Kadhimi et al., 1996) edited tectonic map of Iraq shows also some faults, of the same directions which support the presentation above.

Many ring structures are developed in the Western Desert. One ring structure is identified within Hussainiyat Formation in the upper reaches of Wadi Ghadaf. The diameter of the feature is about 500 m. Its formation is related to block movements. In the Western parts of the Western Desert, tens of ring structures are developed, they are either of karst origin or hydrocarbon explosion (Hagopian, 1979). The diameters range from few hundred meters to few kilometers which Usually from depressions on surface of the Ratga Plateau. Tens of circular and oval depressions of different sizes are located in the western part of the Western Desert. They are developed in flat areas, built up by Ratga Formation, locally are called "Faidhah". Some of them are interpreted by geophysical means as ring structures.

1-5-3 Geomorphology

The Western Desert is considered as rocky desert of a large plateau comprising mainly carbonate rocks. It is characterized by low rainfall, Low seasonal vegetation like short grass and thick soil cover in general and tends to be featureless. It can to be described as flat to semi flat area, rises gradually from east to west to a maximum elevation of 987 m, above sea level. The main topographic features are positive and negative features. The main features are mesas, kuestas, Hogbacks, buttes, hills, cliffs, canyons, valleys and depressions. Several canyons cut the desert from the west towards north, northeast and east. The largest depression is represented by Ga`ara,

The landforms of the desert are the result of the interaction between structure, lithology and climate, as indicated by the variable forms of the geomorphological units and features. The landforms of the Western Desert are grouped in many major units related to the agents and processes contributing to their development. Some of these units that are close to the study area are: Units of structural-denudational origin. Four types of landforms are developed under this topic, these are: Mesas, Cuestas, Hogbacks and Plateaus. The major plateau is: Plateau on Umm Er Radhuma Formation, Plateau on Tayarat Formation, Plateau on Mulussa Formation and Plateau on Ga`ara Formation. Units of Denudational Origin are characterized by Hills (Buttes) and Depressions in most.

Chapter Two

Materials and

Methods

2- Materials and Methods

2-1 Preface

Scientific contexts follow concrete steps to show the logical sequence for the conduct of scientific research. An urgent need to list and explain the most important methods of work used in this study, as well as the equipments and techniques used. Field, laboratory and office works are described in details that will provide the basic foundation and roadmap for this study.

2-2 Field work

Field work has been done on Akashat and Digma Formation in the Western Desert of Iraq. Before starting on detailed fieldwork, some of the requirements have been taken to make this mission a success. These requirements, were conducting reconnaissance field trip from Trafawi at the south of the study area to the Ga'ara depression to the north of the study area of about 80km north Rutba city (Figure 2-1). Through this trip, the nature of the area has been viewed and the accessible outcrops of the studied geological formations which contain palygorskite-rich sediments are determined using detail geological maps and GPS. Thereafter, many trips of detailed field work have been carried out. Clay deposits have been investigated and followed up in the field to search for palygorskite. Then the exposures of clay-bearing beds have been marked and sampled. Many stratigraphic sections representing different facies of the basin were investigated for the units of palygorskite. Palygorskite is commonly associated with phosphatic sediments, carbonates and siliceous rocks (Yalcin and Bozkaya, 1995).

Samples are collected from the accessible geological sections and outcrops. Fifty samples are collected from 11 sites (Figure 2-1). These sampling sites with geographic coordination are listed in Table 2-1. Then the suitable samples were chosen, where the samples of no or poor palygorskite were then neglected.

Sample 1D is collected from the trench of 2m depth, where porcellanite extends subsurface with thickness varying between 0.8 to 1 m within the Digma Formation (Figure 2-2). The main facies of Akashate Formation is marine phosphatic deposits (Figure 2-3). Safra Bed, a part of Digma Formation is well exposed near Akashat village on the right side of the main road between Akashat and Qaim (Figure 2-4). Facies of Digma Formation changes to kaolinite-palygorskite claystone interbedded with opal-CT eastward

(Figures 2-5 and 2-6). Sample 12D was collected from section rich with claystone and dolomite (Figure 2-7).

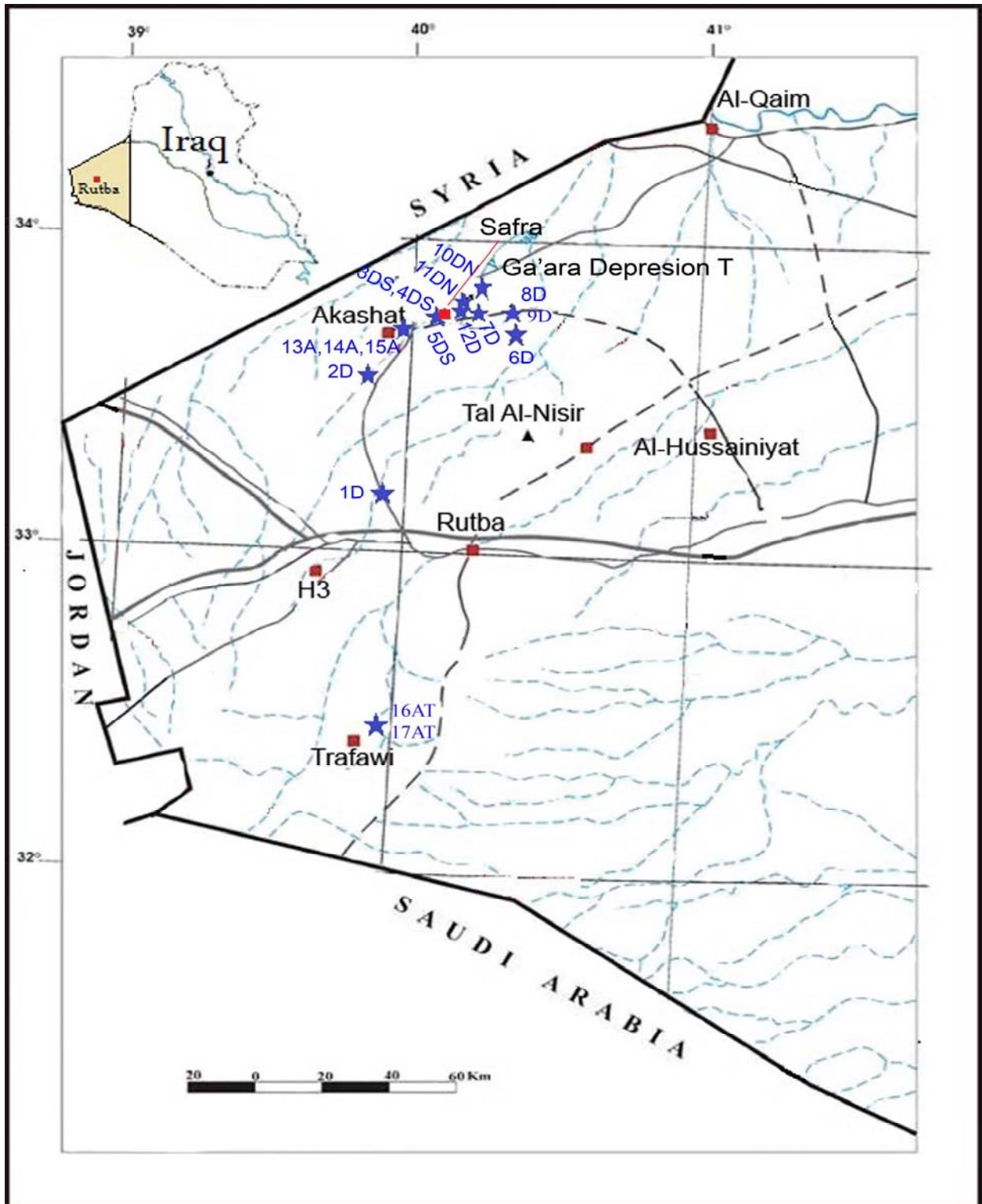


Figure 2-1: Location map shows the study area and the sampling sites, (after Al-Basam, 2007)

Table 2-1: Coordinates of samples and field and laboratory description.

Sample No.	Formation	Elev. (m)	Longitude	Latitude	Description	
1D	Digma	765	E 39 55 50.3	N 33 12 41.7	Porcellanite (opal-CT)-rich sediments, quartz, little dolomite and apatite	
2D		642	E 39 56 44.6	N 33 38 55.9	Phosphate-rich clay	
13A	Akashat		E 30 57 59.9	N 33 40 24.5	Palygorskite-rich claystone, Opal-CT, Quartz, calcite and apatite.	
14A			E 30 57 59.9	N 33 40 24.5	Palygorskite –rich clay with siliceous sediment and dolomite	
15A			E 39 57 59.9	N 33 40 24.5	Siliceous claystone.	
3DS	Digma	597	E 40 02 07.8	N 33 40 35.2	Mainly dolomite with very little clay (Palygorskite).	
4DS		597	E 40 02 07.8	N 33 40 36.2	Mainly dolomite with little clay (Palygorskite).	
5DS		597	E 40 02 07.8	N 33 40 36.2	Mainly Montmorellonite and palygorskite with porcellanite (opal-CT), quartz and dolomite.	
6D		518	E 40 19 57.9	N 33 33 31.3	Claystone (kaolinite) with porcellanite (opal-CT) and quartz.	
7D		518	E 40 19 53.3	N 33 33 36.3	Kaolinitic rich clay (palygorskite)	
8D			E 40 19 53.9	N 33 33 31.3	Claystone composed mainly of kaolinite and palygorskite with little porcellanite (opal-CT) and quartz.	
9DN		585	E 40 08 44.7	N 33 37 38.3	Siliceous claystone (quartz and kaolinite).	
10DN		585	E 40 55 50.3	N 33 40 24.5	kaolinite-rich clay with porcellanite (opal-CT), quartz and apatite.	
11DN		585	E 40 07 55	N 33 38 45.7	Siliceous- calcitic rich clay.	
12D		585	E 40 07 55	N 33 38 45.7	Palygorskite with little clay minerals and dolomite.	
16AT		Akashat Trafawi	744	E 39 50 49.8	N 32 41 64.0	Clay minerals (montmorillonite and palygorskite) with silica as quartz and opal-CT and very little apatite.
17AT			744	E 39 50 49.8	N 32 41 64.0	Clay minerals (montmorillonite and palygorskite) with silica as quartz and opal-CT and very little apatite.

D=Digma Formation; A= Akashat Formation; S=Safra bed, N=Na'aja unit; T=Traifawi member.



Figure 2-2: Porcellanite (opal-CT) facies (0.8-1m) of yellowish white color having conchoidal fracture, site of sample 1D.

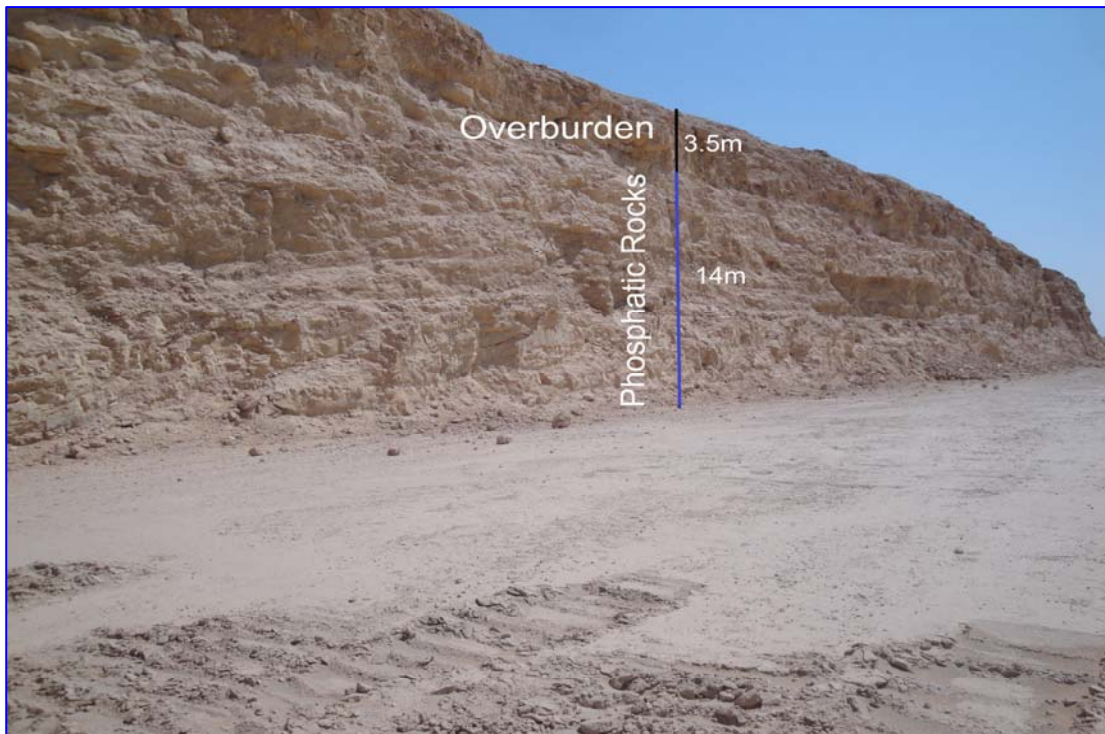


Figure 2-3: Phosphatic rocks (14m thick with carbonate rock overburden of 3.5m) at the main working face of Akashat mine, Akashat Formation.



Figure 2-4: View of Safra bed of Digma Formation which forms from claystone with dolomite. The samples 3DS, 4DS and 5DS collected from this site.



Figure 2-5: Kaolinite-palygorskite claystone interbedded with opal-CT in Digma Formation; Sample 8D was collected from this section.



Figure 2-6: Palygorskite-rich clay with porcellanite (opal-CT) and siliceous deposits in Digma Formation, sample 10DN.



Figure 2-7: Palygorskite-rich calystone with dolomite a part of Digma Formation; sample 12D.

Trafawi site characterizes by claystone mixed with porcellanite of crystabollite and tridymite (opal-CT); dolomite also occurs in this facies (Figure 2-8).



Figure 2-8: Traifawi section (2m thick) illustrates claystone with dolomite. At the ground, quarried bentonite of yellow color exists with papery texture.

2-3 Laboratory work

Laboratory work, as usual, is the work immediately follows the field work. Therefore, all the samples collected were transferred to the laboratory and prepared as necessary as for the purpose of mineralogical identification, chemically analyses and technical testing. Laboratory work focuses on examination of samples in a variety of ways for the purpose of selecting palygorskite-rich samples in order to concentrate (purify) this mineral practically. The laboratory steps are explained below:

2-3-1 Sample preparation

All samples (whole samples) are prepared in the Geochemisrty Laboratory, at Department of Geology, College of Science, University of Baghdad. Preparation processes including drying and gentle grinding. Palygorskite was dried in an electric oven at 80°C for several hours before use in the adsorption tests. Generally, samples are not hard, but dismantle, and after drying they are gently grinded with a plastic pestle and agate mortar. All

samples are subject to the preparation processes for different examination and analyses.

2-3-2 Mineral identification

To be sure of the diagnosis of mineralogical composition, many techniques have been used for this purpose. These techniques include the following:

2-3-2-1 X-ray diffraction technique

The XRD analysis is performed in the laboratories of the Iraqi Geological Survey. The samples are first ground, mounted on holders, then introduced for analysis. The source consisted of Cu K α radiation ($\lambda=1.54 \text{ \AA}$). Each sample was scanned with 2 theta range of 2-50 degrees.

Palygorskite can be detected by means of x-ray powder diffraction analysis (Keller, 1979). This technique is used for the purpose of mineral identification. Fourteen samples were subjected to X-Ray diffraction method in three runs, normal, ethylene glycolated and heated to 550°C. Then, one of these samples is chosen, according to its high concentration of palygorskite; that sample given the name (12D). This sample, then subjected to a series of investigation started from palygorskite separation according to Paul et al., (2000) and Robert (2002). These methods of separation of palygorskite depending on the assumption the specific gravity of the palygorskite are low (2.3) relative to other clay minerals. Carbonates are removed by treatment with the acetic acid. Procedures (normal, heated and glycolated methods) are applied to identify clay minerals. The general steps are as follows:

A. Acetic Acid treatment

It is necessary to dissolve the carbonates in some limestones and sediments before the clay mineral identification. However, treatment with strong acids to remove carbonate can attack the structure of clay minerals (trioctahedral minerals are often destroyed by such treatment), and even dilute acid can attack the silicate layers via interlayer regions and exposed edges. Generally, dilute acetic acid is preferred over hydrochloric acid because it is less likely to affect clay crystallinity. The procedure followed is described below:

1. Add 1 part acid to 4 parts distilled water in the graduated cylinder and mix thoroughly with the glass rod. Caution: acetic acid can cause burns.

Wear safety goggles, plastic gloves, and an apron while working with this chemical.

2. Label 300 ml beakers and add sample.
3. Add 50-75 ml of the acetic acid solution slowly to avoid foaming and overflow of beaker. A glass pipette may be used to transfer the acid solution. When effervescence subsides, add another 50-75 ml of acid. Stir and allow standing overnight. Repeat until suspension no longer effervesces.
4. Allow the suspension to settle and carefully siphon or pour off the supernatant liquid or wash sample by centrifuging. Dispose of acid waste properly. Sample now free of carbonate.

B. Random powder mounts

1. Tape the glass slide over the opening of the sample holder. Leave tabs on each side for later removal of this cover, but fold the extra tape against itself so that it will not stick to other objects or the sample. Place the holder glass side down on a piece of weighing paper.
2. Grind the dried sample thoroughly so that it is easily brushed through the sieve. The particles should be much finer than 0.062 mm to avoid fractionation of the minerals. The sieve is used only to achieve even distribution and to ensure that the grinding is complete.
3. Place a second holder over the first as a mask. This enables the buildup of a thick enough layer of sample for later packing, while maintaining a clean metal surface on the final holder.
4. Place the sieve over the sample holder and brush the sample from the mortar.
5. Use the spatula to loosen any sample that has stuck to the mortar and brush the material into the sieve.
6. Brush the sample through the sieve into the cavity of the sample holder. The purpose of the brushing is to obtain an even distribution and to minimize preferred orientation of the particles.
7. Remove the sieve and mask.
8. Place the sample holder on a clean piece of weighing paper, tap the

powder remaining on the mask onto the first weighing paper, and replace the mask over the sample holder.

9. Pour the excess powder onto first weighing paper into the sample holder. Distribute the powder evenly.
10. Use a glass slide to pack the sample into the cavity firmly enough so that it will not fall out, deform, or slide, but not so firmly that preferred orientation will be produced on the opposite surface (which will later become the top surface). The glass slide can also be used to scrape any sample that has flattened onto the holder surface during packing back over the holder opening.

C. Thermal treatment

Thermal treatment at various temperatures is commonly used to help identify clay minerals by revealing changes in crystal structure spacing or loss of the structure. Depending on the temperature and the mineral species, these treatments can collapse the structure by dehydration, or in the case of other minerals destroy the crystal structures. However, it is important for the analyst to remember that some of the changes caused by the heat treatments may be temporary, and that partial or complete rehydration may occur during cooling. Samples are heated to 550°C. Procedure is described below:

1. Preheat the oven to 550°C.
2. Place the oriented aggregate mount in the furnace using the tongs. Leave sample in the furnace at 500°C for 2h.
3. Remove mount by pulling it forward with tongs. It is ready to be run on the diffractometer.

Separated palygorskite is also activated by heating for 200°C, 400°C, 600°C and 800°C to investigate the effect of temperature on palygorskite sorption.

D. Ethylene Glycol vapor treatment

Pour ethylene glycol to about 1 cm depth in base of desiccator. Place oriented aggregate mounts on the shelf of desiccator. Additional shelves may be stacked if necessary. Place desiccator in oven at 60 to 70°C for about 4

hours or overnight. Longer times will not damage samples. Do not remove mounts until running in the X-ray diffractometer.

2-3-2-2 Separation of palygorskite

Since one of the objectives of this study is to test sorptive properties of palygorskite of some elements (Pb, Cd, Ni, Co, Cr, V, Zn, Cu, Mn, Fe and B), A sample of pure palygorskite must be prepared. To meet this issue, two major processes were performed. First is that, clay minerals are separated from the whole samples of palygorskite-rich sediments. Second, palygorskite is separated from clay mineral suits to obtain a sample of as pure palygorskite as possible as. The detail procedures of Pual et al. (2000) and Robert and Dennis (2002) where done on whole sample (crude sample). It has been done for separating the clay mineral from whole sample, and then, palygorskite is extracted from clay minerals. The procedure followed is described below:

1. Whole (crude) sample (12D) has chosen for extracting palygorskite, because of is rich with palygorskite according to the result of XRD and chemical analysis.
2. The slurry was prepared by mixing of 50 gm of crushed crude sample with tap water 1.0 L; then stirs it at a speed of 1500 rpm for 30 minutes.
3. Pass the slurry through sieve of 200 mesh US standard to separate clay which pass the sieve, while the non clay minerals retain on the sieve.
4. Add dispersant agent (Tetra Sodium Pyrophosphate) 8 gm to 1L.
5. Allow suspension to rest and hence separated by gravity sedimentation (settling).
6. The clay suspension is decanted and subjected to be centrifuged at 2000 rpm for 15 minutes.
7. The result will be of pale gray residue at the bottom consisting of montmorillonite (sp.gr 2.53), dolomite (sp.gr 2.74) and kaolinite (sp.gr 2.9). These specific gravity values are according to Grim (1968). Palygorskite will be at the top (sp.gr 2.3) which can be distinguished by its brown color (Figure 2-9). At every patch, 8 test tubes have been used, and for the purpose of obtaining a sufficient amount of palygorskite, enough to complete all the required tests, the separation process was repeated several times. The extracted palygorskite was wet, and then was dried and grinded gently (Figure 2-10).

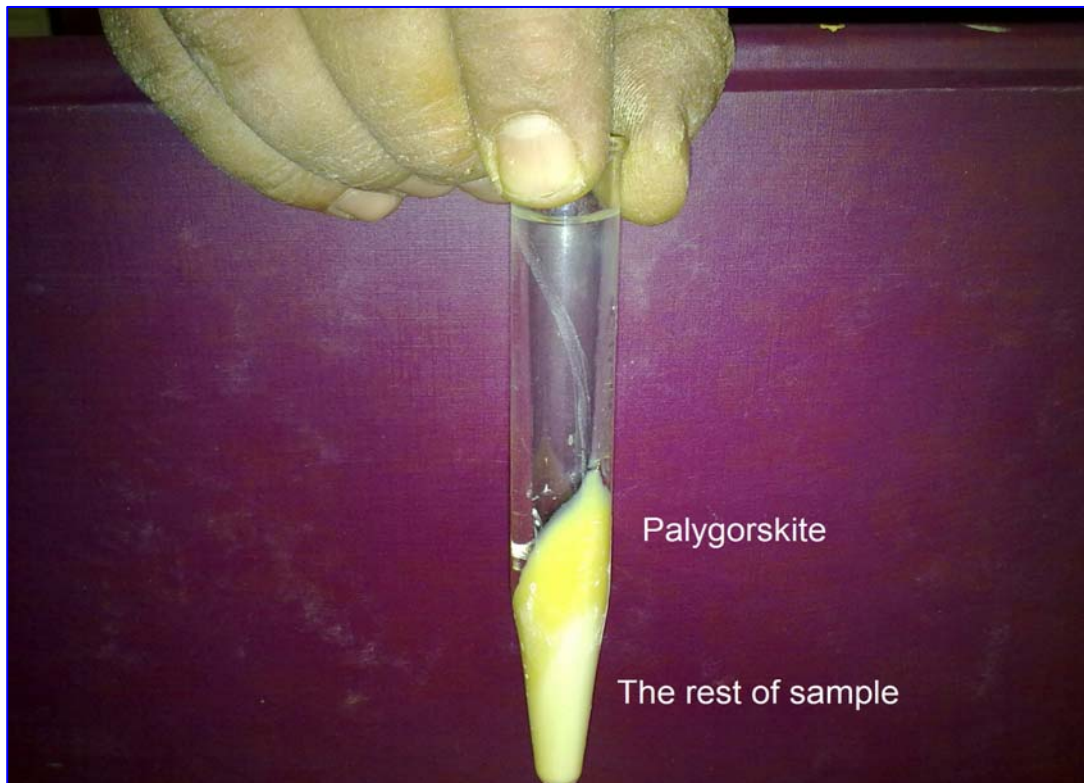


Figure 2-9: Separated palygorskite from whole sample centrifugally, Sample no 12D.



Figure 2-10: Wet (left) and dry samples (right) of separated palygorskite.

2-3-2-3 Scanning Electron Microscope (SEM)

SEM is a powerful technique applied in micro-imaging of a variety of surfaces. This technique can be used in exploring the surface structure to determine particle size and texture on that surface.

Palygorskite can be detected with the use of transmission or scanning electron microscope (Zumwalde, 1976). Scanning electron microscopy (SEM) was used to study the morphology of the palygorskite powders (Figure 2-11). This technique is carried out the Nanotechnology and Advance Materials Research Center at the University of Technology with a device type of VIGA TESCAN II SBH MS12, and on the South Oil Company (SOC) in Basra.



Figure 2-11: Studying the palygorskite mineralogy using SEM at the Nanotechnology and Advance Materials Research Center at the University of Technology with a device type of VIGA TESCAN II SBH MS12.

2-2-2-4 FTIR technique

Infrared spectroscopy is an important technique in mineralogy. It is an easy way to identify the presence of certain functional groups in a molecule. This technique measures the absorption of various infrared light wavelengths

by the material of interest. With the advent of Fourier Transform Infrared Spectroscopy (FTIR), the range of applications and the materials amenable to study has increased sensitivity, speed, wave number accuracy and stability.

The FTIR instrument consists of an IR light source, a sample container, a prism to separate light by wavelength, a detector, and a recorder (which produces the infrared spectrum) (Connor et al. 2003).

A Fourier transform infrared spectrometer (FTIR) was used to detect the absorption peaks of untreated and thermally treated palygorskite powders. The samples were prepared using the KBr pellet technique. Laboratory work at Ibn-Sina Company (Baghdad) was the laboratory in which the FTIR were performed.

Thirty whole samples obtained from Akashat and Digma Formations as well as the separated palygorskite are tested by FTIR. The KBr and the powdered sample must be entirely dry.

2-3-3 Laboratory experiment

Laboratory tests included the preparation of stock solutions from standard solutions, and adsorption experiments. A set of 110 laboratory experiments (11 heavy metals for 10 different concentrations) was made at the Geochemistry lab in the Department of Geology at the University of Baghdad.

2-3-3-1 Preparation of stock solutions

Ten concentrations as stock solutions (10, 25, 50, 75, 100, 125, 150, 175, 200 and 225 ppm) for each of the elements (Pb, Cd, Ni, Co, Cr, V, Fe, Mn, Zn, Cu and B) were prepared. This means, this study dealt with a total of 110 solution samples. These stock solutions were prepared by diluting the standard solutions with distilled water. The standard solutions that are used for preparing the stock solutions are listed in Table 2-2.

Table 2-2: Standard solutions used for preparation stock solutions.

Element	Concentration (g/l)	Compound	Color
Pb	1	Pb(NO ₃) ₂	Colorless
Cd	1	Cd(NO ₃) ₂ .4H ₂ O	Colorless
Ni	1	Ni(NO ₃) ₂ .6H ₂ O	Light Blue
Co	1	Co(NO ₃) ₂	Red
Cr	1	Cr(NO ₃) ₃	Blue
V	1	VO ₂ .H ₂ O	Blue
Cu	1	Cu(NO ₃) ₂	Light Blue
Zn	1	Zn(NO ₃) ₂ .4H ₂ O	Colorless
Mn	1	Mn(NO ₃) ₂ .4H ₂ O	Colorless
Fe	1	Fe(NO ₃) ₃	Light Blue
B	5	H ₃ BO ₃	Light Pink

2-3-3-2 Laboratory adsorption experiment

The sorption (adsorption and absorption) measurements are determined by the batch experiment style by adding 1 gm of pure palygorskite with 100 ml of aqueous solutions of Pb, Cd, Ni, Co, Cr, V, Fe, Mn, Zn, Cu and B separately in 200 ml beaker. The sorption mechanisms are carried out by preparing 10 different concentrations from each element of 10, 25, 50, 75, 100, 125, 150, 175, 200 and 225 ppm. The time of reaction is determined to be 1h. The mass of palygorskite is determined to be 1 gm.

The mixtures were stirred by magneto-stirrer at 1 hour. The initial and the final concentration of each of Pb, Cd, Ni, Co, Cr, V, Fe, Mn, Zn, Cu and B in the solution are measured by using inductively coupled plasma (ICP) in the Global ALS Laboratory Group in the Czech Republic-Prague Laboratory.

Temperature, pH, Total dissolved solid (TDS), Electrical Conductivity (EC) and salinity were immediately measured for each experiment in the initial and final solutions. Initial solution means a solution contains a certain concentration of a metals before the start of the experiment; whilst, the final solution means that solution which represents the initial solution itself, but after the completion of the experiment.

2-3-4 Chemical analyses

Whole samples of palygorsike-rich sediments and pure palygorskite separated from the raw samples were analyzed for SiO₂, Al₂O₃, MgO, Fe₂O₃, TiO₂, MnO, Na₂O, CaO, K₂O, P₂O₅, LOI., while solutions that prepared for testing the palygorskite sorption were analyzed as follow:

2-3-4-1 ICP-AES method

After completing experiments of heavy metals adsorption by palygorskite, all filtrate solutions were analyzed to determine the palygorskite sorption efficiency of the elements (Pb, Cd, Ni, Co, Cr, V, Fe, Mn, Zn, Cu and B) by inductively coupled plasma- atomic emission spectrometry. All solutions (110 samples) were chemically analyzed in the Global ALS Laboratory Group in the Czech Republic-Prague and Spain. Samples were fixed by nitric acid addition prior to analysis. The certification of analyses can be seen in appendices (Table Ap-1).

2-3-5 Accuracy and precision

2-3-5-1 Accuracy

The accuracy is defined as the differences in the analysis results of the standard samples from the values installed globally (Maxwell, 1968). Standard samples represented by standard solutions of 100 ppm for each element were analyzed three times (Table 2-3). Here, The mean of the triplicate analysis (X) is compared and revealed that the results of the standard samples are close to the values installed globally (Table 2-3). For all results, the standard deviation is very small. Consequently, the results are accurate.

Table 2-3: Accuracy and precision results of the standard sample compared with their global results; X= Mean; σ = Standard deviation; R. S. D= Relative standard deviation.

Elements	Standard Solution (ppm)	Number of analyses (ppm)			X	$\pm\sigma$	R. S. D%	
		1	2	3			$(\sigma / X)100$	$(2 \sigma / X)100$
Pb	100	100	102	99.4	100.4	1.11	1.106	2.212
Cd	100	99.8	100	100	99.9	0.09	0.094	0.188
Ni	100	99.8	99.6	100	99.8	0.16	0.163	0.327
Co	100	99.7	100.1	99.9	99.9	0.16	0.163	0.327
Cr	100	100	100	99.6	99.8	0.18	0.188	0.377
V	100	100.1	99.4	100	99.8	0.30	0.309	0.619
Cu	100	99.5	100	99.8	99.7	0.20	0.205	0.411
Zn	100	100	99.3	99.9	99.7	0.31	0.309	0.619
Mn	100	100.2	99.5	99.7	99.8	0.29	0.294	0.589
Fe	100	99.6	100	100.2	99.9	0.25	0.249	0.499
B	100	99.5	100.2	100.2	99.9	0.33	0.330	0.660

2-3-5-2 Precision

The term precision is defined as the range of the compatibility and harmony among different results of the sample were analyzed multiple times under the same conditions. For this study, the standard solutions of 100 ppm for each element were triplicates analyzed and the results were comparable together (Table 2-3). Standard deviation used for calculating precision. The following equation shows the relative standard deviation (R.S.D) from the confidence level of 63%, in this point; the precision will be acceptable to the 15% (Stanton, 1966).

$$\text{R.S.D}\% = (\sigma/X) 100$$

The following equation shows the relative standard deviation (R.S.D) from the confidence level of 93%, in this point the precision will be acceptable to the 25% (Maxwell, 1968).

$$\text{R.S.D}\% = (2\sigma/X) 100$$

The relative standard deviation in both cases at a confidence level of 63% and 93% showed that the results are acceptable.

Chapter Three

Mineralogy

3- Mineralogy

3-1 Preface

Common clays have a wide range of physical properties thus making them applicable to many different structural clay products. Palygorskite is a clay mineral with a wide variety of industrial applications. This mineral has some particularly desirable sorptive, colloidal-rheological, and catalytic properties, in comparison with other clay minerals (Jones and Galan, 1988).

Samples are tested with a variety of techniques for the purpose of examining the mineralogy, as well as to determine the palygorskite content, and then to select richest sample in palygorskite as pure mineral to test its efficiency of heavy metal sorption (adsorption and absorption). The techniques that are used for mineralogical study are XRD, Scanning electron microscope (SEM) and Fourier transform infrared spectrometer (FTIR).

3-2 Mineralogical study using XRD, SEM and FTIR

Most palygorskite fibrous have a diameter below the resolution limit of the light microscope (Zumwalde, 1976; Bignon et al., 1980). Thus, the analysis of clays may require the use of both X-ray diffractometry and electron microscopy. When using X-ray powder diffraction analysis, the strongest line at 1.05 nm is best suited for the identification of palygorskite (Christ et al., 1969; Keller, 1979).

In this study, there is a need to identify palygorskite, then to be separated as a pure mineral as possible; therefore, the crude sample (whole sample) which represents palygorskite-rich sediment will be identified and pure palygorskite will be separated. Thereafter, the separated palygorskite will be subjected to many techniques in order to ensure that the separated mineral is palygorskite. Then the palygorskite will be subjected to many laboratory experiments to test its efficiency in adsorbing and absorbing heavy metals. The laboratory experiments are described in chapter four. The mineralogy is described below:

3-2-1 Mineralogy of raw samples

The raw samples mean whole or bulk samples. The minerals that associate palygorskite can also be called as impurities. These impurities include both clay minerals (montmorellonite (smectite), kaolinite) and non-clay minerals (quartz, calcite, dolomite, apatite, cristobalite and tridymite).

Cristobalite and tridymite are often present and called opal C-T. Clay minerals include kaolinite, montmorillonite and palygorskite; whereas the non-clay minerals include calcite, dolomite, quartz and opal-CT (cristobalite and tridymite) and rare amount of apatite.

Mineralogy was investigated using XRD, SEM, and FTIR. Twelve whole (bulk) samples (1D, 3DS, 4DS, 5DS, 6D, 8D, 9DN, 10DN, 11DN, 13A, 16AT and 17AT) are tested by using XRD technique. For the purpose of highlighting the clear picture of mineralogical composition and giving a good idea about each sample under study, they must view the illustrations that would indicate the mineral composition of the samples. Consequently, the results are illustrated in Figures 3-1 to 3-12.

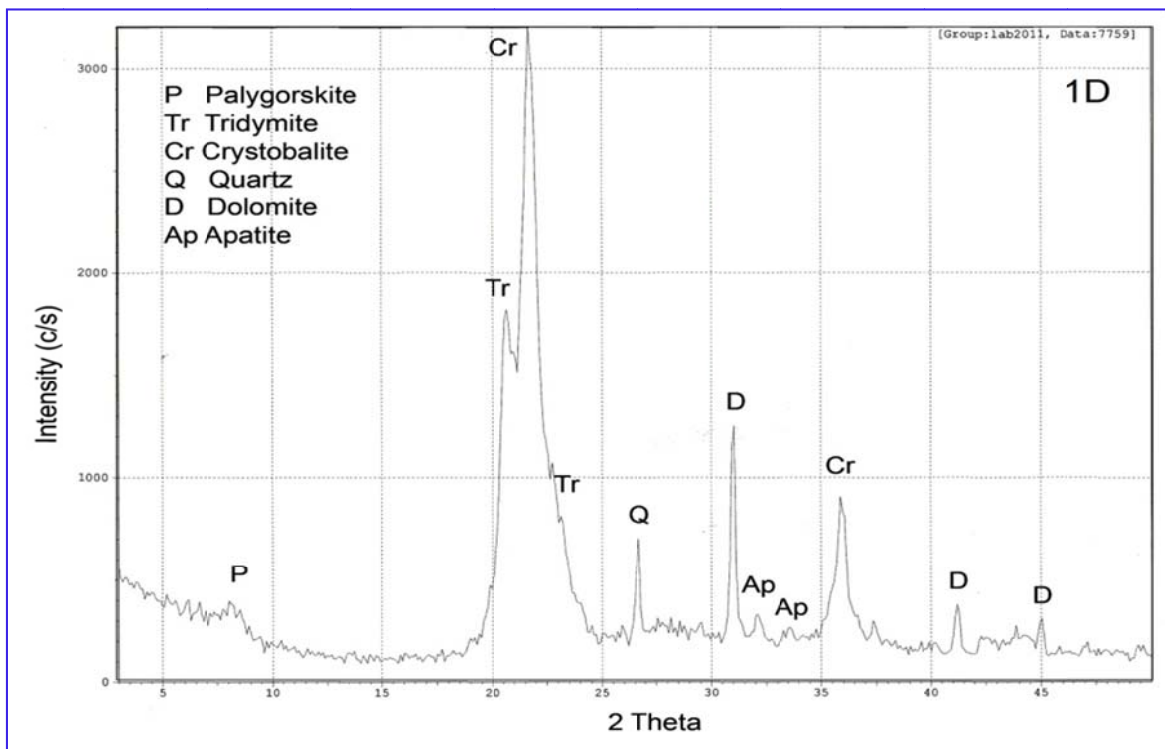


Figure 3-1: X- ray diffractogram illustrates mineral composition in sample no.1D.

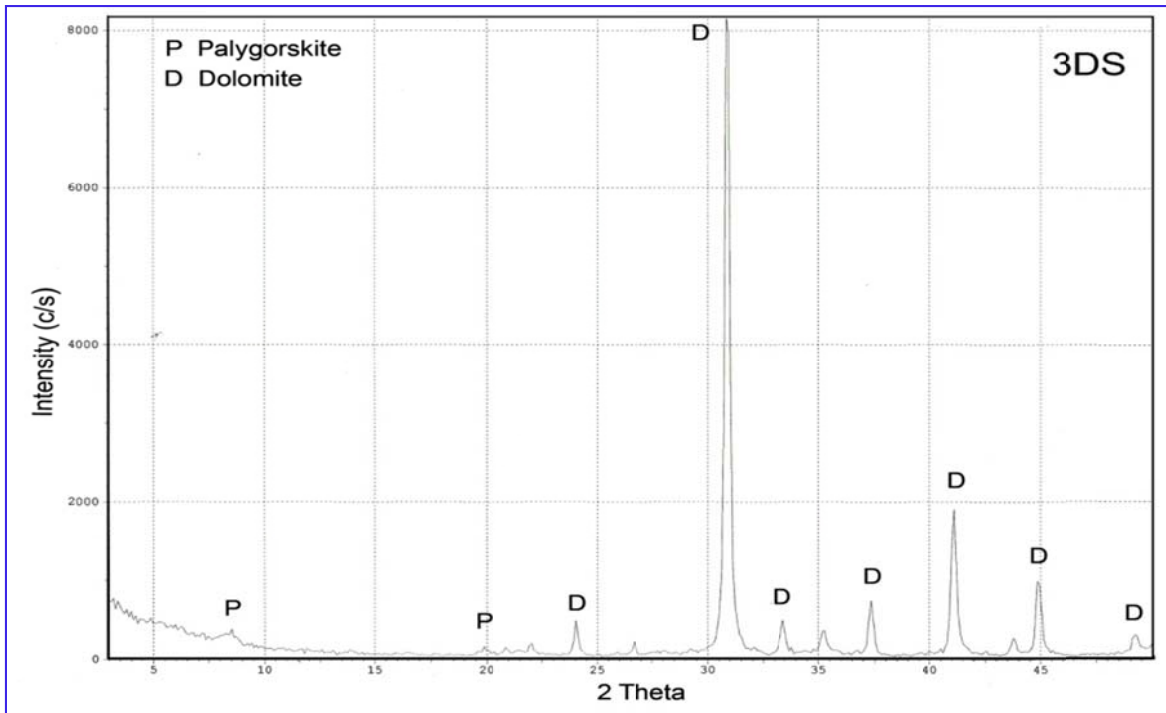


Figure 3-2: X- ray diffractogram illustrates the mineralogical composition in sample no.3DS.

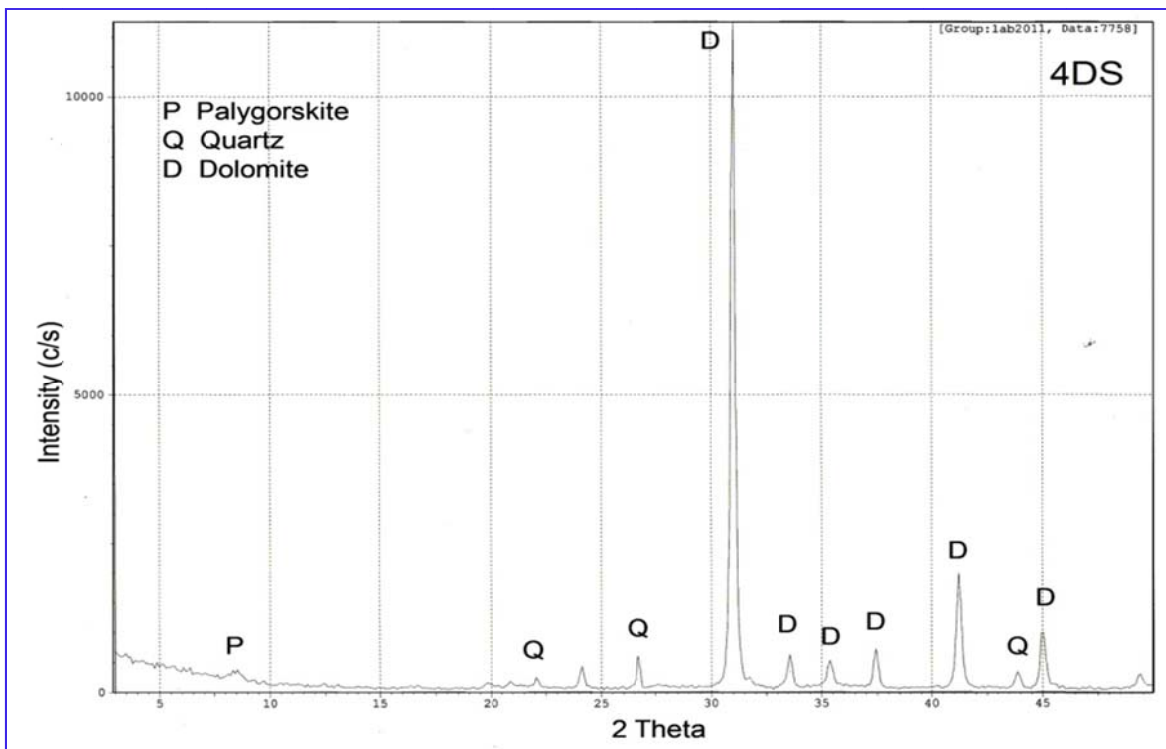


Figure 3-3: X- ray diffractogram illustrates the mineralogical composition in sample no.4DS.

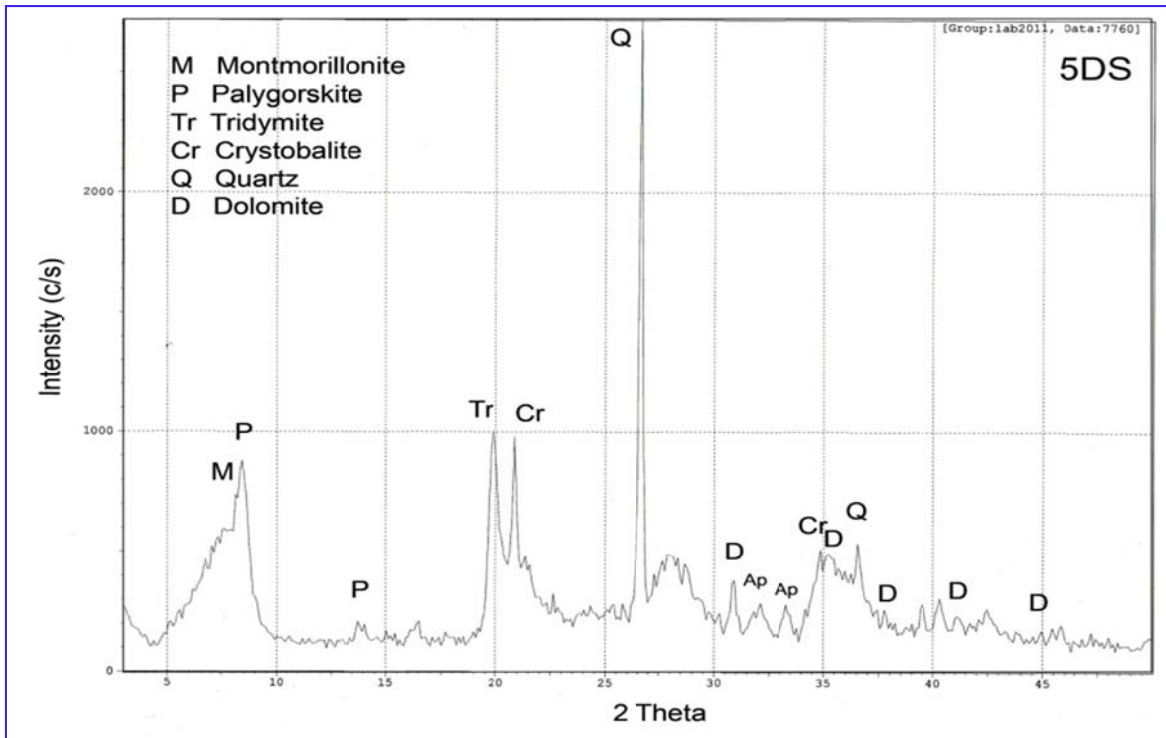


Figure 3-4: X- ray diffractogram illustrates the mineralogical composition in sample no.5DS.

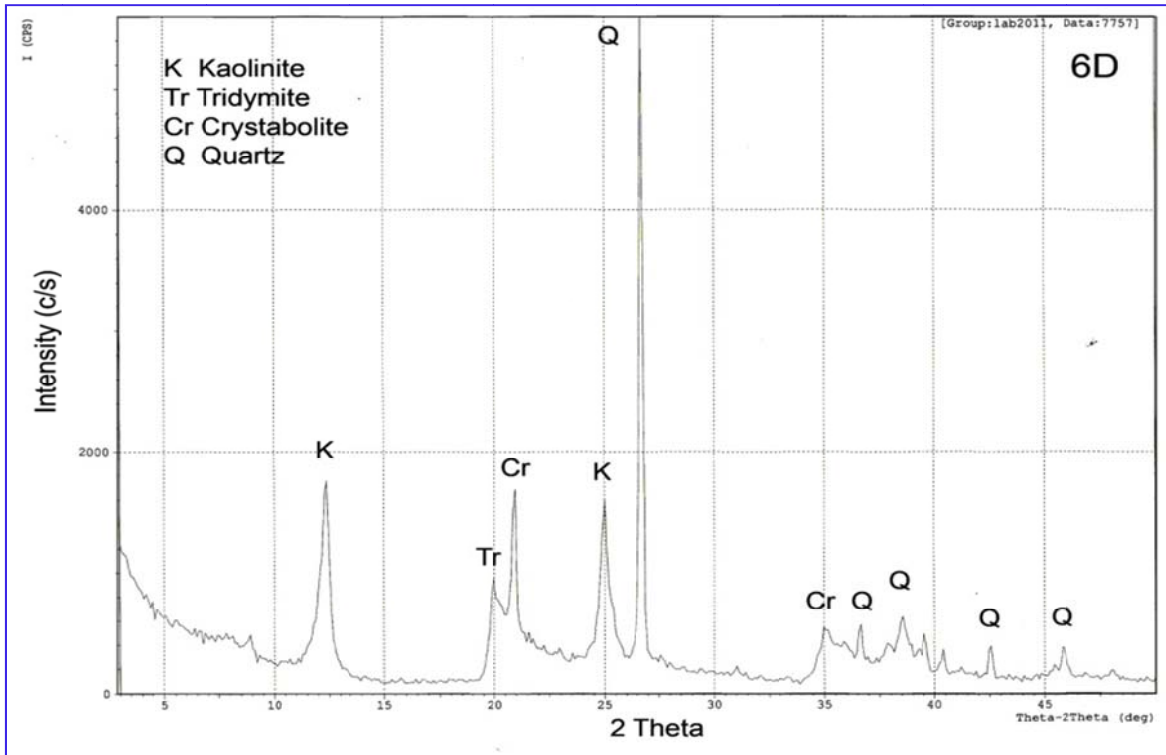


Figure 3-5: X- ray diffractogram illustrates the mineralogical composition in sample no.6D.

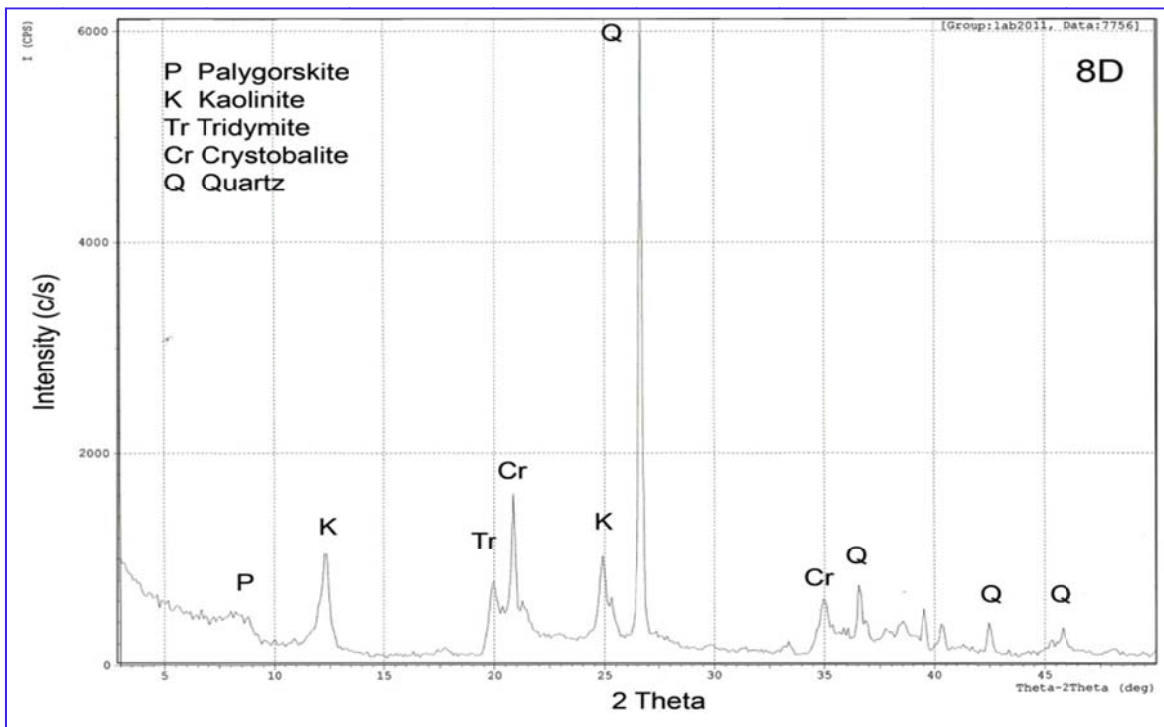


Figure 3-6: X- ray diffractogram illustrates the mineralogical composition in sample no.8D.

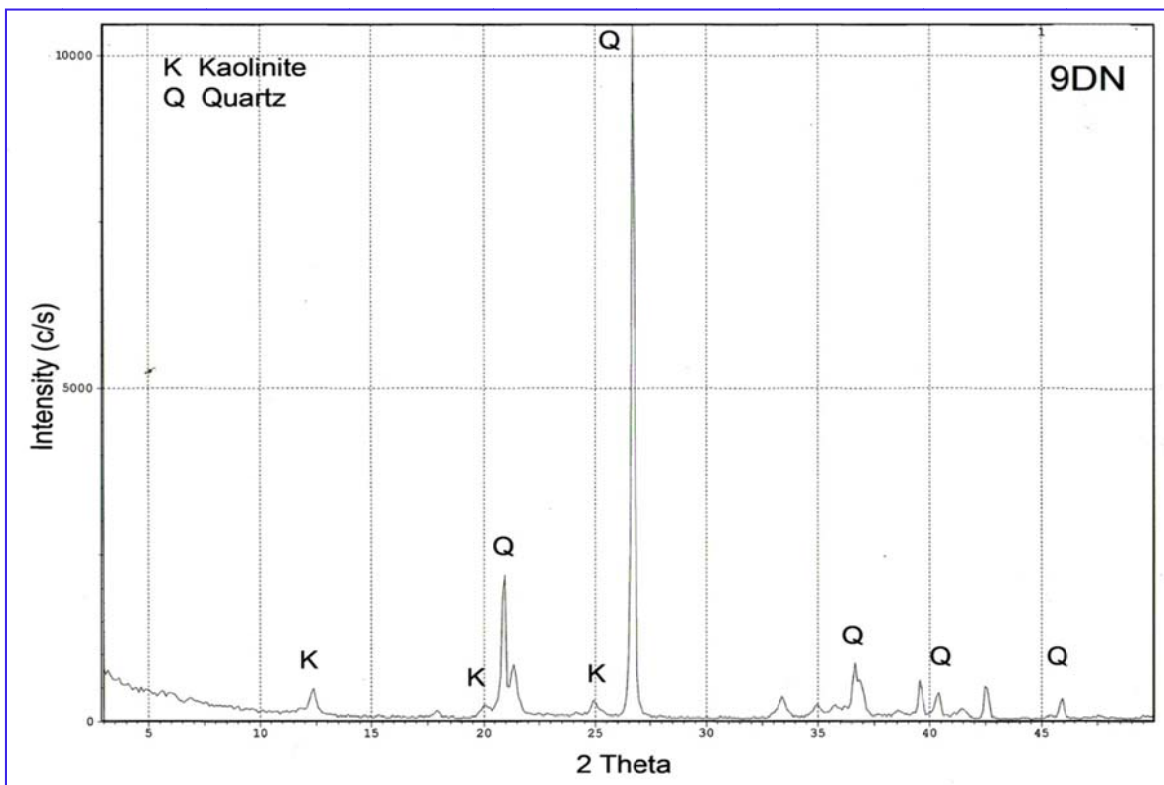


Figure 3-7: X- ray diffractogram illustrates the mineralogical composition in sample no.9DN.

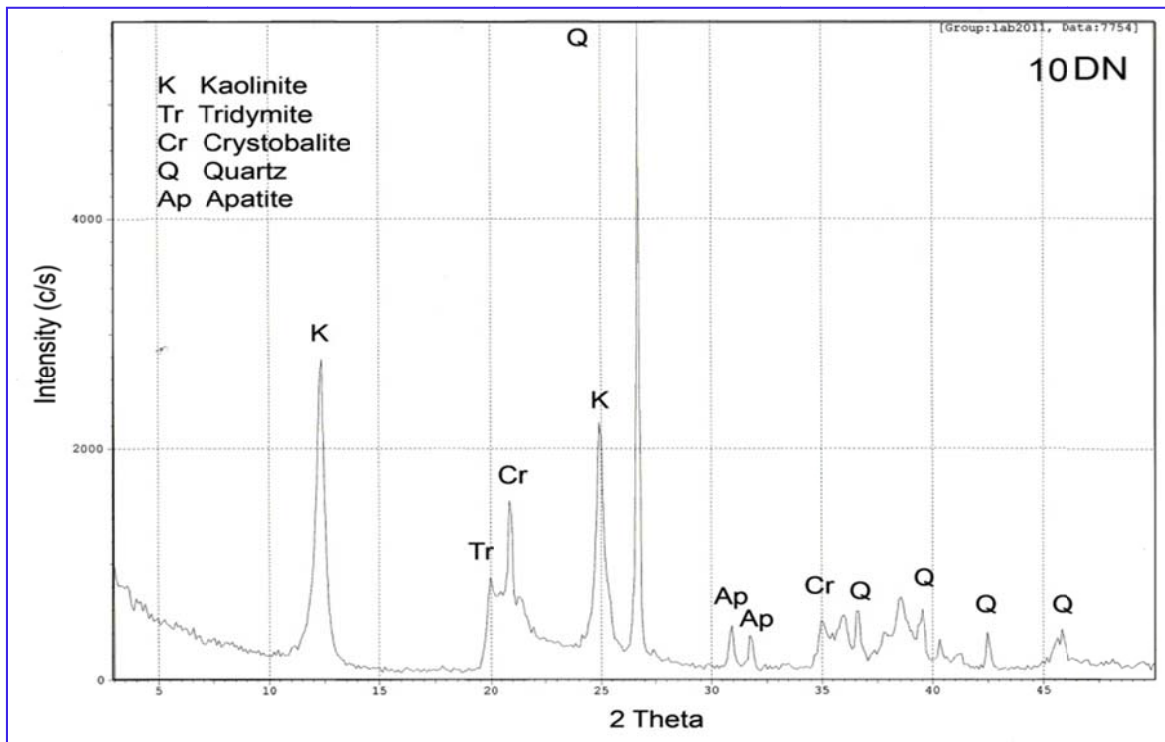


Figure 3-8: X- ray diffractogram illustrates the mineralogical composition in sample no.10DN.

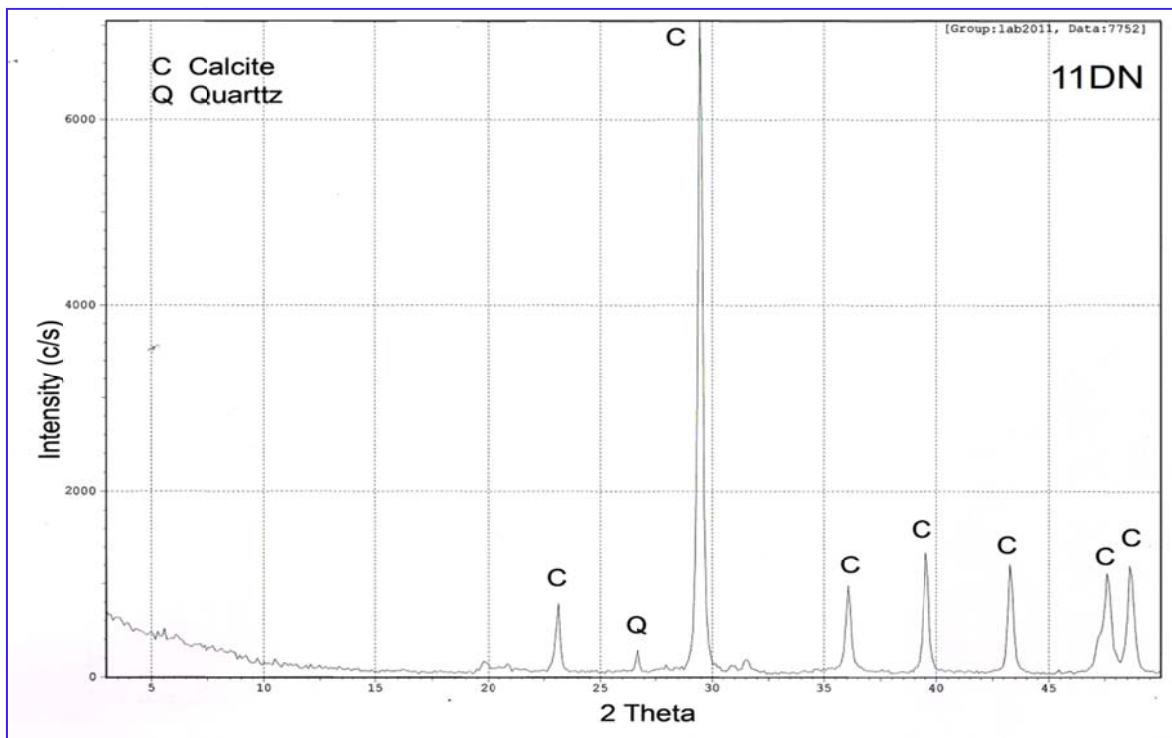


Figure 3-9: X- ray diffractogram illustrates the mineralogical composition in sample no.11DN.

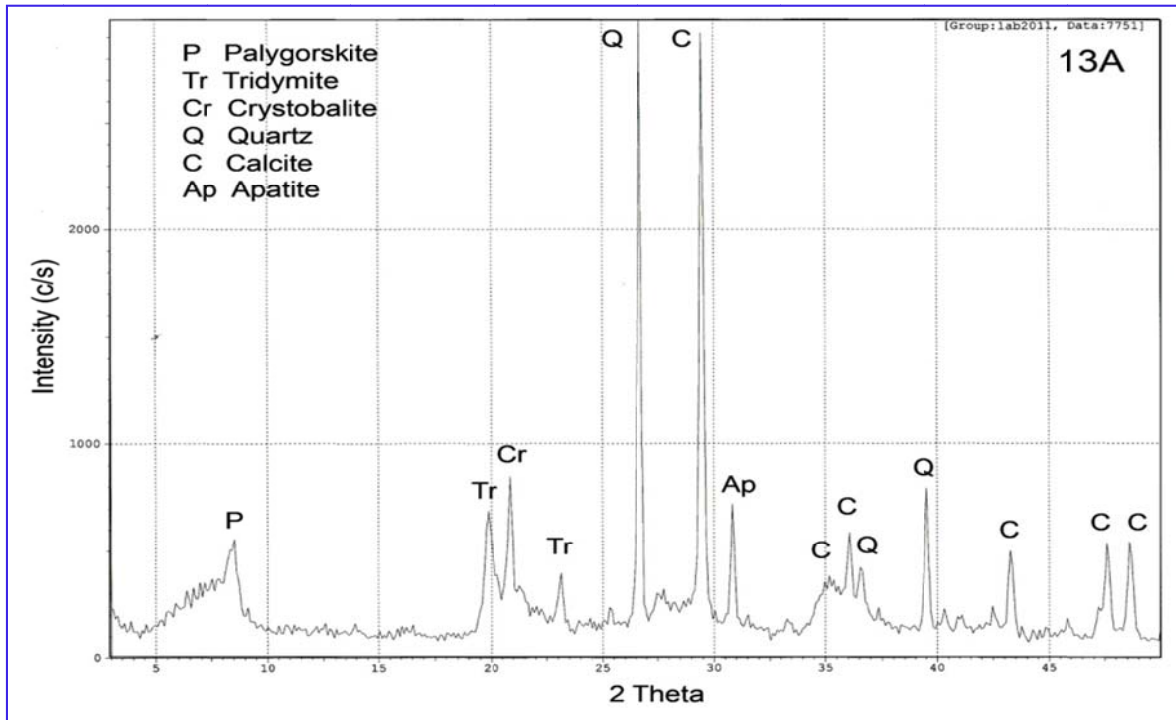


Figure 3-10: X- ray diffractogram illustrates the mineralogical composition in sample no.13A.

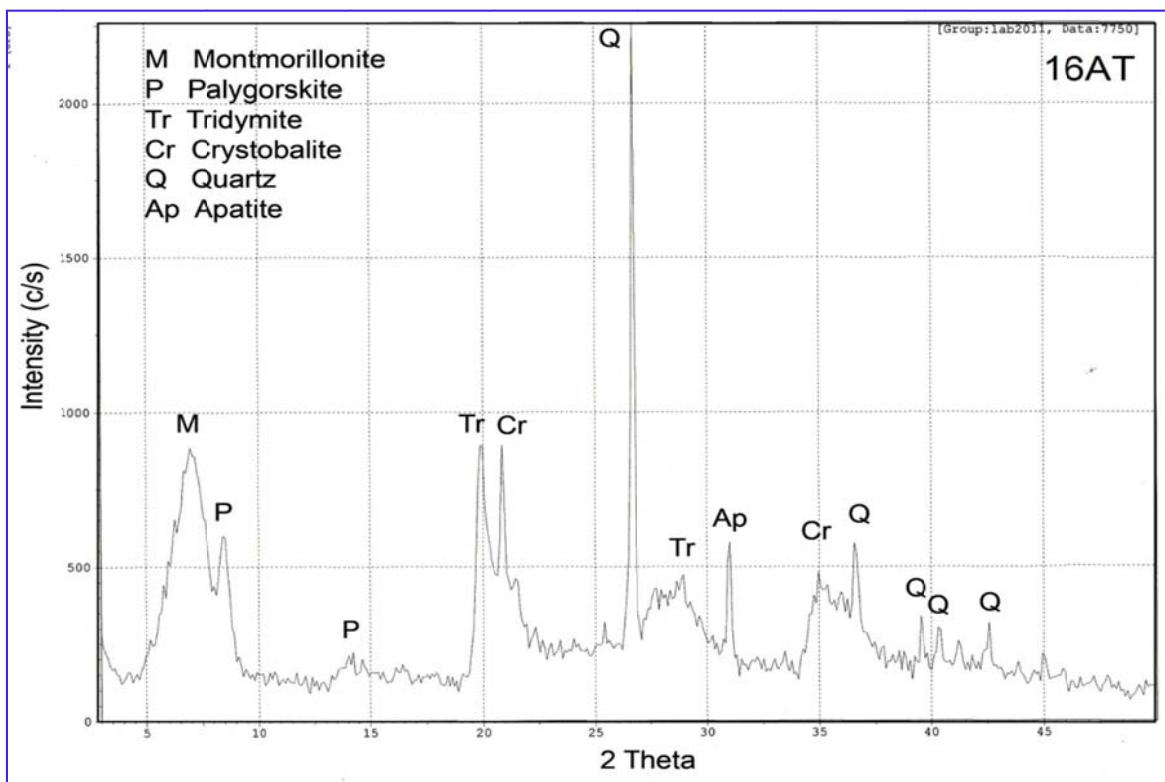


Figure 3-11: X- ray diffractogram illustrates the mineralogical composition in sample no.16AT.

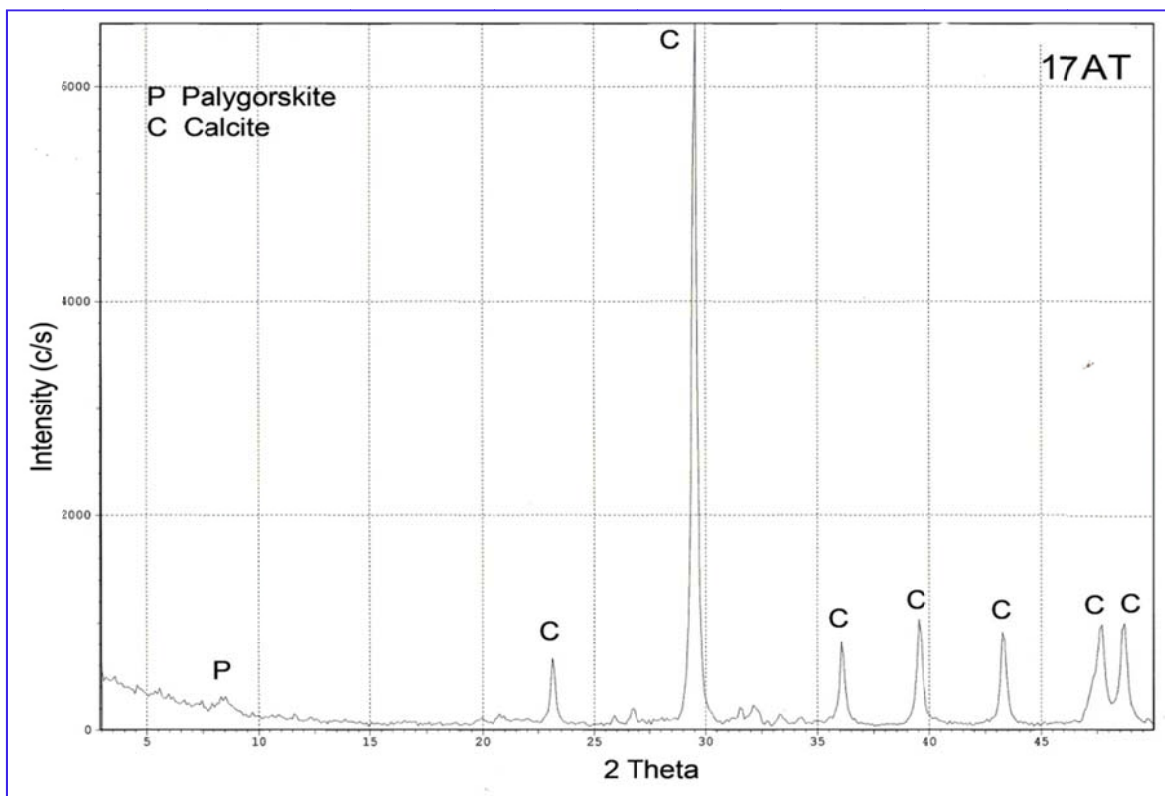


Figure 3-12: X- ray diffractogram illustrates the mineralogical composition in sample no. 17AT.

3-2-2 Clay minerals

The whole or bulk samples that are palygorskite-rich sediments are basically a mixture of clay and non-clay minerals. Clay minerals are dominant, where palygorskite appears to be the main constituent.

Clay minerals in the whole sample make up the most proportion. The remaining part is composed of non-clay minerals. Clay minerals include a variety of minerals such as montmorillonite, kaolinite and palygorskite which are described below:

3-2-2-1 Montmorillonite

Montmorillonite is composed of hydrous aluminum silicates in the form of extremely small particles. It belongs to phyllosilicate group of the clay minerals. It is a very soft mineral and has the chemical formula: $(\text{Na}, \text{Ca})_{0.3}(\text{Al}, \text{Mg})_2\text{Si}_4\text{O}_{10}(\text{OH})_2 \cdot n(\text{H}_2\text{O})$. It is considered as a member of the smectite family, with 2:1 clay, meaning that it has 2 tetrahedral sheets sandwiching a central octahedral sheet (Figure 3-13). It is an expandable mineral of microscopic grains.

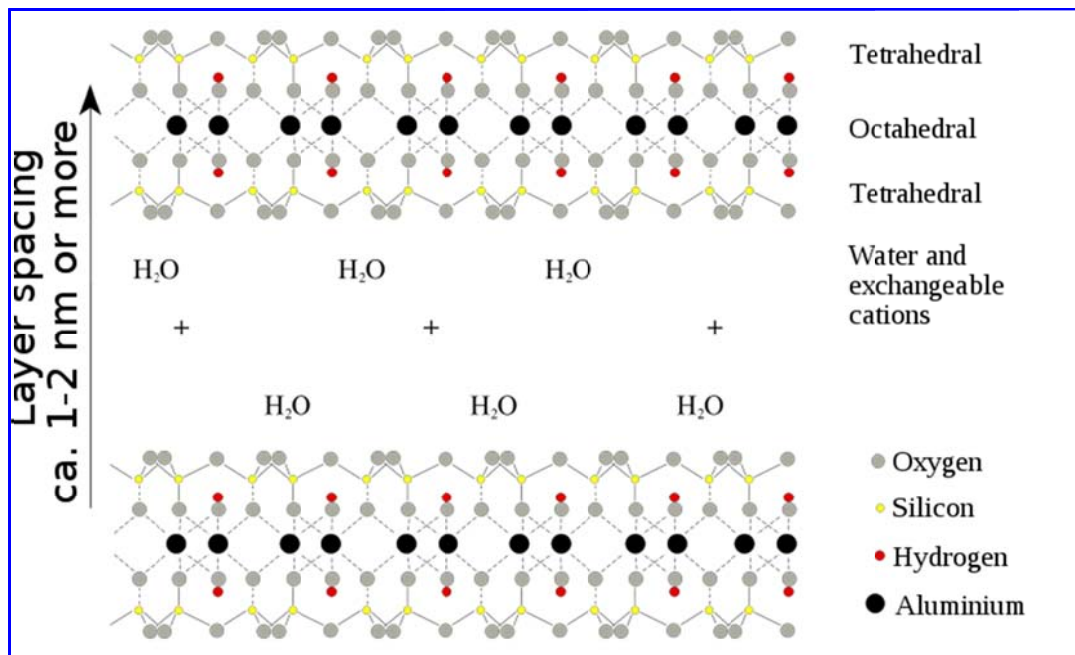


Figure 3-13: Montmorillonite structure (Meunier, 2005).

Montmorillonite in this study is the principal constituent of clay minerals following palygorskite. This mineral contributes a significant amount particularly at Traifawi site. Montmorillonite observed in the form of typical microscopic crystals (Figure 3-14). Some grains carry at the edges a minute fibers branching outward having lath-like morphology. These grains of montmorillonite indicate that the montmorillonite is diagenetically has been changed into palygorskite (Figure 3-15).

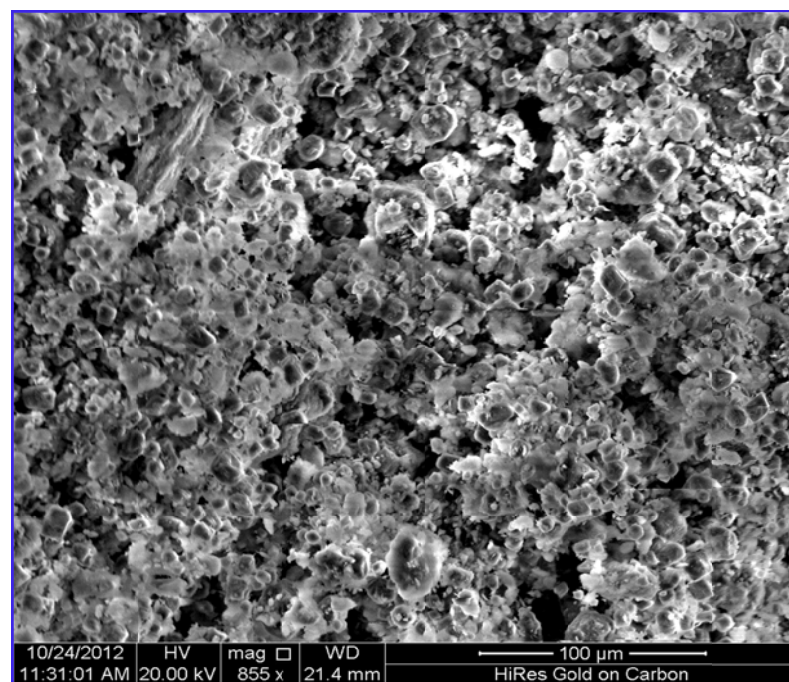


Figure 3-14: Scanning Electron Microscope image of montmorillonite. Sample No. 12D.

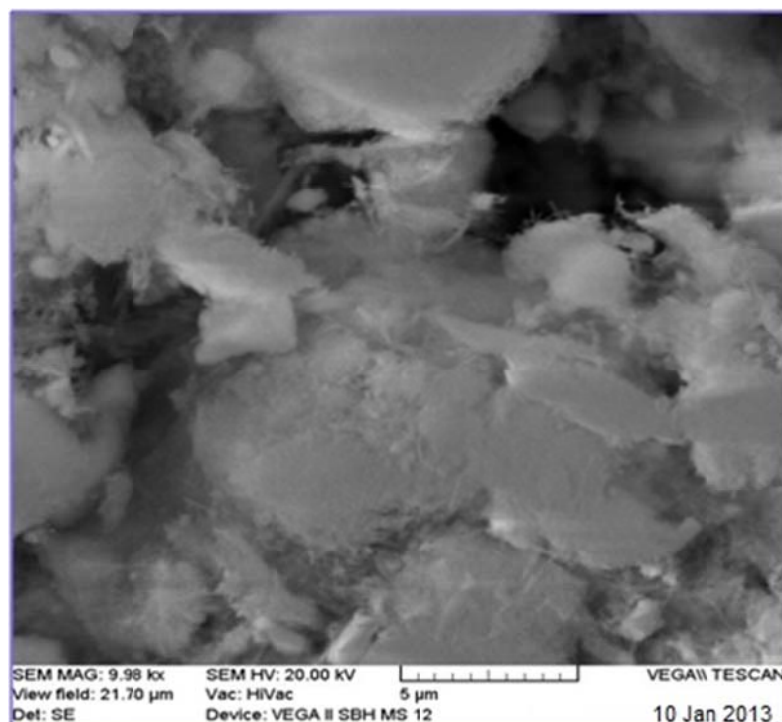


Figure 3-15: Scanning Electron Microscope image of smectite changing to palygorskite. Sample No. 12D.

3-2-2-2 Kaolinite

The ideal formula of kaolinite is $\text{Al}_2\text{Si}_2\text{O}_5(\text{OH})_4$. It consists of an octahedrally coordinated sheet of aluminium ions and tetrahedrally coordinated sheet of silicon ions. When these sheets stack, OH ions of one sheet, O ions of its neighbour sheet provide connection between tetrahedral silicate (SiO_4) and octahedral gibbsite layers ($\text{Al}_2(\text{OH})_6$). As a result the structure of kaolinite becomes tightly bound by H bonding. Therefore, most sorption activity occurs along the edges and surfaces of the structure. It is non-expandable and possesses a cation exchange capacity (CEC) of 3-15 meq /100 g. (Coles et al., 2002 and Hu et al., 2003). The mineralogical purity of samples was tested using XRD. The results showed that the kaolinite in addition to quartz existed as an impurity with palygorskite.

Scanning Electron Microscope image shows that the kaolinite has varying sizes of grains arranged in pattern of face to face (Figure 3-16). Another pattern is that some individual grains well develop to be crystallized with pseudo-hexagonal edge also observed (Figure 3-16).

Kaolins spectra of FTIR can readily be distinguished from other clays by differences in position and relative intensities of their OH stretching bands. The OH stretchings occurring around the $3700\text{-}3620\text{ cm}^{-1}$ doublet are characteristic for kaolin clays (Wilson, 1994). The feature near 3700 cm^{-1} lies well separated from those of most other mineral bands.

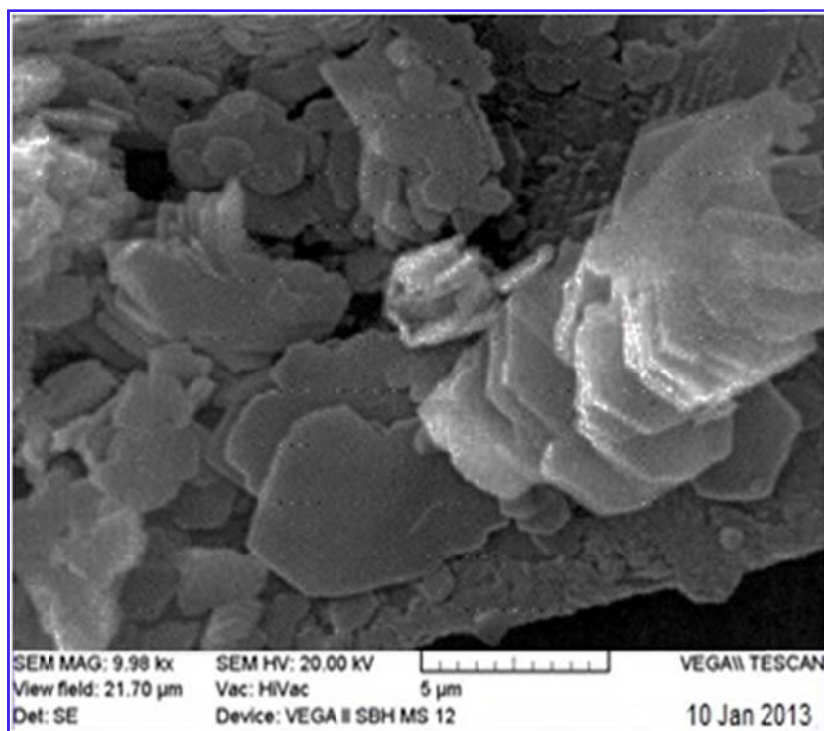


Figure 3-16: Scanning Electron Microscope image of pseudo-hexagonal shape of face to face pattern, Sample No 8D.

The OH deformation bands near $938\text{-}916\text{ cm}^{-1}$ are also typical for the kaolin group minerals and arise from vibrations of the inner and inner surface OH groups within the clay matrix. Other features appearing in the spectrum belong to a variety of Al-OH and Si-O stretching and bending vibrations (Wilson, 1994). A detailed assignment of all the bands rising in the kaolinite spectrum is given in Table 3.1. The FTIR spectrum of natural kaolinite is given in Figure 3-17.

Sample no. 6D is analysed by FTIR technique. It is claystone and consists mainly of kaolinite with little amount of porcellanite (opal- CT) and quartz. The OH group, Al-O, Si-O, Si-O-Al is stretching vibration and bending vibration identifying kaolinite are found. Figure 3-18 illustrates the FTIR spectra for kaolinite-rich sediments, where good agreements in band position are found between the natural kaolinite and kaolinite from this study.

Table 3-1: Assignments of the bands appearing in the FTIR spectrum of natural kaolinite.

Band Position (cm ⁻¹)	Vibration Assignment
3700	Inner surface -OH stretching vibration
3620	Inner -OH stretching vibration
1112, 1038, 1010	Si-O bending vibration
938, 918	Al-OH bending vibration
792, 754	Si-O-Al compound vibrations
692	Si-O stretching vibration
540	Si-O-Al compound vibrations
471, 433	Si-O vibrations

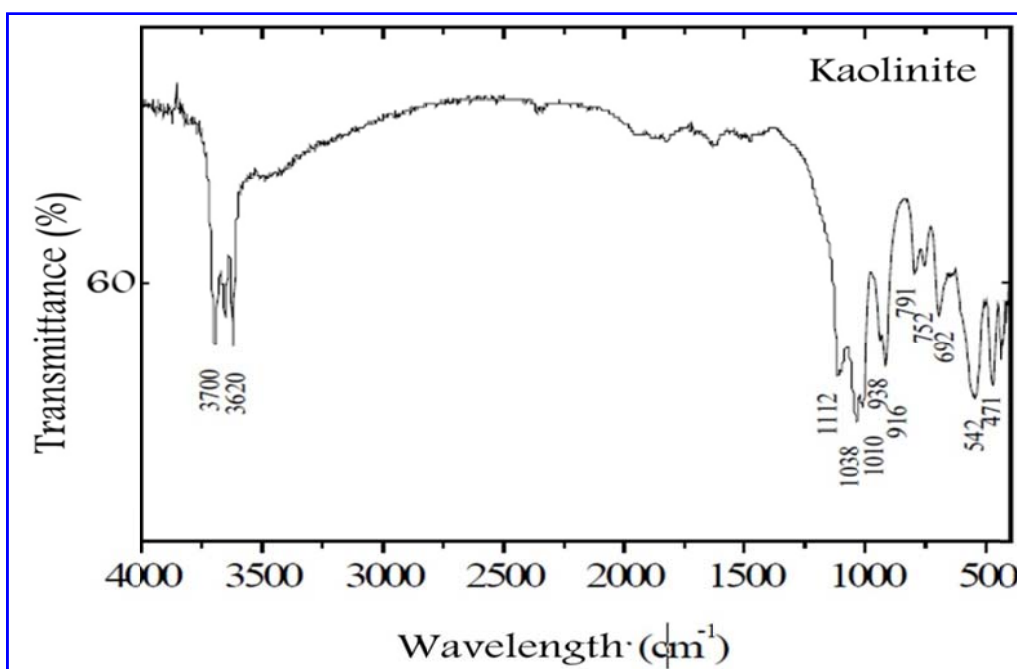


Figure 3-17: FTIR spectra of natural kaolinite.

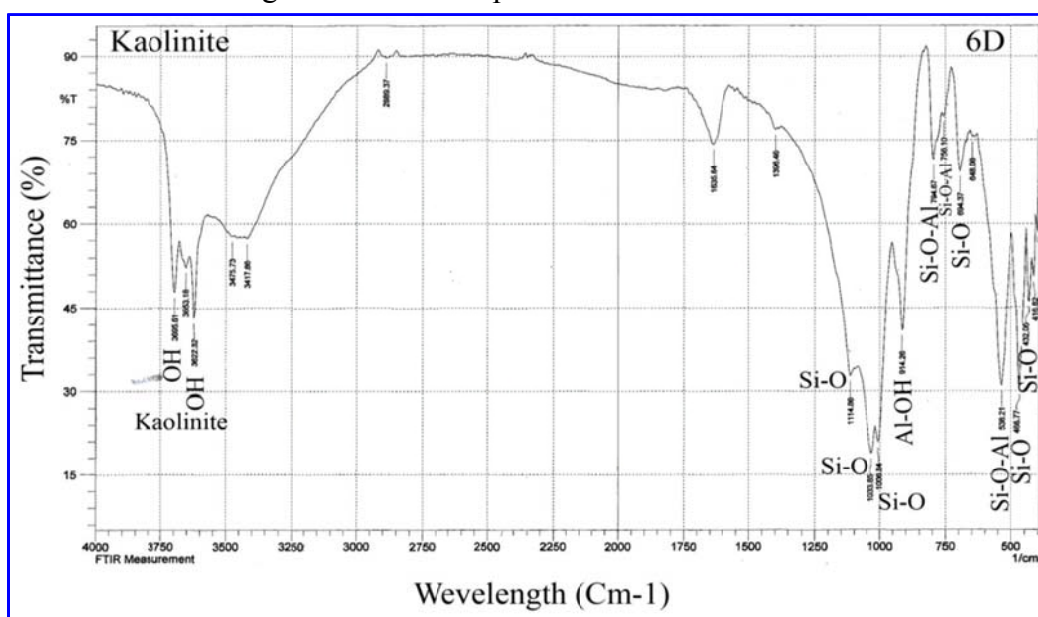


Figure 3-18: FTIR spectra of kaolinite-rich sediments, sample No.6D.

3-2-2-3 Palygorskite

Palygorskite has an elongated morphology and is similar in structure to the minerals of the amphibole group; it has one orthorhombic and three different monoclinic unit cell geometries. The structure of palygorskite contains open channels; the schematic structure is illustrated in Figure 3-19.

The morphology of the palygorskite was investigated by SEM techniques and appears to have a 1-D fibrous structure with a uniform diameter and randomly oriented. The fibrous habit is thin and of threadlike shape accumulating together forming micro tabular fan shape. The particles have a length of 1 to 2 μm with a width of less than 0.1 μm approximately (Figure 3-20). Palygorskite has a three-dimensional network of densely packed rods with a diameter less than 100 nm and a length ranging from hundreds of nanometers to several micrometers for each single rod (Hongxia, Dajun, 2007).

A micro-grain of palygorskite grows from diagenetic montmorillonite grains. Palygorskite appears to be originating from montmorillonite (smectite) with length varying from 0.5 μ to 2.5 μ approximately (Figures 3-20 and 3-21).

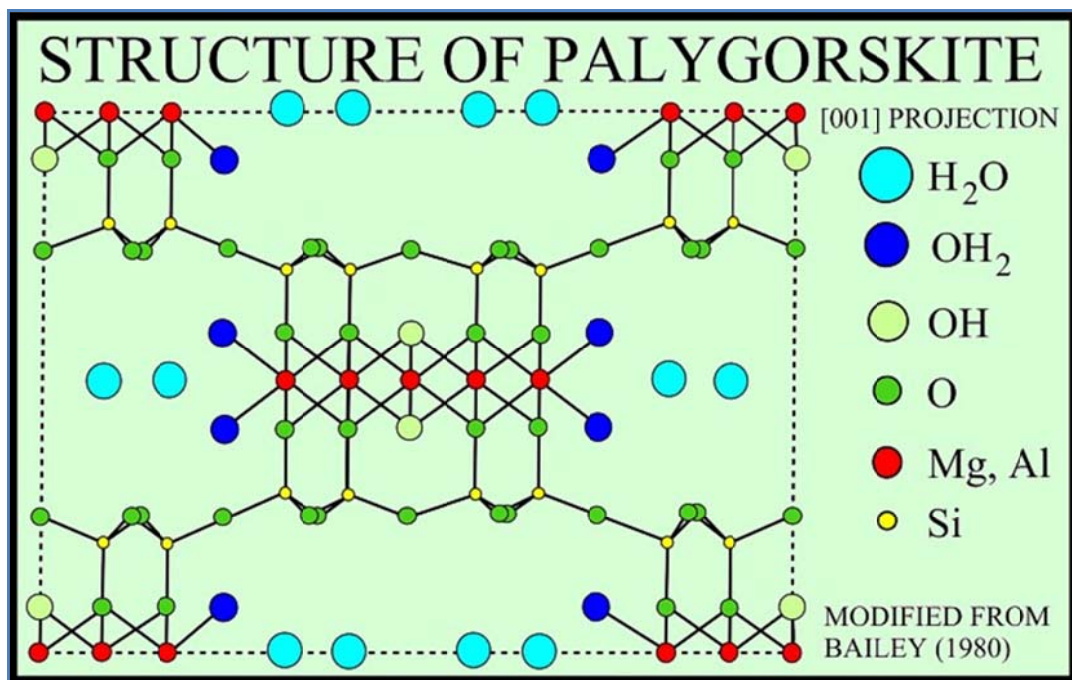


Figure 3-19: Schematic structure of palygorskite (after Bailey, 1980).

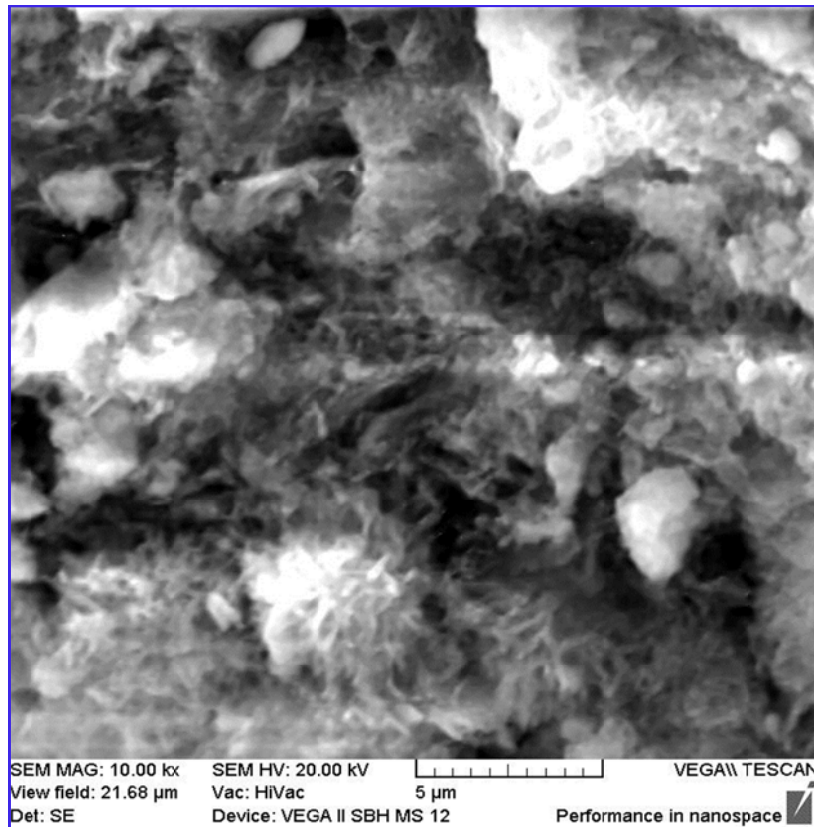


Figure 3-20: Scanning Electron Microscope image of palygorskite derived from smectite, sample No 12D.

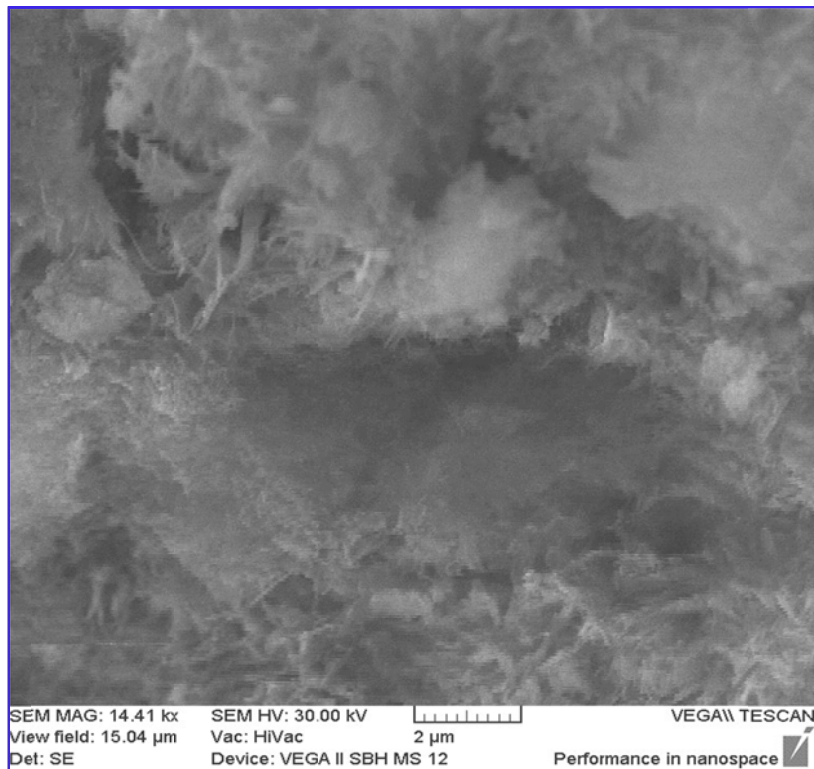


Figure 3-21: Scanning Electron Microscope image of palygorskite, sample No 12D.

Some samples are tested by XRD to detect palygorskite. The d-spacing data for identifying palygorskite are listed in Table 3-2.

palygorskite-rich clay (samples no 7D and 8D) are subjected to XRD test. Three parts are taken from this sample in order to prepare XRD slides as untreated, glycolated (treated with glycol ethylene) and heated to 550°C. Following glycolation, there was no swelling in palygorskite and kaolinite, but kaolinite collapsed at 550°C, whereas palygorskite remains unchanged. Figures 3-22, 3-23, 3-24, 3-25 explain this case.

XRD patterns show that the untreated palygorskite appeared at 2-theta 8.5° and d-spacing (10.4°A). Upon glycolation, the peak intensity of palygorskite peak tends to decrease and shift to 8.3° (10.7°A) (Figure 3-22 to 3-25). This agrees with Jeffers and Reynolds (1987). The observed shifting peak of glycolated palygorskite causes expansion in one straight forward direction along a-axis (Jeffers and Reynolds, 1987). Heating at 550°C replaced palygorskite peak to 2 theta which is slightly greater than 2 theta of untreated sample. The micropores parallel to the long axis of palygorskite (x-axis) are the only sites in the structure that can accommodate ethylene glycol molecules.

The fibrous nature of palygorskite precludes the production of oriented aggregate mounts to enhance the 001 reflection for X-ray powder diffraction (Wilson, 1994). However, strong reflections from the 011 planes yield intense peak at 10.4 or 10.5 angstroms. This peak is unaffected by treating with ethylene glycol, but changes during heat treatments.

Table 3-2: XRD data of palygorskite under condition of Cu K α λ 1.54056°A.

d (°A)	h	k	l
10.4	100	1	0
6.36	20	2	0
5.38	16	1	3
4.46	20	0	4
4.36	4	-1	2

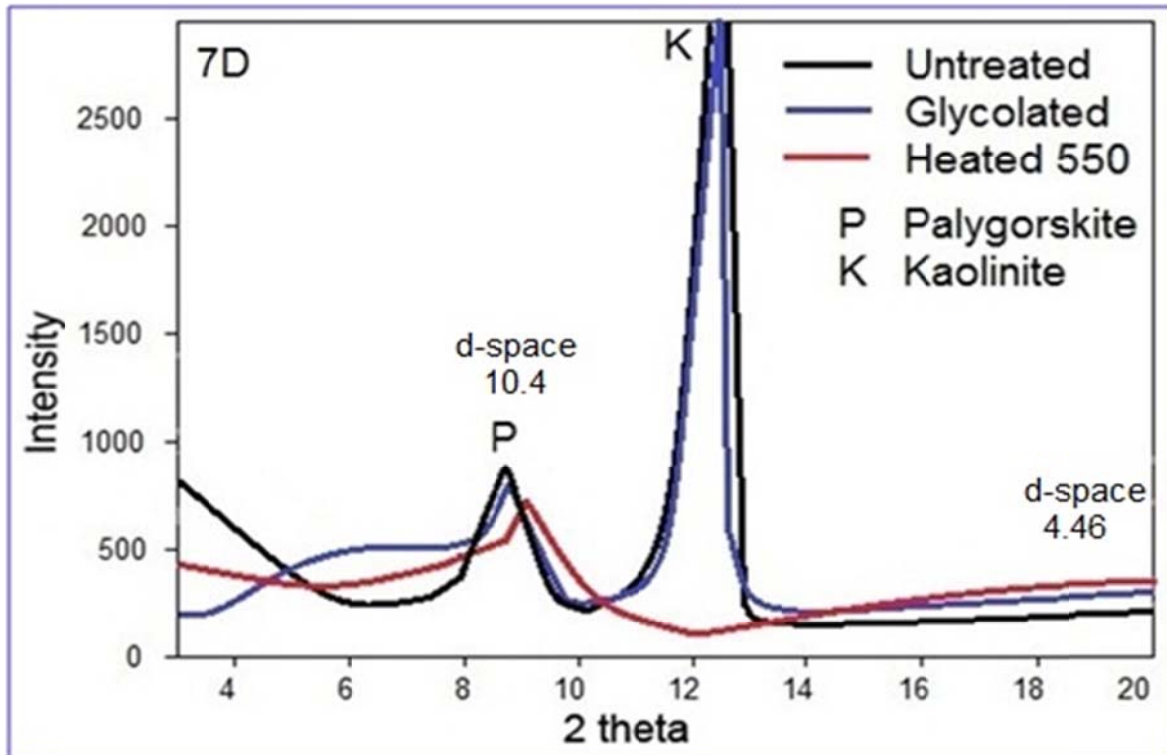


Figure 3-22: X-ray diffractogram of sample no.7D.

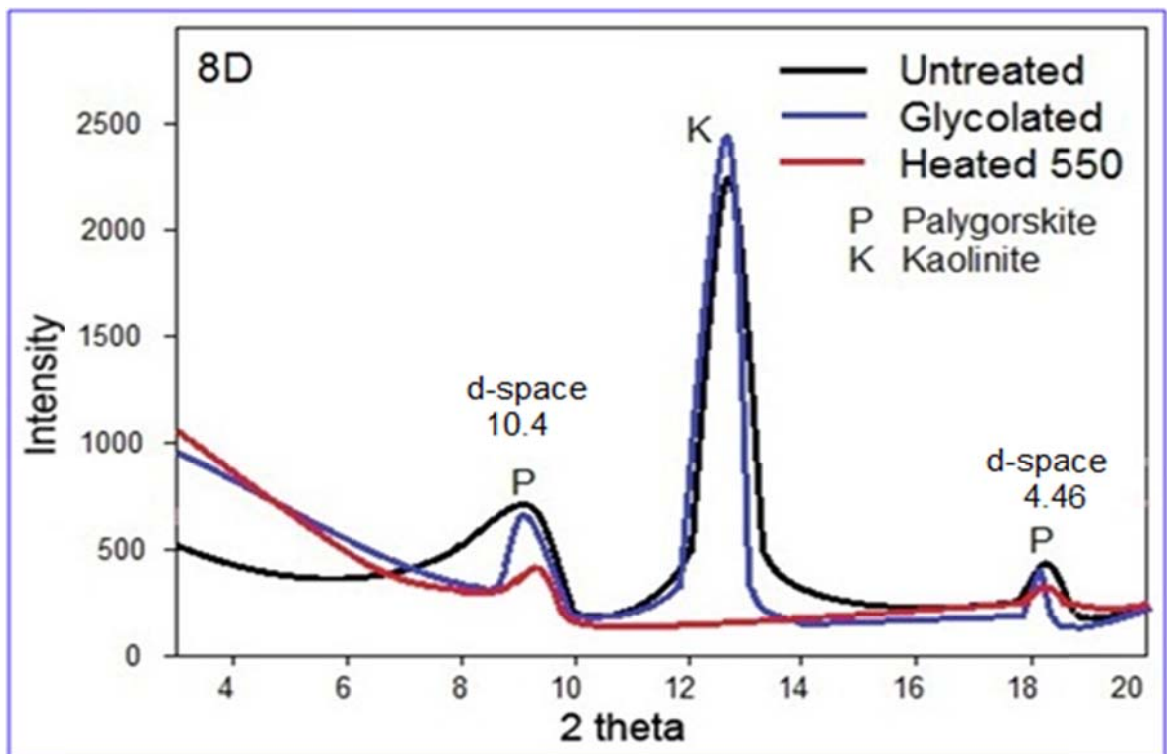


Figure 3-23: X-ray diffractogram of sample no.8D.

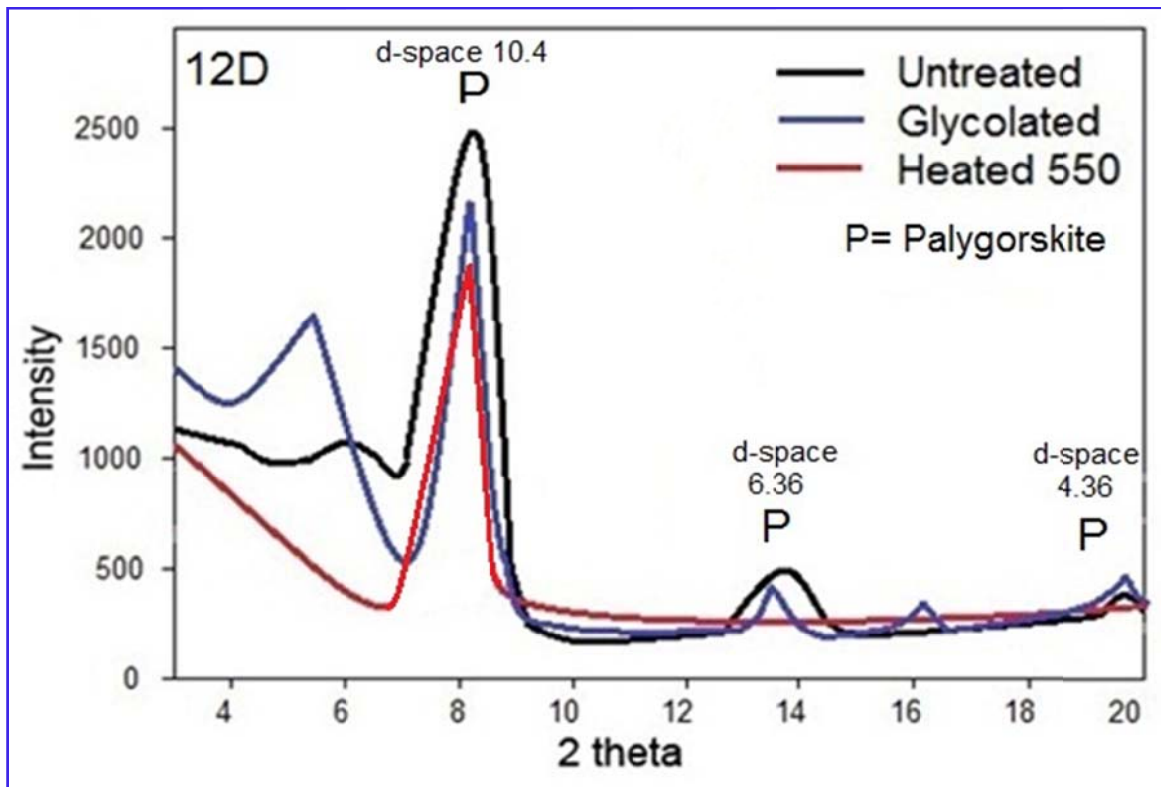


Figure 3-24: X-ray diffractogram of sample no.12D.

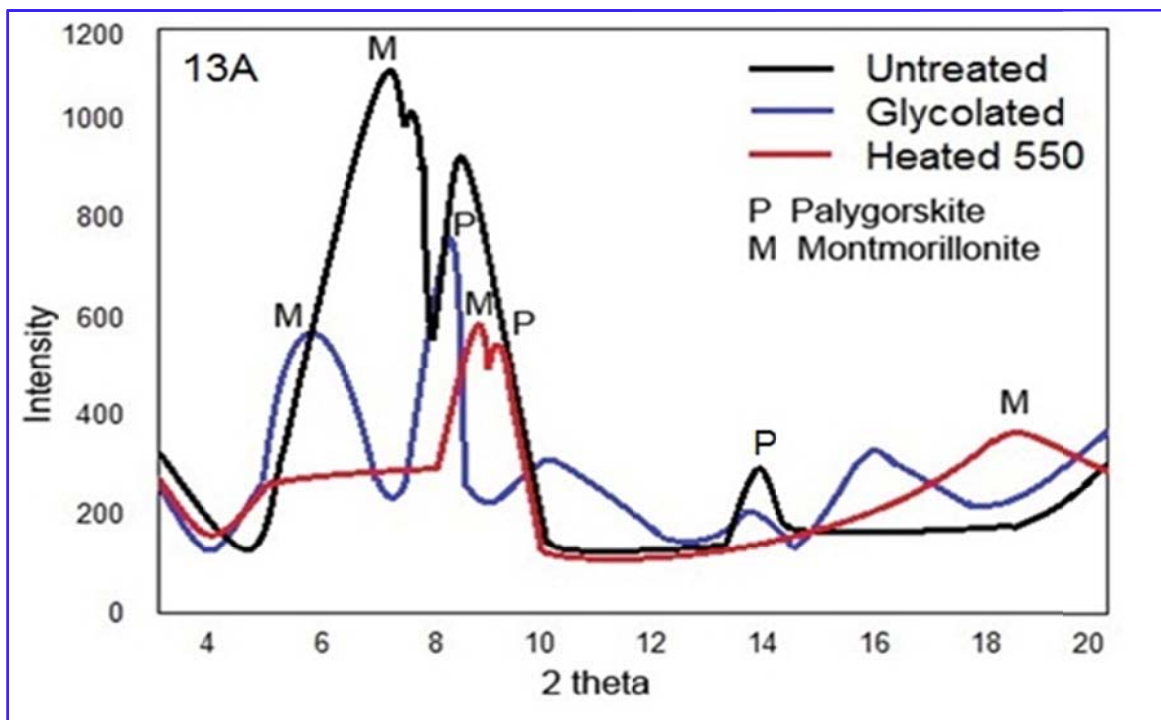


Figure 3-25: X-ray diffractogram of sample no.13A.

The structure of palygorskite is tested at 200°C, 400°C, 600°C, and 800°C; at 200°C and 400°C, its structure tends to be stable (Figure 3-26). When heated to 600°C, some peaks disappear indicating water release. At 800°C the palygorskite structure completely collapses (Figure 3-26). From the knowledge of the background, the peak at a lower temperature of 149°C, palygorskite did not release its coordinated water stepwise. The complete dehydroxylation occurred below 500°C. Above 500 ° C, there is no water left. The decomposition of palygorskite according to Jones and Galan (1988), palygorskite is amorphous above 700 °C.

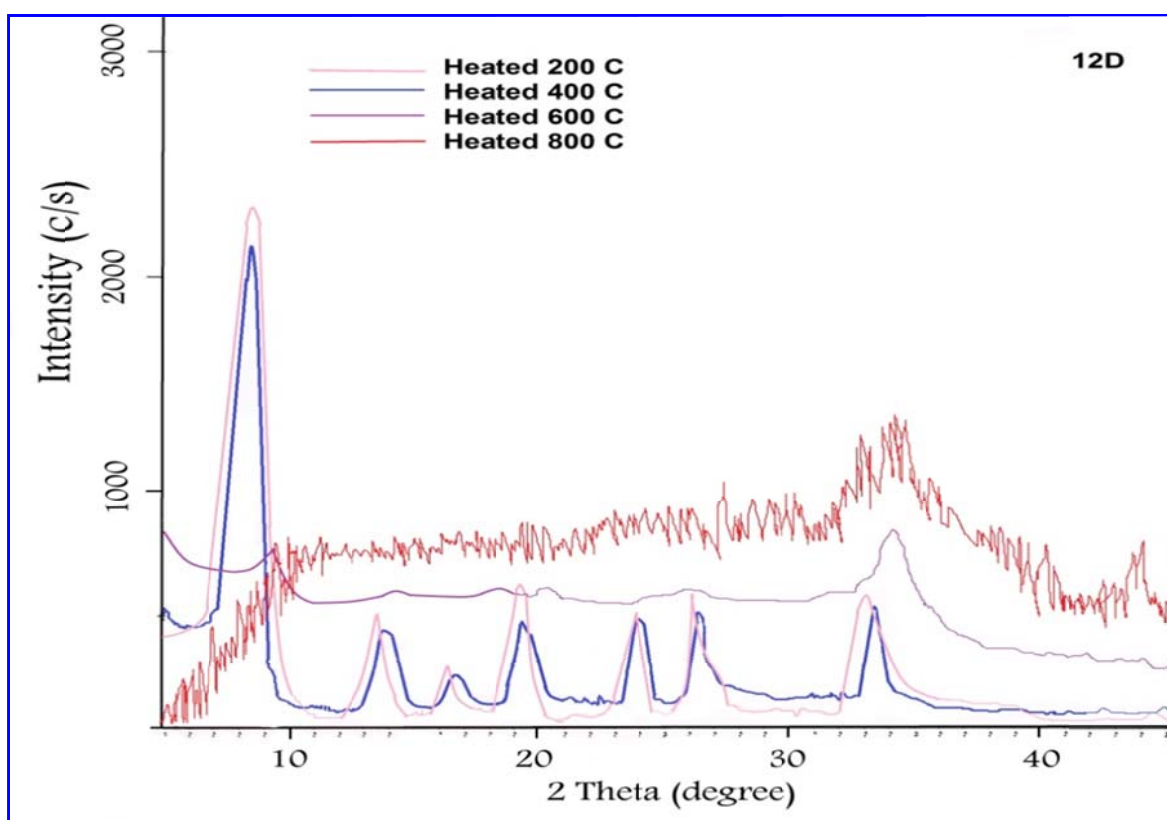


Figure 3-26: X-ray diffractogram of separated palygorskite from sample no. 12D which was heated to different temperatures.

Fourier transform infrared spectroscopy provides a potentially rapid method of relatively non-destructive analysis which can be used to establish a database on the crystallinity and trace mineral components of rocks (Parthasarathy et al., 2001 and 2003). Infrared Spectroscopy is an easy way to identify the presence of certain functional groups in a molecule.

Palygorskite was also investigated by using the FTIR technique. Palygorskites studied have different chemical composition. There is one

sample that corresponds to Mg-rich palygorskites obtained by separation palygorskite from palygorskite-rich sediments. On the other hand, many of the whole samples that consist of palygorskite in little quantity are subjected to FTIR tests. The position of the bands identified in the FTIR spectra of the palygorskites studied is similar for all samples, but there are some significant differences in their intensity, which are significant. Regarding to the structure of palygorskite, there are several bonds that can give absorption effects in the IR region. The most intense absorptions are related to water and hydroxyl stretching bending vibrations. This mineral has three types of water in its structure (Suárez and Garcia-Romero, 2006). The spectra can be divided into two regions for simplicity, OH-stretching vibration region and the water bending vibration. OH-stretching vibration region in the higher wave number region of the samples studied, the following can be observed (Figure 3-27):

- (1) A sharp peak at 3614 cm^{-1}
- (2) A peak or shoulder at 3541 cm^{-1} , which appears only in some samples.
- (3) Peaks at 3400 cm^{-1}

The first effect, at 3614 to 3616 cm^{-1} , is described in all bibliographic references on FTIR of palygorskite (McKeown et al., 2002; Chahi et al., 2002) and it seems to be characteristic of this mineral. There is good agreement in the literature recording the position at water molecules (coordinated and zeolitic water), but according to Ausburger et al. (1998) the band at 3543 cm^{-1} is excessively strong and sharp to be assigned only to coordinate water. Absorbance peak at 3543 cm^{-1} can be attributed to the anti-symmetric stretching modes of molecular water coordinated with the magnesium at the edges of the channel (Frost et al., 2001). The peak at 1654 cm^{-1} is associated with the hydroxyl zeolitic water, and the peak at 984 cm^{-1} with the bending vibration of OH group. The peak at 800 cm^{-1} indicates the presence of Si-O-Al and O-Al bonds (Augusburger et al., 1998). The typical FTIR of palygorskite published by Xu et al. (2009) is illustrated in Figure 3-28. Palygorskite content varies from one sample to another, as the accompanying minerals (impurities) vary in type (montmorillonite, kaolinite, dolomite, calcite, cristabollite, tridymite, quartz and apatite). All these mineral types are associated with palygorskite in different amounts and influence on the IR transmittance. For this reason, the pattern of FTIR changes depending on these variables. Palygorskite associated with porcellanite (opal-CT), quartz and calcite illustrate a different pattern (Figure 3-29), where Ca-O and C-O refer to calcite and Si-O refers to quartz,

tridymite and cristabolite, while Si-O-Si indicates a tetrahedral layer which refers with OH to palygorskite.

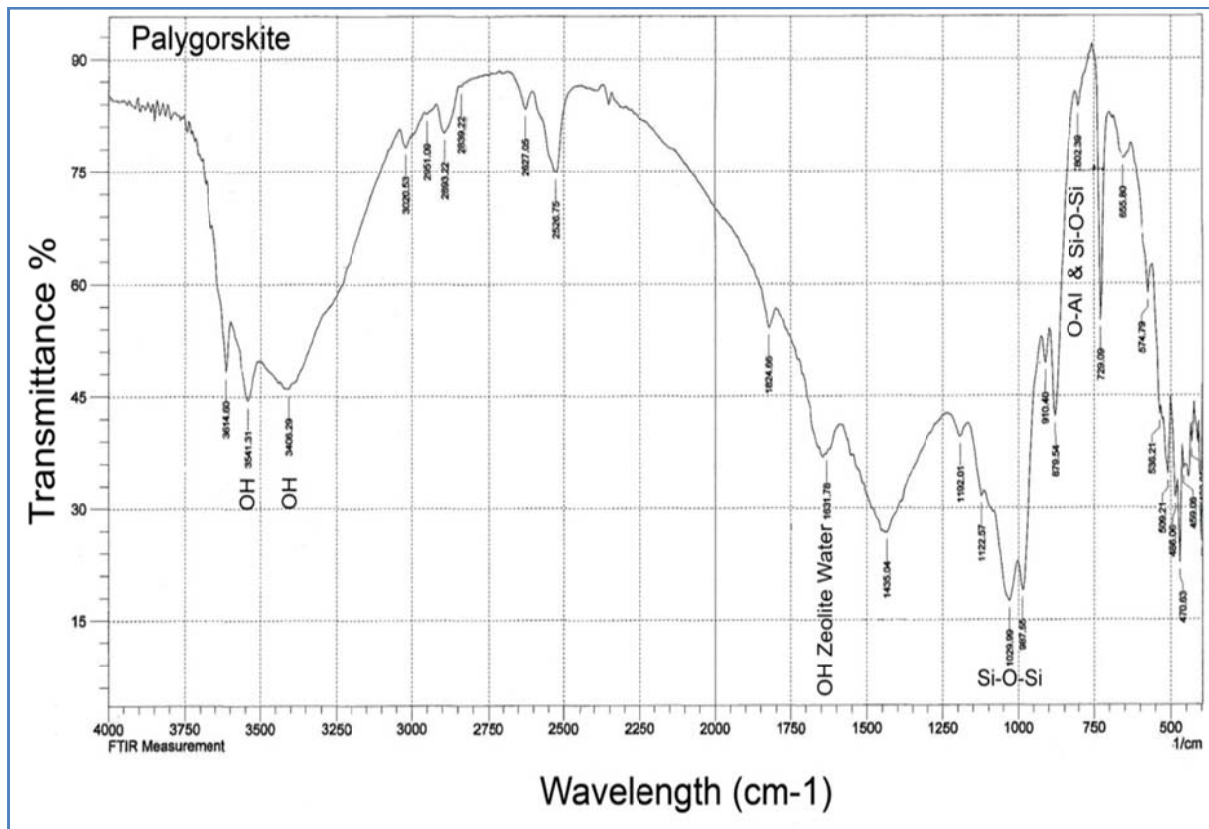


Figure 3-27: FTIR spectra of pure palygorskite separated from sample no.12D.

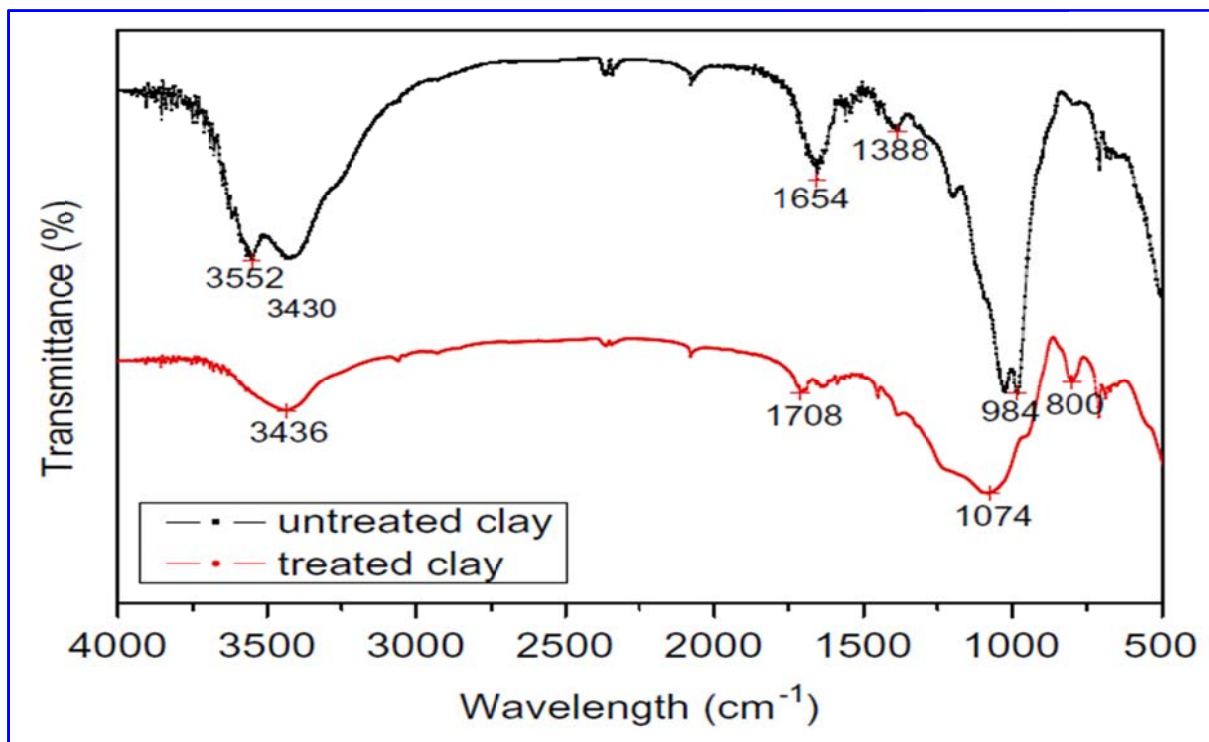


Figure 3-28: FTIR spectra of typical pure palygorskite, (after Xu et al., 2009).

The FTIR pattern in Figure 3-30 illustrate a similar one of Figure 3-29 but different in intensity or transmittance (%) of IR. This difference was attributed to the content (%) of each mineral type in this sample. The influence of calcite and polymorph silica such as quartz, tridymite and cristobalite on FTIR pattern is clear where all these minerals associate palygorskite (Figure 3-31). Some samples studied are similar in position but not in intensity due to the mineral content (%).

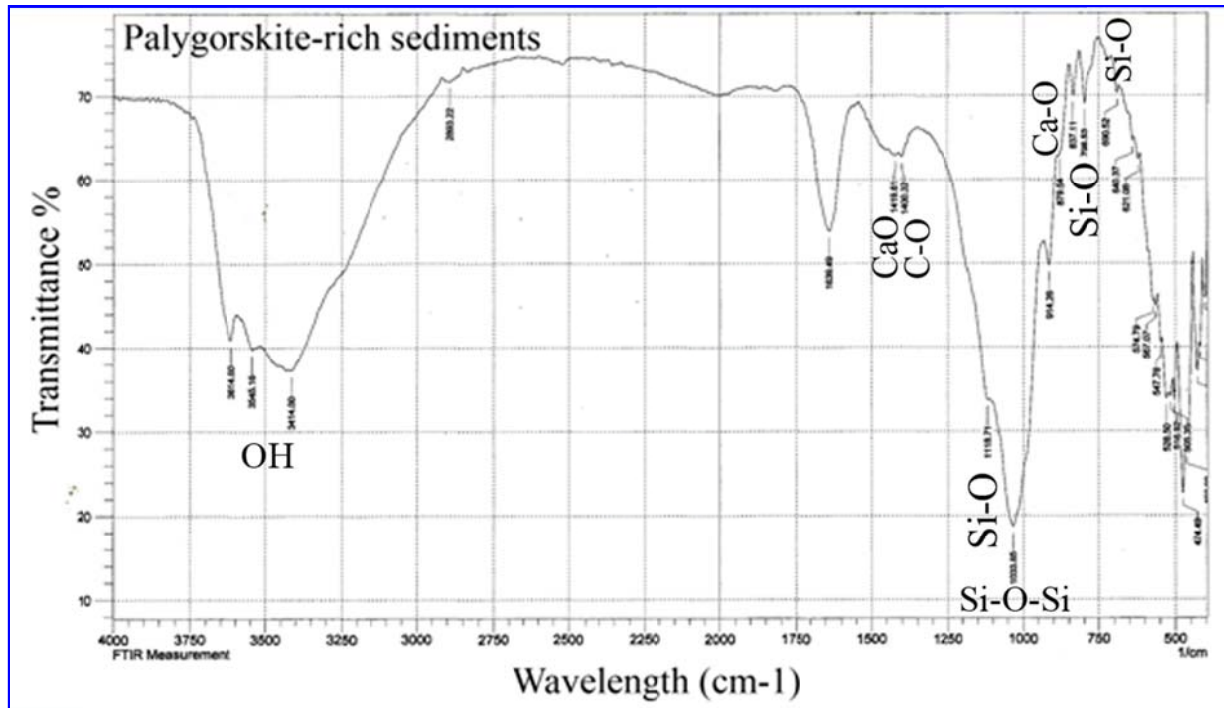


Figure 3-29: FTIR spectra of palygorskite-rich sediments, sample no.5DS.

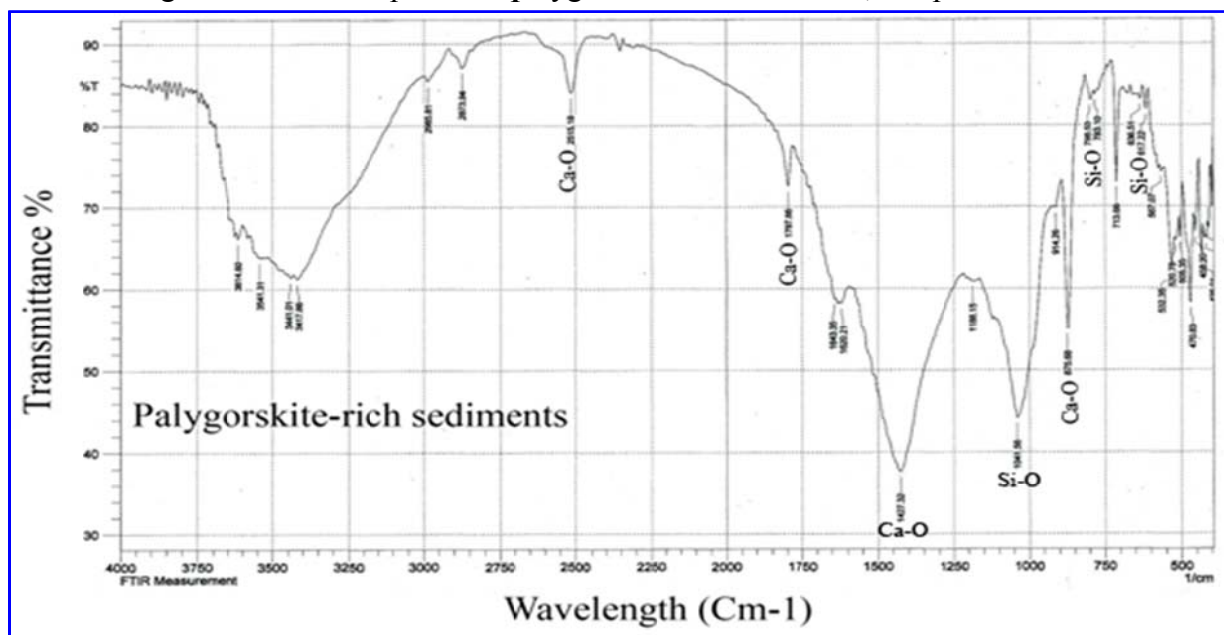


Figure 3-30: FTIR spectra of palygorskite-rich sediments, sample no.13A.

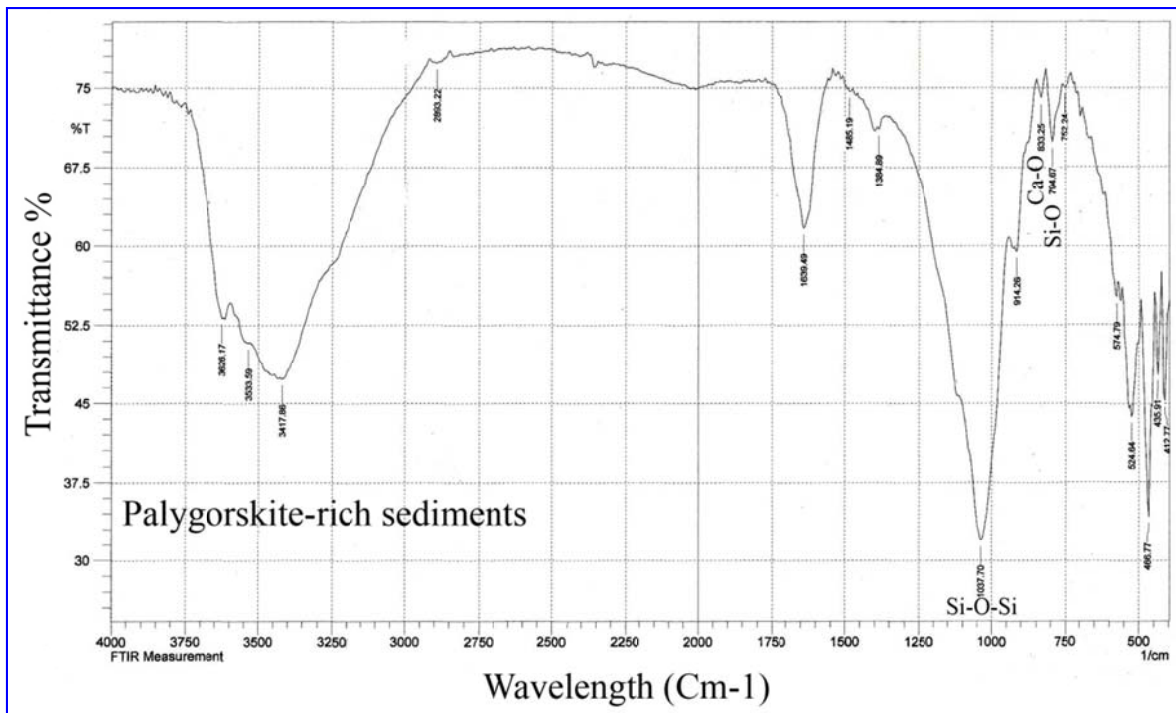


Figure 3-31: FTIR spectra of palygorskite-rich sediments, sample no.16AT.

3-2-3 Non-clay minerals

3-2-3-1 Calcite and dolomite

Calcite (CaCO_3) can exist in three polymorphs; calcite, aragonite, and vaterite. Calcite is the most thermodynamically stable mineral at room temperature and atmospheric pressure, but vaterite is the least stable. It has a hexagonal structure with the trigonal carbonate ions being coplanar (Smyth and Ahrens, 1997).

XRD reveals that there is a calcite in some samples (Figures 3-9, 3-10 and 3-12). Dolomite occurs more than calcite and tend to exist mostly in all samples (Figures 3-1, 3-2, 3-3 and 3-4).

The FTIR spectrum of calcite is shown in Figure 3-32. The bands appearing near 1428 , 878 , and 714 cm^{-1} are diagnostic for calcite (Wilson, 1994). Dolomite can be identified by FTIR absorption features at 2626 cm^{-1} and 730 cm^{-1} and calcite at 713 cm^{-1} . Calcite and dolomite do not exist individually, but exist mixed with other minerals. In this study, these minerals are expressed as impurities. The presence of small quantities of impurities can easily be detected in the FTIR spectrum. Calcite is detected within sample no. 5DS by its characteristic band at 1430 cm^{-1} and a shoulder at 876 cm^{-1} (see Figure 3-29) (Suárez and Garcia-Romero, 2006).

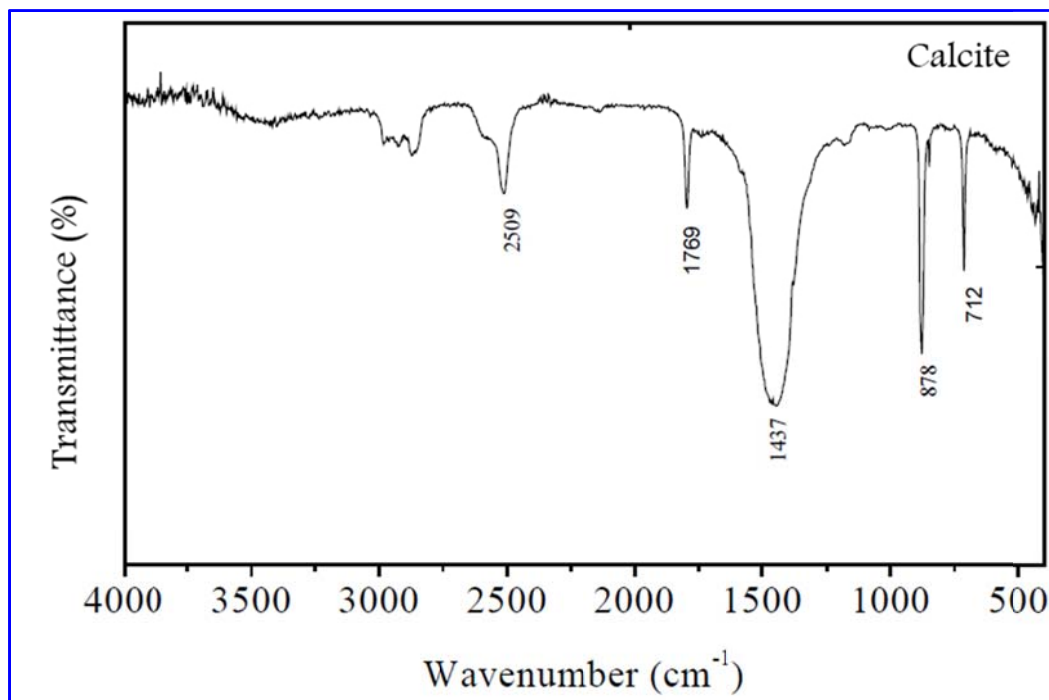


Figure 3-32: FTIR spectra of calcite.

3-2-3-2 Quartz, cristobalite and tridymite

The main basic reflection of quartz mineral is (101), major peak of quartz: $d=3.34\text{\AA}$, $2\Theta=(26.63)^\circ$ and (110): $d=2.45\text{\AA}$, $2\Theta=(36.54)^\circ$ and (102): $d=2.28\text{\AA}$, $2\Theta=(39.46)^\circ$. Peaks of quartz are quite clear in XRD patterns of all samples as in Figures 3-1, 3-4, 3-5, 3-6, 3-7, 3-8, 3-9 3-10 and 3-11). Cristobalite and tridymite are the other most common forms of which are commonly known as crystalline silica. Silica mineral phases appear to be scattered as a thin bed within Digma Formation. Cristobalite and tridymite are clearly identified by XRD (Figures 3-1, 3-4, 3-5, 3-8, 3-10, and 3-11).

The infrared spectra of the quartz-rich sample, is investigated by using the frequency range 500– 2000 cm^{-1} . The mid infrared spectra of silicate between the range 1200–400 cm^{-1} are classified into four characteristic bands around 1000, 780, 695 and 450 cm^{-1} with reference to the standard quartz spectra. Among these four characteristic peak regions (Table 3-3), the peak at 695 cm^{-1} is unique to the crystalline materials. The bands around 1000 cm^{-1} appear due to the silicon-oxygen stretching vibrations and the tetrahedral–tetrahedral ion vibrations affecting the band around 780 cm^{-1} for silicate, the tetrahedral dimensions are generally considered to be little affected by pressure and temperature (Saikia et al., 2008).

It is well known that in the infrared spectra of amorphous silica the symmetrical bending vibration of the Si–O group found at 695 cm^{-1} is absent. Therefore, the symmetrical bending vibrations of Si–O group obtained at 695 cm^{-1} is a diagnostic peak of the quartz, whether it is crystalline or amorphous (Saikia et al., 2008 and Suárez and Garcia-Romero, 2006).

Table 3-3: Characteristics of IR bands associated with quartz. V=vibration.

SiO₄ tetrahedra	Type of IR band modes of vibration	Frequency (cm⁻¹)
V3	Si–O asymmetrical stretching vibration	1080–1175
V1	Si–O symmetrical stretching vibration	780–800
V2	Si–O symmetrical bending vibration	695
V4	Si–O asymmetrical bending vibration	464

The crystallinity obtained from this infrared investigation represents the ratio of characteristic amorphous peak at 695 cm^{-1} and the tetrahedral characteristic peak at 778 cm^{-1} which is found to be good for structure elucidation. The presence of the 695 cm^{-1} peak and the crystallinity provide that the SiO₂ mineral in all the samples is in crystallized form. From the value of crystallinity we can identify purity of the samples.

3-3 Palygorskite separation from clay minerals

In this study, for the purpose of obtaining a pure palygorskite, it has been separated from the clay fraction that was already separated mainly from the whole sample. The non-processed palygorskite called natural palygorskite or crude palygorskite which represents the whole sample, while the separated palygorskite is called separated or pure palygorskite. The pure palygorskite (separated) is investigated by XRD and FTIR techniques (Figure 3-26 and 3-27). The separation processes are carried out on sample no. 12D.

Bish and Guthrie (1993) had mentioned that the palygorskite commonly is found with smectite, amorphous silica, and other minerals. In the studied samples, palygorskite-rich sediment samples consist of palygorskite and considerable amount of impurities of clay minerals (montmorillonite and kaolinite) and non-clay minerals including calcite, dolomite, quartz, apatite, and opal C-T. All components other than palygorskite are considered as impurities.

In this study, palygorskite is separated using the procedure proposed by Paul et al., (2000) and Robert and Dennis (2002); and then it is concentrated for processing in the laboratory experiment to test the efficiency of palygorskite in adsorbing and absorbing the heavy metals.

Since one of the objectives of this study is to test the sorption efficiency and sorptive properties of palygorskite of some elements (Pb, Cd, Ni, Co, Cr, V, Fe, Mn, Zn, Cu and B) with different concentrations (10, 25, 50, 75, 100, 125, 150, 175, 200, 225 and 250 ppm), so a sample of pure palygorskite must be prepared. To achieve this target, two major processes are performed. The first one is that, clay minerals are separated from the whole samples of palygorskite-rich sediments and the second is restricted to separate palygorskite from clay mineral suits in order to obtain a sample of pure palygorskite as possible as. The detail procedures of Paul et al., (2000) and Robert and Dennis (2002) were done on whole sample (crude sample, 12D) was done for separating the clay mineral from whole sample, and then, palygorskite was extracted from clay minerals. The detail procedure is described in chapter two. The detailed identification of the pure palygorskite was confirmed by XRD and FTIR (See Figures 3-26 and 3-27 respectively). These figures support the accuracy of the separation procedure.

3-4 Origin of palygorskite

Palygorskite are commonly associated with phosphatic sediments, salt deposits, sulfates, carbonates, zolites, and siliceous rocks (Jones and Galan, 1988). It appears chronologically within Upper Cretaceous and particularly Tertiary age sediments (Yalcin and Bozkaya, 1995). Palygorskite occurs extensively in shallow water such as coastal lagoon, pedogenic (Singer, 1984), and lacustrine environments (Jones, 1986); It is unique to deep sea sediments (Toyoda et al., 1990). Most major deposits were originally formed in shallow seas and lakes as chemical sediments or by the reconstitution of smectites, in open oceans by the hydrothermal alteration of volcanic materials, and in calcareous soils by direct crystallization (Calan and Castello, 1984).

The cohesion of the palygorskite with the smectite indicates that the origin of palygorskite is authigenic from transformation or alteration smectite. Palygorskite is bedded in Akashat and Digma Formations interstratified with dolomite, siliceous, calcareous clays and phosphatic zones. Lithology suite of dolomite, cherty dolomite, marly limestone, phosphatic

sediments, siliceous minerals such as tridymite and cristobalite indicates shallow marine environment of inner platform in arid and semi arid environment.

There are no considerable differences among the study sites regarding to palygorskite characteristics. The in-situ replacement was the dominant process forming palygorskite by the transformation of montmorellonite with presence of Mg-rich solution. Occurrence of palygorskite with dolomite was interpreted as suggested authigenic origin rather than detrital (Esteoule-Choux, 1984). Two models are proposed:

- 1- The reaction of pore water rich in silicic acid with dolomite suggests the sepiolite formation as below:



Then the sepiolite was transformed to palygorskite $(\text{Mg},\text{Al})_2\text{Si}_4\text{O}_{10}(\text{OH})_4(\text{H}_2\text{O})$ by taking Al from the surrounding area.

- 2- Transformation of smectite to form palygorskite: The transformation of another clay illite (Galan and Castillo, 1984), smectite (Singer, 1984) or detrital phyllosilicates (Torres-Ruiz et al., 1994) to generate palygorskite are proposed. There is evidence on SEM observation of palygorskites which was accompanied by smectite. Ca is generally related to the carbonate minerals in the surrounding area, Al and some Si are related to the other type of clay minerals, other few Si is originated from silicic acid. The presence of chert in the carbonate rocks indicates that the environment was saturated with silicic acid.

3-5 Discussion

Palygorskite is a crystalline hydrated magnesium aluminum silicate with a unique chain structure of unusual colloidal and sorptive properties. It consists of a double chain tetrahedra of silicon and oxygen (Si_4O_{11}) running parallel to the long axis. A layer of magnesium atoms in six-fold coordination links upper and lower parts of each double chain. The overall structure resembles a channeled wall where every second brick is missing (Haden and Schwint, 1967). Palygorskite has two unusual characteristics. First, the clay cannot swell because the structure consists of three dimensional chains. Second, an unusual needle-like shape is formed by cleavage parallel to the 110 plane along the Si-O-Si bonds holding the strips together. These needle-

like formations generally remain in bundles, similar to haystacks, giving palygorskite products their principle structural feature (Haden, 1963).

The detection of palygorskite by many techniques (XRD, SEM and FTIR) in most samples refers to the success of the sampling process. Investigation of the separated palygorskite sample again by these techniques and along treatment with heating confirms that the laboratory separation process is successful and the separated palygorskite becomes ready for subjecting to a set of tests such as its efficiency for heavy metals sorption which will be discussed in the next chapter.

The position of the bands identified in the FTIR spectra of the palygorskites studied is almost similar for all samples, but there are some differences in their intensity, which are significant. Analyzing these intensities, valuable information about the distribution of cations along the octahedral sheet has been obtained (Suárez and Garcia-Romero, 2006).

Palygorskite appears to be commonly associated with a component of montmorillonite and calcium carbonates, particularly dolomite. Therefore, arid conditions appear to be essential for the formation of palygorskite. These conditions presumably provide the high Mg concentration and the high pH necessary for its formation, where, arid climatic conditions also favour the formation of palygorskite in desert soils.

Palygorskite is invariably associated with montmorillonite and in some situations is believed to weather to montmorillonite (Barshad et al., 1956) and by others to be transformed from montmorillonite by the addition of magnesium (Loughnan, 1959). A micro-grain of palygorskite was grown from diagenetic montmorillonite grains. It epigenetically originated from montmorillonite (smectite) with grain length varies from 0.5μ to 2.5μ approximately as micro-grain growth outside smectite forming micro fan shape. Palygorskite is unstable in most soil environments and may be transformed to smectite again (Bighamm et al., 1980), but in this study there is no evidence refers to palygorskite alteration.

Porcellanite (opal-CT) with phosphatic facies occur in association with palygorskite provide a significant environment evidence. Apatite in Marl-phosphatic facies may indicate shallow to deep inner platform. Phosphorite facies is characterized by discontinuous extension of thick light gray color bed reflecting a shallow water of inner platform. Porcellanite facies indicates open inner platform.

Chapter Four

Geochemistry and Sorption Efficiency

4- Geochemistry and Sorption Efficiency

4-1 Preface

Palygorskite has a high sorption capacity for cations. It is fibrous silicate clay mineral, called special clay and used in more than 100 different applications (Galan, 1996). The sorption capacity of palygorskite is experimented for eleven elements, these are lead (Pb), cadmium (Cd), nickel (Ni), chromium (Cr), cobalt (Co), vanadium (V), zinc (Zn), copper (Cu), iron (Fe), manganese (Mn), and boron (B). Absorption and adsorption are two properties related to the surface area of clay minerals.

Absorption is the penetration of fluid molecules into the bulk of an absorbing solid, whereas adsorption implies some interaction between the fluid molecules and the solid surface. Both types of phenomena are encompassed by the term sorption. Technological applications are based on the mineral physicochemical properties, principally in composition, surface area, porosity, among others, and particularly in its fibrous structure.

Influence of sorbent mass (solid to liquid ratio), equilibrium reaction time, Effect of concentration, effect of pH, effect of ionic potential and effect of calcinations at different temperatures are tested and discussed.

4-2 Geochemistry

In order to determine the best samples containing palygorskite, seven samples rich with clay minerals have been chosen, and then analyzed for major oxides (SiO_2 , Al_2O_3 , MgO , Fe_2O_3 , TiO_2 , MnO , Na_2O , CaO , K_2O , P_2O_5 , LOI). The results are listed in Table 4-1.

Sample 5DS comprises clay minerals and opal-CT (cristobalite and tridymite), quartz, dolomite, montmorellonite, and palygorskite (Figure 3-4). MgO which has 4.42% arises mainly from dolomite and palygorskite. Consequently, palygorskite can be considered as the mineral with low concentration in this sample. Sample 6D looks like it doesn't contain palygorskite, where MgO is very low (0.61). The chemical composition appeared in Table 4-1 is a reflection of its mineralogical composition, where it consists of kaolinite quartz and opal-CT (cristobalite and tridymite) (Figure 3-5). This sample contains the highest Al_2O_3 due to kaolinite content. Palygorskite is also found in the sample 8D, but of little quantity; where MgO (1.79%) is mainly originated and reflects palygorskite. This sample comprises kaolinite, palygorskite, quartz, and opal-CT (cristobalite and tridymite) (Figure 3-6). Sample 10DN tend to be free from palygorskite, while it

contains kaolinite, apatite, quartz, and opal-CT (cristobalite and tridymite) (Figure 3-8). Samples 8D, 10DN and 16AT contain iron oxide which has heterogeneous distribution. The irregular distribution of iron in the samples was reflected in the lack of appearance of iron by XRD, while it is reflected in the chemical analyses. Sample 12D is the richest within palygorskite. Consequently, all the chemical sorption tests have been carried on this sample. Sample 13A contain a wide suite of minerals, these are palygorskite, calcite, apatite, quartz, and opal-CT (cristobalite and tridymite) (Figure 3-10). Sample no. 16AT formed of montmorellonite, palygorskite, apatite, quartz, and opal-CT (cristobalite and tridymite) (Figure 3-11). MgO in this sample reflects the content of palygorskite. The association montmorellonite with palygorskite confirm the authigenic palygorskite which is formed in situ under arid climate.

Table 4-1: Chemical analyses of the whole samples collected from Digma and Akashat Formations.

Oxides %	5DS	6D	8D	10DN	12D	13A	16AT
SiO ₂	40.09	41.12	38.85	41.21	17.9	39.09	39.80
Al ₂ O ₃	18.11	29.87	20.31	14.13	21.5	6.63	15.90
MgO	4.42	0.61	1.79	4.20	17.11	2.51	4.03
Fe ₂ O ₃	8.55	5.73	10.13	10.24	3.73	5.13	6.58
TiO ₂	2.80	4.06	3.06	2.81	0.9	1.86	3.29
MnO	0.01	0.01	0.01	0.01	0.11	0.05	0.01
Na ₂ O	0.41	0.28	0.31	0.12	0.11	0.28	0.66
CaO	8.41	1.86	12.32	11.35	8.5	16.55	11.19
K ₂ O	0.37	0.78	1.11	0.04	0.05	0.21	0.21
P ₂ O ₅	0.015	0.040	0.020	0.030	0.02	0.020	0.040
LOI	16.06	14.85	13.02	15.21	29.5	26.87	17.51
Total	99.24	99.21	100.9	99.35	99.61	99.2	99.22

4-2-1 Geochemistry of separated palygorskite

Concentration of palygorskite by separation of specific particle-size fractions was ineffective in improving the adsorption capacity (Kannevischer, 2006). In this study, the separated palygorskite appears to be of high grade, with containing very few impurities. This means that the separated

palygorskite is not a mixed clay, but it is of high purity. An isomorphism is the essential process that happens between palygorskite and the surrounding environment. A specific evidence of isomorphism in palygorskite occurs and may involve:

- 1- Substitution of Al for Si in positions of tetrahedral layer in the crystal lattice.
- 2- Substitution of Fe for Al in octahedral layer.
- 3- Substitution of Mg for Al in octahedral layer.
- 4- Substitution of Ti for Fe in octahedral layer.
- 5- Substitution of varied kind of cations like Ca, Na and K for other kinds of cations in interlayer positions.

In nature, palygorskite contains substantial quantities of Al_2O_3 and there is no evidence for a continuous solid solution with sepiolite which is a hydrous magnesium silicates. Accordingly, it probably contains exchangeable cations like Ca, Na and K. Palygorskite occurs in soil, sediment (clay deposits) and alteration products of certain basic igneous rocks, sometime forms in situ from alteration of montmorillonite.

The raw sample (12D) is composed of a mixture of palygorskite and dolomite as well as a little amount of clay minerals. Consequently, it is distinct its enrichment with MgO (17.11), CaO (8.5%) and LOI (29.5%) (Table 4-2) reflecting a mixture of palygorskite and dolomite. The laboratory separation process of palygorskite from the raw sample (bulk sample) led to the decline of the content of alumina, magnesia and lime. This means the success of the separation process in the removal the both of dolomite and clay minerals. The separation process here is considered as palygorskite purification. The chemical composition of the separated palygorskite is of high grade and fit or of minimal differences with the global palygorskite of Georgia and Pereja palygorskite; the chemical composition of separated palygorskite is seen in Table 4-2. It is characterized by containing a high MgO (10.2%) and high content of silica (52.5%). Such contents in palygorskite give its structure credibility as a good adsorbent. Loss on ignition (19.1%) fits with typical palygorskite and confirms that MgO belongs to palygorskite, and not dolomite. If dolomite exists, it will cause a significant increase in LOI.

The $\text{Al}_2\text{O}_3/\text{MgO}$ ratio is relatively constant in palygorskite, varying from 0.64 to 1.08. The $\text{Al}_2\text{O}_3/\text{MgO}$ ratio in separated palygorskite in this

study is 0.86. CaO, Na₂O, K₂O along with some of the magnesia, is probably present as exchangeable cations; however, in most samples these cations are more abundant than can be accounted for by the cation exchange values. Exchange values of 5-30 mequiv/100 g seem to be most characteristic of the relatively pure samples (Weaver and Pollard, 1973). The structural formula of palygorskite is computed (Table AP-2, see appendix).

Table 4-2: Chemical results of whole palygorskite-rich sediments and separated palygorskite compared with palygorskite from world.

Oxides	Palygorskite			
	Raw sample (12D)	Separated palygorskite (12D)	¹ Georgia palygorskite	² Pareja palygorskite (Tajo basin)
SiO ₂	17.9	52.3	53.64	56.5
Al ₂ O ₃	21.5	8.8	8.76	7.87
MgO	17.11	10.2	9.05	10.81
Fe ₂ O ₃	3.73	3.1	3.59	3.55
CaO	8.5	5.2	2.02	0.2
K ₂ O	0.05	0.7	---	0.28
Na ₂ O	0.11	0.13	---	0.07
TiO ₂	0.9	0.8	0.6	0.05
MnO	0.11	0.1	---	0.04
P ₂ O ₅	0.2	0.02	---	---
LOI	29.5	19.1	20.01	19.84
Total	99.61	100.4	97.67	99.29

1:Bradley, 1940; 2: Lopez et al.,1996.

4-2-2 Ionic substitutions

Ionic substitution is described in tetrahedral layer, octahedral layer and interlayer

A. Tetrahedral substitutions

The structural formula of palygorskite is calculated (Table 4-3) depending on the basis of 20 oxygen atoms (Weaver and Pollard, 1973). In palygorskite, the ionic substitution most frequently observed in the tetrahedral sheet is Si⁴⁺ replaced by Al³⁺. The difference of valency between both ions produces a negative charge (0.14) which means positive charge deficiency

(Table 4-3) and changes the symmetry of the tetrahedral sheet. The overall positive charge in this layer within unit cell is 31.86 (Table 4-3). From the structural formula, it can be seen that there is very little tetrahedral Al for Si substitution (0.42), but it is relatively high in comparison with other clay like sepiolite resulting in an increase of the layer charge.

Table 4-3: Cations and charge distribution of separated palygorskite.

Cation	Tetrahedral layer	Charge
Si ⁴⁺	7.86	31.44
Al ³⁺	0.14	0.42
	8.00	31.86
	Octahedral layer	
Al ³⁺	1.42	4.26
Mg ²⁺	2.30	4.60
Fe ²⁺	0.35	0.70
Ti ⁴⁺	0.08	0.32
	4.15	9.88
	Interlayer (Exchangeable cations)	
Ca ²⁺	0.84	1.68
Na ⁺	0.04	0.04
K ⁺	0.13	0.13
	1.01	1.85

B. Octahedral substitutions

In octahedral layers, three types of ionic substitution are likely to happen, these are:

- Homovalent substitutions: it happens between Al³⁺ and Fe³⁺ or between Mg²⁺ and Fe²⁺
- Heterovalent substitutions: it happens between Fe³⁺, Fe²⁺ and Ti⁴⁺. The overall positive charge in this layer within unit cell is 9.88 (Table 4-3).

In this layer, Mg is the dominant cation in the octahedral site, accompanied by minor amounts of Al, Fe and Ti.

C. Interlayer substitution

This layer lies between tetrahedral and octahedral layers. It includes three cations (Ca, Na and K), that play a role in the ionic exchange process. These cations have a net valence of 1.85 in this layer (Table 4-3).

4-2-3 Types of Solid Solution

The three types of solid solutions in the clay mineral layers according to Meunier (2005) are:

- 1. Substitution Solid Solutions:** These are formed by the isomorphous replacement of ions or atoms in equivalent sites of the crystal structure. In the case of ions, valency must be identical. This is the case of Fe^{2+} replacing Mg^{2+} in the octahedral sheet of phyllosilicates (the difference in their ionic radii is only 7.5%).
- 2. Addition Solid Solutions:** In the case of heterovalent substitutions, the electrical neutrality may impose the presence of additional ions that are located in particular sites. This is the case of the ions in the interlayer sheet of phyllosilicates.
- 3. Omission Solid Solutions:** As heterovalent substitutions change the charge balance, the latter is restored by the incomplete occupation of a crystallographic site (vacancies). This is the case of trioctahedral chlorites in which the substitution rate of R^{3+} for R^{2+} in the octahedral sheet imposes vacancies.

4-2-4 Cation Exchange capacity (CEC)

Two types (external and internal) of cation exchange capacity can be distinguished. The external CEC depends on the number of binding sites of cations on the external surfaces. These negatively charged sites correspond to charges resulting from the tetrahedral or octahedral substitutions of those sheets forming the (001) faces, or to defects emerging on these faces. The properties of external sites depend on pH. The internal CEC depends on the permanent charges of clay species.

The exchange capacity is defined as the amount of cations retained by all the negative charges (permanent charges) in 100 g of clay at pH 7; while, Anion Exchange Capacity (AEC) of clays involves only those sites on the edges of crystals where OH groups cannot totally compensate for their valency (Hower and Mowatt, 1966). It is expressed in milliequivalents (meq)

per 100 g of clay. The milliequivalent is equal to $(\text{charge}/\text{mass}) \times 1000$; it equals to one centimole of unit charge per kilogram of dry matter (cmol kg^{-1}) (Meunier, 2005). The exchange capacity is calculated following the relation:

$$\text{CEC} = (\text{charge}/\text{mass}) \times 1000 \times 100$$

The total CEC is equal to the sum CEC variable charges + CEC permanent charges. The CEC of palygorskite is reported to vary from below 10 to 35 meq/100g

4-3 Sorption efficiency of of palygorskite

Palygorskite used in many applications omit industrially and pharmaceutically, where they are used as antidiarrhoeaics, dermatological protectors, as emulsions and creams, and in several other industrial applications (Carretero et al., 2006). Palygorskite particles can adsorb many exchange cations owing to isomorphic substitution during its formation. Its porous structure and absorbed cations provide it to be with large specific surface area and moderate cation exchange capacity (Galan, 1996), making it beneficial for the adsorption of heavy metals from solution. Technological applications are based on its physicochemical properties, principally in composition, surface area, porosity, among others, and especially in its fibrous structure. Bradley (1940) described the structure of palygorskite; as a 2: 1 phyllosilicate in which the sheets of silica tetra-hedra are periodically inverted with respect to the tetrahedral bases. Owing to their absorptive properties, palygorskite is used commercially for many purposes as carriers, fillers, clarifying agents, and in used lubricant reclamation, Here, in this study, palygorskite adsorption tested for ten heavy metals as well as boron by conducting laboratory experiments which has explained below.

4-3-1 Procedure of laboratory experiments

A series of adsorption tests are conducted as kinetic batch experiments to test the sorption capacity of palygorskite using separated palygoskite and heavy metal ions of Pb, Cd, Ni, Co, Cr, V, Cu, Zn, Mn, , Fe, and B. The standard solutions used for preparing the stock solutions are listed in Table 4-4. The stock solutions are prepared by dilution of $\text{Pb}(\text{NO}_3)_2$, $\text{Cd}(\text{NO}_3)_2 \cdot 4\text{H}_2\text{O}$, $\text{Ni}(\text{NO}_3)_2 \cdot 6\text{H}_2\text{O}$, $\text{Co}(\text{NO}_3)_2$, $\text{Cr}(\text{NO}_3)_3$, $\text{VOSO}_4 \cdot \text{H}_2\text{O}$, $\text{Cu}(\text{NO}_3)_2$, $\text{Zn}(\text{NO}_3)_2 \cdot 4\text{H}_2\text{O}$, $\text{Mn}(\text{NO}_3)_2 \cdot 4\text{H}_2\text{O}$, $\text{Fe}(\text{NO}_3)_3$ and H_3BO_3 in deionized water.

Hundred mls from each stock solution are slowly added on 1gm of separated samples of dry palygorskite powder in glass beaker of 250 mls. For

these experiments, ten concentrations (10, 25, 50, 75, 100, 125, 150, 175, 200 and 225 ppm) for each Pb, Cd, Ni, Co, Cr, V, Cu, Zn, Mn, Fe, and B are tested with reaction time of 1h at room temperature. The reaction beaker is covered and stirred continuously using a magnetic stirrer. After finishing the reaction time, the samples are filtered. Patch reaction system is followed, where each concentration of each element is conducted separately.

Table 4-4: Specifications of the standard solutions used for preparing the stock solutions that are used for laboratory experiments of palygorskite sorption.

Element	Concentration (g/L)	Compound	Color
Pb	1	Pb(NO ₃) ₂	Colorless
Cd	1	Cd(NO ₃) ₂ .4H ₂ O	Colorless
Ni	1	Ni(NO ₃) ₂ .6H ₂ O	L. Blue
Co	1	Co(NO ₃) ₂	Red
Cr	1	Cr(NO ₃) ₃	Blue
V	1	VO ₂ SO ₄ .H ₂ O	Blue
Cu	1	Cu(NO ₃) ₂	L. Blue
Zn	1	Zn(NO ₃) ₂ .4H ₂ O	Colorless
Mn	1	Mn(NO ₃) ₂ .4H ₂ O	Colorless
Fe	1	Fe(NO ₃) ₃	L. Blue
B	5	H ₃ BO ₃	L. Pink

Adsorption experiments are carried out at the desired contact time, temperature, metal concentrations and palygorskite mass using the necessary adsorbents in a 250 ml conical flask containing 100 ml of metal solution, pH value, initial solutions with different concentration of metals were prepared by proper dilution from stock standards. All experiments were conducted at room temperature. Solid to liquid ratio (1gm/100ml), conditioning time (1h), effect of solution pH, and effects of heavy metal ions was adjusted accurately.

The palygorskite suspension was stirred for 1 h (as conditioning time reaction) with a magnetic stirrer. The palygorskite sample used in this study has been separated and purified from the raw sample (12D). It was collected from Digma Formation.

After being stirred and filtered, filtrate solutions were collected in vials for analysis. Final metal concentration was determined using ICP in the Global ALS Laboratory Group in the Czech Republic-Prague Laboratory.

All experiments were carried out in the Laboratory of Geochemistry at the College of Science, University of Baghdad. The sorption (%) of metals was calculated by using the following equation:

$$\text{Sorption (\%)} = [(C_i - C_f) / (C_i)] \times 100$$

Where, C_i and C_f are the initial and final metal ion concentrations, respectively.

4-3-2 Laboratory experiment conditions determination

4-3-2-1 Influence of sorbent mass (solid to liquid ratio)

The sorption (%) of Pb on palygorskite is studied at different palygorskite masses (0.25, 0.5, 1.0, 1.5, 2.0, 2.5, and 3 g/100 ml) keeping initial Pb concentration (100 and 200 ppm), temperature (25 °C) and contact time (1 h) constant. The results of the experiment are listed in Table 4-5.

Such approximate conditions have been used by Hefne et al. (2008). The results showed that with increase in the palygorskite mass, adsorption (%) of Pb increases and the maximum removal was observed with 1 gm dose (Figure 4-1). With increasing palygorskite mass, the corresponding increase in adsorption (%) is less, because the cations find difficult to approach the adsorption sites due to overcrowding of clay mineral particles (Palygorskite) termed as a kind of solid concentration effect (Garg et al., 2004). Accordingly, the solid to liquid ratio was determined to be 1gm palygorskite to 100 ml metal solution.

Consequently, and depending on the result of the experiment, the sorption (%) of Pb, Cd, Ni, Co, Cr, V, Cu, Zn, Mn, Fe, and B on palygorskite was studied at palygorskite mass of (1.0 g /100 ml metal solution) and at concentrations of 10, 25, 75, 100, 125, 150, 175, 200, 225 and 250 ppm, keeping room temperature, stirring speed, and contact time (1 h) constant. The room temperature is changed slightly according to the atmospheric conditions. In addition higher adsorbent amount creates particle aggregation, resulting in a decrease in the total surface area and an increase in diffusional path length; both of which contribute to decrease in adsorbed amount per unit mass (Shukla et al., 2003).

Table 4-5: Results of sorption (%) on different masses of palygorskite.

Mass (gm)	Sorption (%)	
	100 ppm	200 ppm
0.25	20.0	12.0
0.5	35.0	20.0
1.0	83.0	82.9
1.5	83.0	83.0
2.0	82.6	83.1
2.5	82.9	82.6
3.0	83.0	82.8

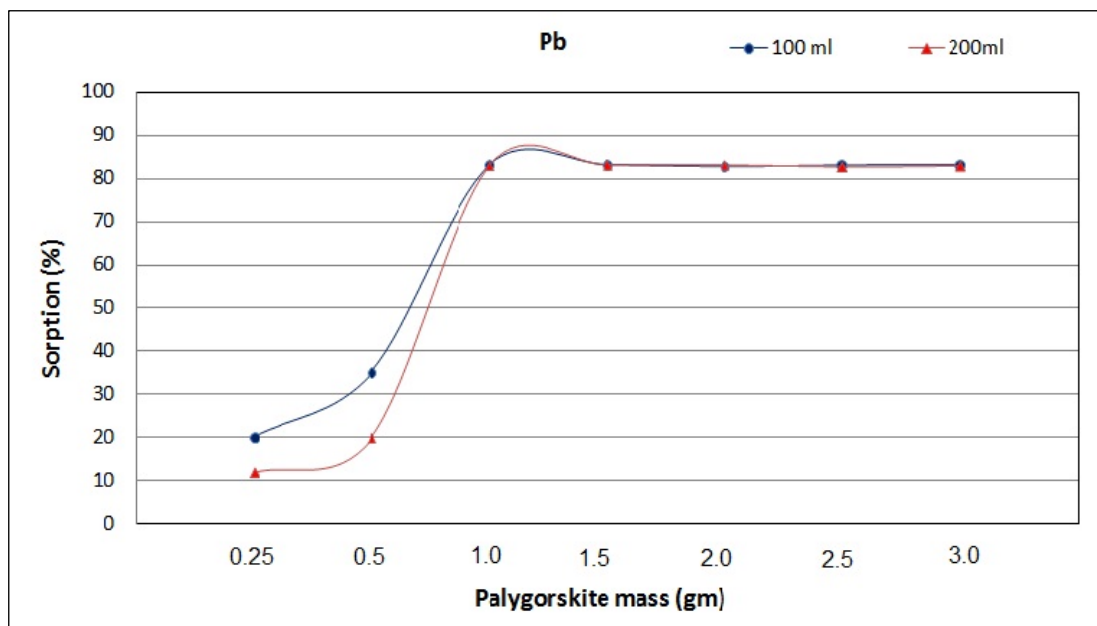


Figure 4-1: Effect of palygorskite mass on adsorption % of Pb at different concentrations (100 and 200 ppm) and 25°C.

4-3-2-2 Influence of the equilibrium reaction time

These experiments are performed in order to know the time required for complete adsorption and absorption of metals onto palygorskite. In order to perform accurate sorption (%) experiments, the effect of conditioning time on sorption (%) of metals onto palygorskite must be determined. The results of conditioning time versus 100 ppm Pb sorption (%) are listed in Table 4-6. The sorption (%) increases proportionally to the time where the maximum sorption (%) can be seen at 60 minutes (Figure 4-2). On this basis, the equilibrium time is determined to be 1h.

Table 4-6: Results of sorption (%) of 100 ppm Pb (100 ml) onto 1 gm palygorskite with time.

Time (Min.)	Sorption (%)
10	25
20	47
30	60
40	70
50	79
60	89.9
70	89.7
80	89.8

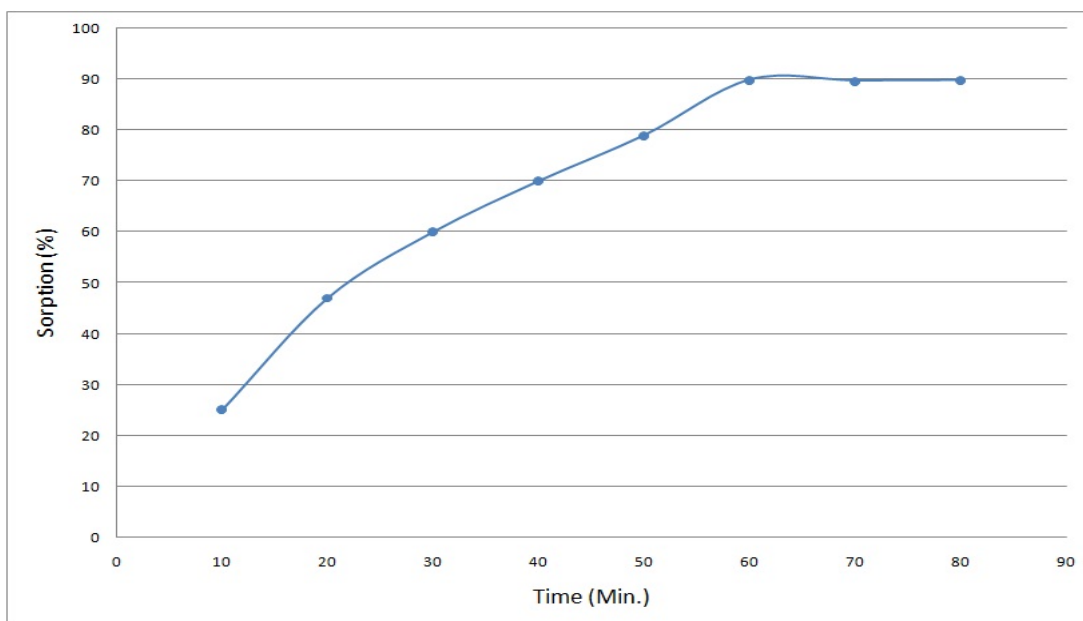


Figure 4-2: Equilibrium time of sorption (%) of 100 ppm Pb onto palygorskite.

4-3-3 Sorption experiments

4-3-3-1 Lead (Pb)

The experiment results of lead treated with palygorskite for ten concentrations are listed in Table 4-7. The Pb concentrations in the initial solutions that have been treated with 1 gm palygorskite are reduced after the end of the experiment. The adsorption (%) at the initial concentration (10 ppm) is 99.8% and then begin to decrease with the increasing Pb concentration. Pb adsorption (%) for the initial solutions (25, 50, 75, 100, 125, 150, 175, 200, 225 ppm) is 96.72, 91.1, 81.9, 76.48, 67.2, 31.43, 23.5, 22.2 % respectively (Table 4-7). Figure 4-3a clearly shows the status of decrease adsorption efficiency with increase concentration.

Table 4-7: Results of laboratory experiments of lead (Pb) sorption on palygorskite in ten solutions of various concentrations.

Sample number	Before experiment						After experiment							
	Initial conc. (ppm)	Total Vol (ml)	PH	TDS (mg/l)	EC ($\mu\text{s/cm}$)	T $^{\circ}\text{C}$	PH	TDS (mg/l)	EC ($\mu\text{s/cm}$)	T $^{\circ}\text{C}$	Final conc. (ppm)	Sorption (ppm)	Sorption (%)	Salinity (%)
1Pb	10	100	2.9	850	1691	24.5	7.0	482	960	24.6	0.05	9.95	99.5	0.2
2Pb	25	100	2.33	2125	3610	24.4	5.01	880	1760	24.2	0.06	24.94	99.8	0.7
3Pb	50	100	2.02	4250	7020	24.4	4.4	2060	3130	23.9	1.64	48.36	96.72	1.5
4Pb	75	100	1.86	6370	10820	24.4	4.1	3160	4510	24	6.67	68.33	91.1	2.3
5Pb	100	100	1.73	8510	15300	24.3	3.45	4012	5900	24.0	18.1	81.9	81.9	3.2
6Pb	125	100	1.62	10600	18020	24.3	3.22	5400	7500	24.0	29.4	95.6	76.48	4.1
7Pb	150	100	1.54	12700	22225	24.3	2.97	6710	8600	23.9	49.2	100.8	67.2	4.8
8Pb	175	100	1.46	14870	25279	24.2	2.48	8720	10900	24.0	120	55	31.43	6.2
9Pb	200	100	1.41	17000	30600	24.2	2.32	9920	12400	24.1	153	47	23.5	7.1
10Pb	225	100	1.36	19120	33840	24.1	2.37	11900	14000	23.9	175	50	22.2	8.2

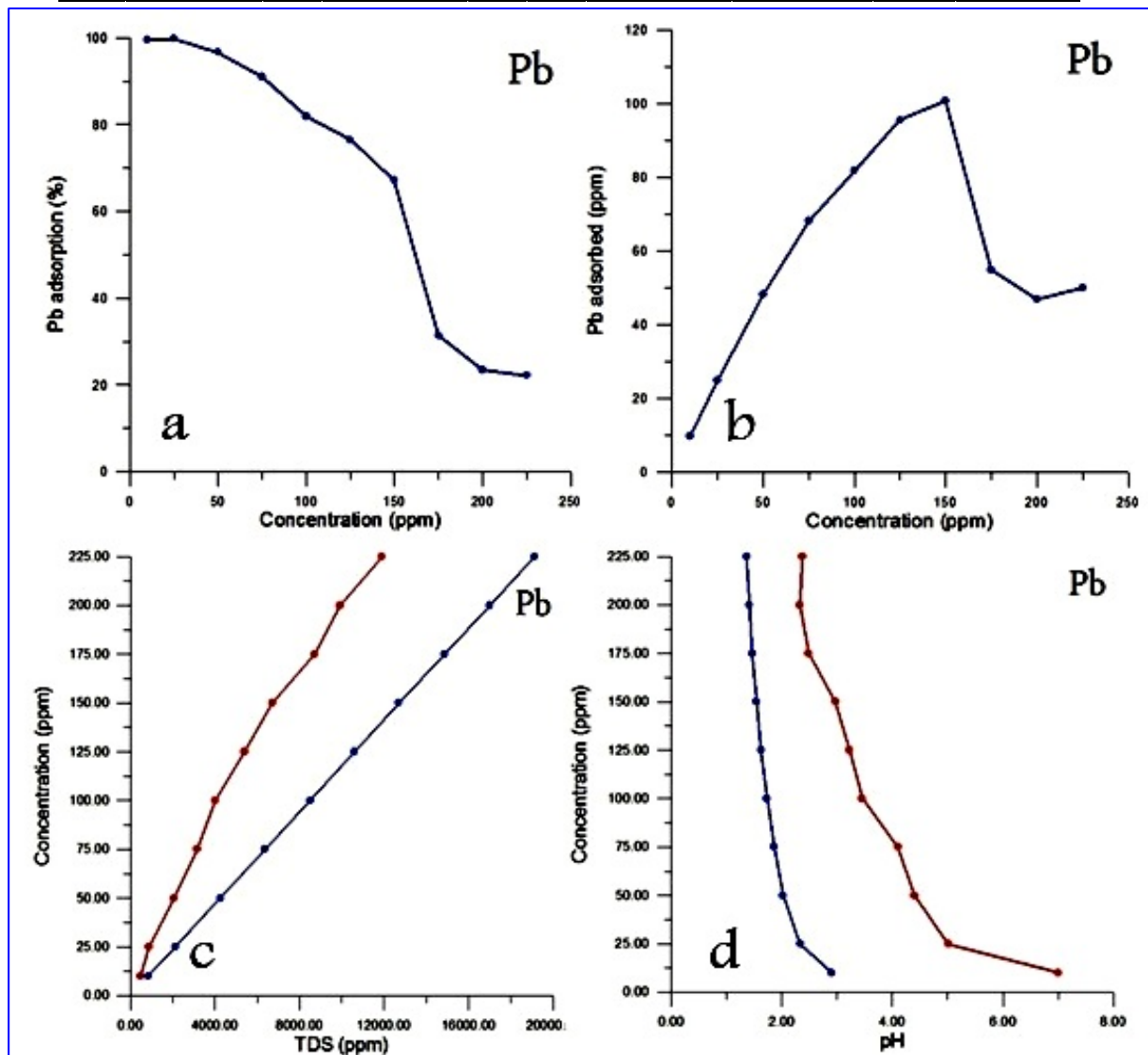


Figure 4-3: The effect of Pb adsorption on palygorskite; a: adsorbance (%) for ten initial solutions of different concentrations, b: the effect of concentration on adsorption, c: TDS pattern for initial solutions (blue line) before experiment and final solutions (red line) after experiment, d: changes of pH before the experiment (blue line) and after the experiment (red line).

It represents the amount of lead adsorbed onto palygorskite with increasing concentration of the initial solution. In case of the initial solution has 10 ppm, the amount of pb tend to be almost totally adsorbed (9.95 ppm); but in case of the initial solution has 150 ppm, the amount of pb that adsorbed on palygorskite is 100.8 ppm (Figure 4-1b); this is the maximal sorption (%) of Pb on palygorskite. Amount of adsorption decreased sharply for solutions of high concentrations (175, 200 and 225 ppm) (Figure 4-3b). Basically, as is known, the Total Dissolved Solid (TDS) is directly proportional to the increase in concentrations; this means a positive relationship between TDS and concentration (Figure 4-3c). The decrease of TDS value is an evidence for adsorption (Figure 4-3c). TDS of initial solutions ranges between 850 ppm and 19120 ppm (Table 4-5) due to the Pb concentration in each solution. As the experiment ended, TDS decreased and became varies between 482 ppm 11900 ppm indicating the adsorption process. For this set of experiments, pH (2.9-1.36) of the initial solutions is increased with the increase of adsorption until it varyies between 7.0-2.37 (Table 4-7 and Figure 4-3d). A significant amount of Pb adsorption is found at pH 2.97.

4-3-3-2 Cadmium (Cd)

The experimental results of cadmium treated with palygorskite for ten concentrations are listed in Table 4-8. The Cd concentration in the initial solutions (10, 25, 50, 75, 100, 125, 150, 175, 200, 225 ppm) that have been treated with 1 mg palygorskite were 0.004, 1.8, 4.9, 5.6, 22.5, 45, 67.9, 91.7, 115 and 140.8 ppm) respectively. This indicates that the sorption (%) was 99.96, 92.8, 90.2, 92.5, 77.5, 64, 54.7, 47.6, 42.5 and 37.4%) respectively (Figure 4-4a). The maximal sorption of the Cd is 77.5% when the initial concentration was 100 ppm (Figure 4-4b). The sorption efficiency at the high concentration seems to decrease at initial solutions of 125 to 225 ppm, where it decreases from 64% to 37.4% (Table 4-8). This is very clear in the amount Cd sorption (ppm), where it reduces to range from 80 to 84.2 ppm for the initial solutions of 125- 125 ppm (Table 4-8). The decrease of sorption efficiency at solutions of high concentrations can be attributed to the strong competition between cations on the negative sites in palygorskite.

Before the starting the experiment, TDS ranges between 933 and 20990 ppm; then after the experiment, it clearly decreases between 468 and 6360 ppm (Figure 4-4c and Table 4-8).

Table 4-8: Results of laboratory experiments of cadmium (Cd) sorption on palygorskite in ten solutions of various concentrations.

Sample number	Before experiment						After experiment							
	Initial conc. (ppm)	Total Vol (ml)	PH	TDS (mg/l)	EC ($\mu\text{s/cm}$)	ToC	PH	TDS (mg/l)	EC ($\mu\text{s/cm}$)	ToC	Final conc. (ppm)	Sorption (ppm)	Sorption (%)	Salinity (‰)
1Cd	10	100	1.9	933	1260	27.5	6.77	468	940	27.4	0.004	9.99	99.96	0.2
2Cd	25	100	1.56	2332	3730	27.5	5.87	832	1662	27.4	1.8	23.2	92.8	0.7
3Cd	50	100	1.27	4665	7510	27.5	4.7	1415	2830	27.4	4.9	45.1	90.2	1.8
4Cd	75	100	1.13	6997	11330	27.5	4.11	1955	3950	27.4	5.6	69.4	92.5	2.5
5Cd	100	100	1.04	9330	13065	27.5	3.28	2419	5760	27.4	22.5	77.5	77.5	3.1
6Cd	125	100	0.92	11660	16555	27.5	3.32	2808	6850	27.4	45	80.0	64	3.6
7Cd	150	100	0.86	13990	20000	27.5	2.03	3852	8960	27.4	67.9	82.1	54.7	5.0
8Cd	175	100	0.81	16320	22670	27.5	2.13	3896	9740	27.4	91.7	83.3	47.6	5.5
9Cd	200	100	0.75	18660	26125	27.5	1.54	5500	13750	27.4	115	85.0	42.5	8.0
10Cd	225	100	0.73	20990	29385	27.5	1.41	6360	15900	27.4	140.8	84.2	37.4	9.4

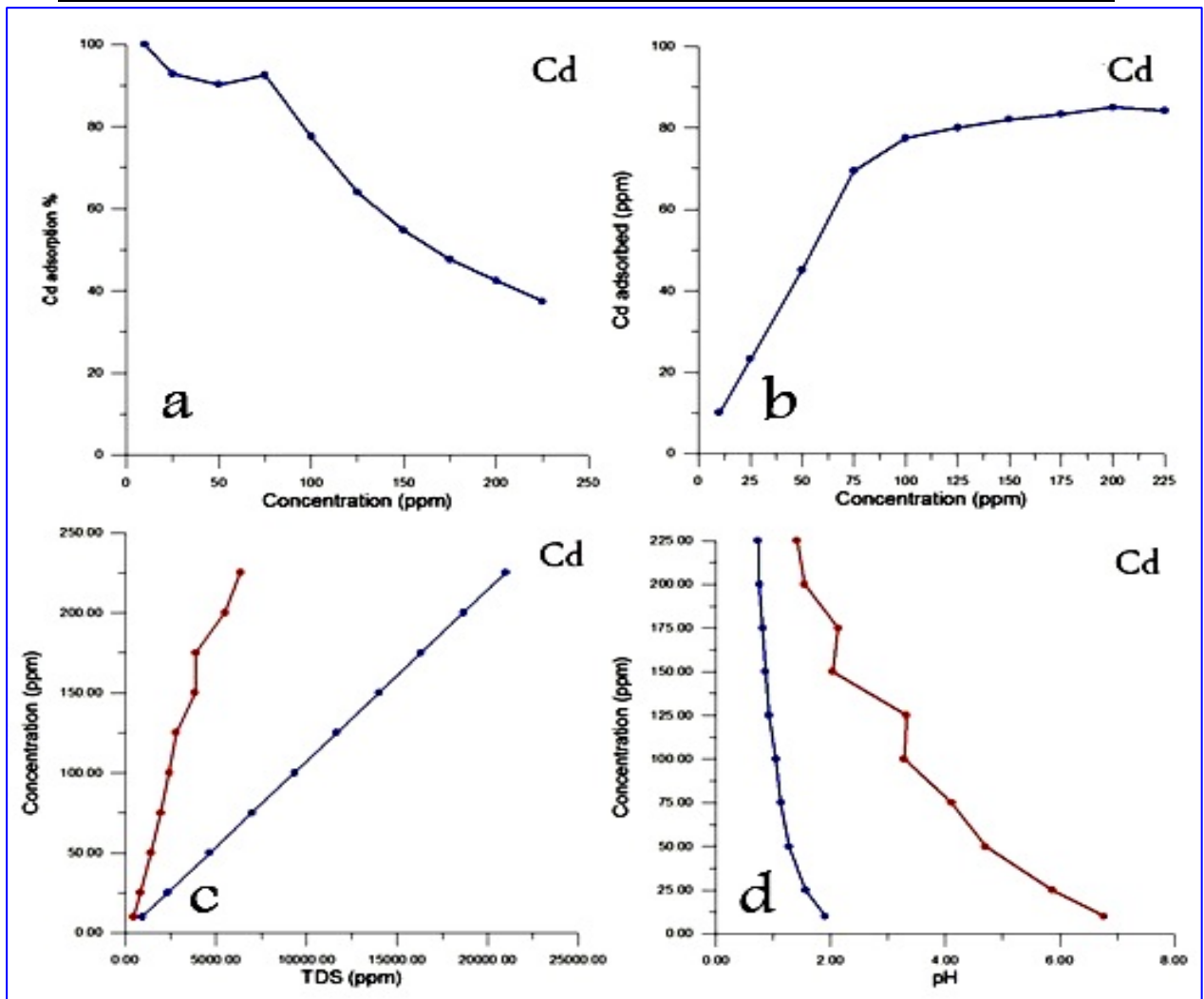


Figure 4-4: The effect of Cd adsorption on palygorskite; a: adsorbance (%) for ten initial solutions of different concentration, b: the effect of concentration on adsorption, c: TDS pattern for initial solutions (blue line) before experiment and final solutions (red line) after experiment, d: changes of pH before experiment (blue line) and after experiment (red line).

This proves that the absorption process has proceeded. Basically, the electrical conductivity (EC) is positively correlated with TDS. The hydrogen number (pH) was changed in the initial solutions from 1.9-0.73 toward alkaline between 6.77 and 0.73 (Table 4-8). The change in pH toward alkaline refers to the occupation of protons (H^+) some negative sites in palygorskite structure.

4-3-3-3 Nickel (Ni)

The experimental results of Ni treated with palygorskite for ten concentrations are listed in Table 4-9. The Ni concentration in the initial solutions (10, 25, 50, 75, 100, 125, 150, 175, 200, 225 ppm) that have been treated with 1 gm palygorskite are 2.22, 7.8, 16, 25, 32.4, 50, 67.7, 87.6, 111.5 and 135.8 ppm) respectively. This indicates that the sorption (%) was 77.8, 68.8, 68, 66.6, 67.6, 60, 54.8, 49.9, 44.3 and 39.6%) respectively (Figure 4-5a).

The maximal sorption of Ni is 67.6% when the initial concentration was 100 ppm (Figure 4-5b). The sorption efficiency at the high concentration seems to decrease at initial solutions of 125 to 225 ppm, where it decreases from 60% to 39.6% (Table 4-9). This is very clear in the amount Cd sorption (ppm), which reduced to 75 to 89.2 ppm for the initial solutions of 125- 125 ppm (Table 4-9). The decrease of sorption efficient at solutions of high concentrations can be attributed to the strong competition between cations on the negative sites on palygorskite.

Before the start of the experiment, TDS ranged between 895 and 19327 ppm; then after the experiment, it clearly decreased to between 394 and 6850 ppm (Figure 4-5c and Table 4-9). This proves that the absorption process has happened. Basically, the electrical conductivity (EC) is positively correlated with TDS and also it decreased during the end of the sorption experiment.

The hydrogen number (pH) was changed in the initial solutions from 2.02-0.61 toward alkaline between 6.85 and 2.05 (Figure 4-5d and Table 4-9). The change in pH toward alkaline is just referring to the occupation of protons (H^+) some negative sites in palygorskite structure.

Table 4-9: Results of laboratory experiments of Nickle (Ni) sorption on palygorskite in ten solutions of various concentrations.

Sample number	Before experiment						After experiment							
	Initial conc. (ppm)	Total Vol (ml)	PH	TDS (mg/l)	EC (µs/cm)	T°C	PH	TDS (mg/l)	EC (µs/cm)	T°C	Final conc. (ppm)	Sorption (ppm)	Sorption (%)	Salinity (‰)
1Ni	10	100	2.02	859	1716	26.5	6.85	394	875	24.5	2.22	7.78	77.8	0.2
2Ni	25	100	1.6	2148	4295	26.5	5.7	875	1735	24.5	7.8	17.2	68.8	0.8
3Ni	50	100	1.3	4290	9050	26.5	5.01	1445	2880	24.5	16	34	68	1.5
4Ni	75	100	1.27	6442	12240	26.5	5.17	1536	3070	24.5	25	50	66.6	1.6
5Ni	100	100	1.0	8590	16750	26.5	4.52	3010	6040	24.5	32.4	67.6	67.6	3.3
6Ni	125	100	0.85	10737	21151	26.5	4.25	3702	7220	24.5	50	75	60	4.0
7Ni	150	100	0.76	12885	25512	26.5	3.75	4185	8290	24.5	67.7	82.3	54.8	4.6
8Ni	175	100	0.72	15032	29763	26.5	3.89	5148	9990	24.5	87.6	87.4	49.9	5.6
9Ni	200	100	0.68	17185	33682	26.5	3.11	5189	10250	24.5	111.5	88.5	44.3	5.8
10Ni	225	100	0.61	19327	40586	26.5	2.05	6850	13600	24.5	135.8	89.2	39.6	7.6

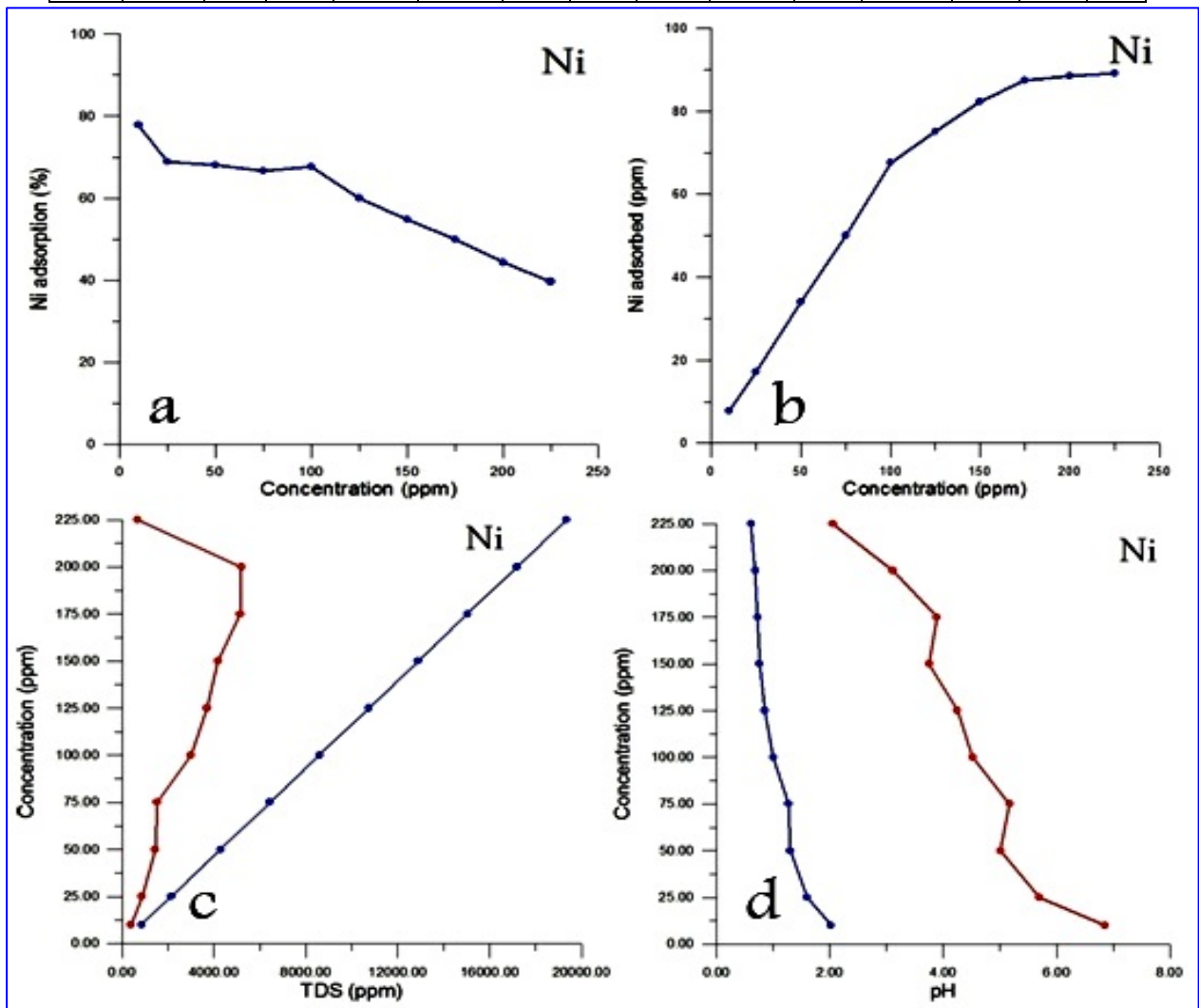


Figure 4-5: The effect of Ni adsorption on palygorskite; a: adsorbance (%) for ten initial solutions of different concentration, b: the effect of concentration on adsorption, c: TDS pattern for initial solutions (blue line) before experiment and final solutions (red line) after experiment, d: changes of pH before experiment (blue line) and after experiment (red line).

4-3-3-4 Chromium (Cr)

The experimental results of Chromium treated with palygorskite for ten concentrations are listed in Table 4-10. The Cr concentrations in the initial solutions that have been treated with 1 gm palygorskite were reduced after the end of the experiment. The adsorption (%) of Cr at the solution of initial concentration (10 ppm) was 99.8% and then began to decrease with the increased Pb concentration (Figure 4-6a).

The Cr concentrations in the initial solutions (10, 25, 50, 75, 100, 125, 150, 175, 200, 225 ppm) have been treated with 1 gm palygorskite, then became as 0.02, 0.2, 3.9, 12.4, 14.5, 18, 40, 50, 60, 75 ppm respectively. The Cr adsorption (%) for the initial solutions (25, 50, 75, 100, 125, 150, 175, 200, 225 ppm) was 99.3, 92.2, 85, 85.5, 85.6, 73.5, 71.5, 70 and 66.7% respectively. Figure 4-6a clearly shows the status of decrease adsorption efficiency with increase concentration.

It represents the amount of Cr adsorbed onto palygorskite with increasing concentration of the initial solution. In case of the initial solution has 10 ppm, the amount of Cr tends to be almost totally adsorbed (9.98 ppm); but in case of the initial solution has 100 ppm, the amount of Cr that adsorbed on palygorskite is 85.5 ppm, and the maximal adsorption (125 ppm) was with the initial solution of concentration 225 ppm (Figure 4-6b); this is the maximal sorption (%) of Cr on palygorskite. Basically as also known, the Total dissolved solid (TDS) is directly proportional with the increase in concentrations; this means a positive relationship between TDS and concentration (Figure 4-6c). The decrease of TDS value is just an evidence for the happening of adsorption process (Shukla, et al., 2003) (Figure 4-6c).

TDS of initial solutions varies from 944 to 21240 ppm (Table 4-10) due to the Cr concentration in each solution. After the experiments; TDS clearly decreases and became varies between 413 and 8027 ppm indicating to the adsorption process. For this set of experiments, pH (2-0.65) of the initial solutions increased with the increase of adsorption until it reaches between 6.17 and 1.78 (Table 4-10). The change in pH toward alkaline refers to the occupation of protons (H^+) some negative sites in the palygorskite structure.

Table 4-10: Results of laboratory experiments of chromium (Cr) sorption on palygorskite in ten solutions of various concentrations.

Sample number	Before experiment						After experiment							
	Initial conc. (ppm)	Total Vol (ml)	PH	TDS (mg/l)	EC ($\mu\text{s}/\text{cm}$)	T $^{\circ}\text{C}$	PH	TDS (mg/l)	EC ($\mu\text{s}/\text{cm}$)	T $^{\circ}\text{C}$	Final conc. (ppm)	Sorption (ppm)	Sorption (%)	Salinity (‰)
1Cr	10	100	2.0	944	1889	27.5	6.17	413	917	26.5	0.02	9.98	99.8	0.2
2Cr	25	100	1.51	2360	4484	27.5	5.14	856	1744	26.5	0.2	24.8	99.3	1.0
3Cr	50	100	1.25	4720	9440	27.5	4.34	1433	2986	26.5	3.9	46.1	92.2	2.0
4Cr	75	100	1.07	7080	13806	27.5	3.96	2515	5030	26.5	12.4	62.6	85	2.7
5Cr	100	100	0.91	9440	18690	27.5	3.51	3360	6720	26.5	14.5	85.5	85.5	3.7
6Cr	125	100	0.86	11800	23485	27.5	2.86	4220	8401	26.5	18.0	107	85.6	4.7
7Cr	150	100	0.82	14160	28320	27.5	2.19	6366	10680	26.5	40	110	73.5	6.1
8Cr	175	100	0.8	16520	32544	27.5	2.02	6837	12555	26.5	50	125	71.5	7.3
9Cr	200	100	0.71	18880	37760	27.5	1.82	7308	14470	26.5	60	140	70	8.5
10Cr	225	100	0.65	21240	42055	27.5	1.78	8027	15950	26.5	75	150	66.7	9.4

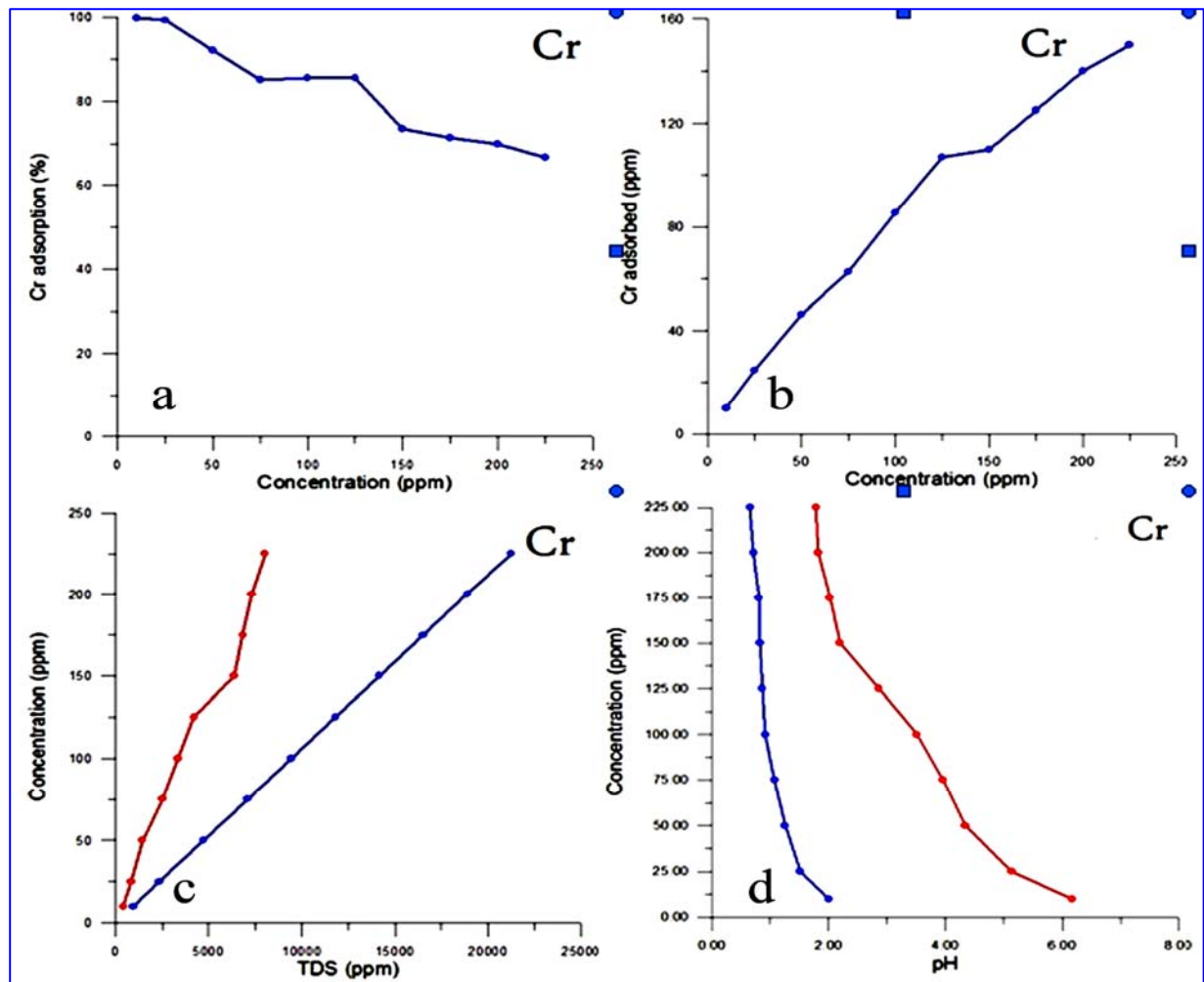


Figure 4-6: The effect of Cr adsorption on palygorskite; a: adsorbance (%) for ten initial solutions of different concentration, b: the effect of concentration on adsorption, c: TDS pattern for initial solutions (blue line) before experiment and final solutions (red line) after experiment, d: changes of pH before experiment (blue line) and after experiment (red line).

4-3-3-5 Cobalt (Co)

The experimental results of cobalt treated with palygorskite for ten concentrations are listed in Table 4-11. The Co concentration in the initial solutions at the beginning of the experiments (10, 25, 50, 75, 100, 125, 150, 175, 200, 225 ppm) that have been treated with 1 gm palygorskite were reduced to 2.21, 7.7, 14.7, 33, 50 66.4, 90, 113.5, 138.9 and 162.8 ppm) respectively. This indicates the sorption (%) was 77.9, 69.2, 71, 56, 50, 46.9, 40, 35, 30.6 and 26) respectively (Figure 4-7a). The optimize sorption of Co is 46.9% when the initial concentration was 125 ppm (Figure 4-7b). The sorption efficiency at the high concentration seems to be slowly elevated as at initial solutions of 150 to 225 ppm, where it increased from 60% to 64% (Table 4-11). The decrease of sorption efficient at solutions of high concentrations can be attributed to the strong competition between cations on the negative sites on palygorskite.

Before the start of the experiment, TDS was ranged between 968-21780 ppm; then after the end of the experiment, it clearly decreased to be varied between 386 and 6245 ppm (Figure 4-7c and Table 4-11). This confirms that the absorption process was happened. Basically, the electrical conductivity (EC) is positively proportional with TDS. The hydrogen number (pH) changed in the initial solutions from 1.92-0.75 toward alkaline to between 6.56 and 2.26 (Table 4-11). The change in pH to alkaline referring to the occupation of protons (H^+) some negative sites in palygorskite structure.

Table 4-11: Results of laboratory experiments of cobalt (Co) sorption on palygorskite in ten solutions of various concentrations.

Sample number	Before experiment						After experiment							
	Initial conc. (ppm)	Total Vol (ml)	PH	TDS (mg/l)	EC (μ s/cm)	T $^{\circ}$ C	PH	TDS (mg/l)	EC (μ s/cm)	T $^{\circ}$ C	Final conc. (ppm)	Sorption (ppm)	Sorption (%)	Salinity (‰)
1Co	10	100	1.92	968	1931	27.4	6.56	386	855	27.4	2.21	7.79	77.9	0.2
2Co	25	100	1.54	2420	4622	27.4	5.78	821	1640	27.4	7.7	17.3	69.2	0.7
3Co	50	100	1.29	4840	9244	27.4	5.21	1412	2830	27.4	14.7	35.5	71	1.6
4Co	75	100	1.16	7260	13866	27.4	4.89	2260	4520	27.4	33.0	42.0	56	2.4
5Co	100	100	1.07	9680	18488	27.4	4.23	2890	5780	27.4	50.0	50.0	50	3.1
6Co	125	100	1.0	12100	23111	27.4	2.3	3880	7760	27.4	66.4	58.6	46.9	4.3
7Co	150	100	0.89	14520	27733	27.4	2.34	4515	9030	27.4	90.0	60.0	40	5.1
8Co	175	100	0.83	16940	32355	27.4	2.08	5090	10180	27.4	113.5	61.5	35	5.8
9Co	200	100	0.8	19360	36977	27.4	1.54	7140	14280	27.4	138.9	61.1	30.6	7.2
10Co	225	100	0.75	21780	41599	27.4	2.26	6245	12490	27.4	162.8	64.0	28	8.3

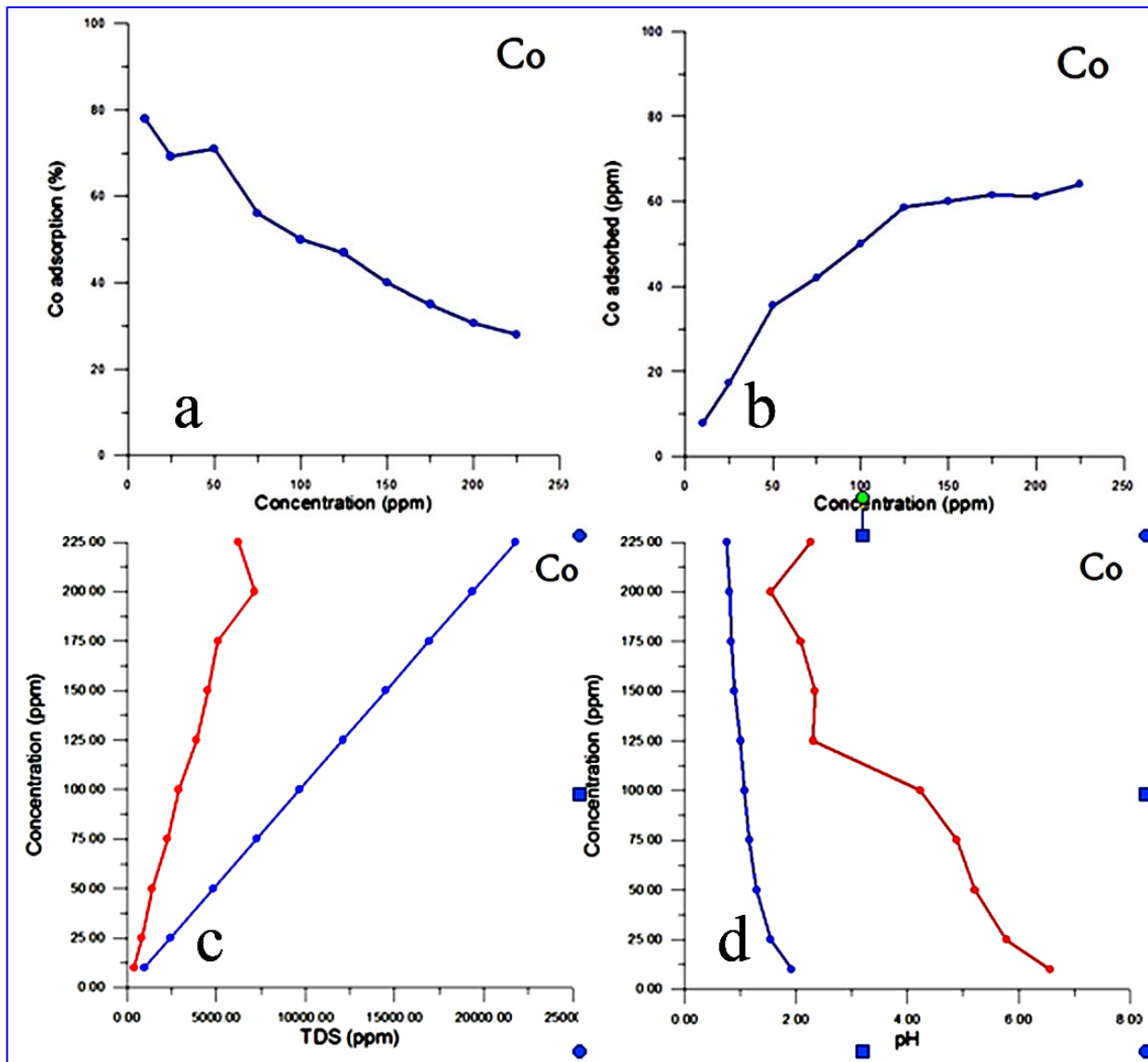


Figure 4-7: The effect of Co adsorption on palygorskite; a: adsorbance (%) for ten initial solutions of different concentration, b: the effect of concentration on adsorption, c: TDS pattern for initial solutions (blue line) before experiment and final solutions (red line) after experiment, d: changes of pH before experiment (blue line) and after experiment (red line).

4-3-3-6 Vanadium (V)

The experimental results of Vanadium treated with palygorskite for ten concentrations are listed in Table 4-12. The V concentrations in the initial solutions that have been treated with 1 gm palygorskite were reduced after the end of the experiment. The adsorption (%) of V at the solution of initial concentration (10 ppm) was 86.1% and then started to decrease slightly with the increased V concentration (Figure 4-8a). The V adsorption (%) for the initial solutions (25, 50, 75, 100, 125, 150, 175, 200, 225 ppm) was 86.1, 78.1, 60.8, 58.6, 55, 50.4, 49.3, 47.4, 45.5 and 45.3) respectively. Figure 4-8a clearly shows the status of decrease adsorption efficiency with increase

concentration due to the competition among ions of positive charge on the negative sites on palygorskite. The V concentrations in the initial solutions (10, 25, 50, 75, 100, 125, 150, 175, 200, 225 ppm) decrease to be 1.39, 5.49, 19.6, 31, 45, 62, 76, 92, 109, 123 ppm) respectively after end the experiments. It represents the amount of V adsorbed onto palygorskite with increasing concentration of the initial solution. The relationship between the V adsorbed and concentration of the solution is found to be clearly positive (Figure 4-6b). In case of the initial solution has 10 ppm, the amount of V tends to be adsorbed (8.61 ppm) on palygorskite; but in case of the initial solution has 225 ppm, the amount of V that adsorbed on palygorskite is 102 ppm which is 45.3%. Figure 4-8b illustrates the linear relations between concentration and adsorption. Basically is also known, the Total dissolved solid (TDS) is directly proportional to the increase in concentrations; this means a positive relationship between TDS and concentration and the decrease of TDS value is an evidence for the happening of adsorption process (Figure 4-8c). TDS of initial solutions varies from 1469 to 33052 ppm (Table 4-12) due to the V concentration in each solution. After the end of the experiments; TDS clearly decreased between 350 and 9622 ppm indicating the adsorption process. For this set of experiments, pH (1.78-0.650.73) of the initial solutions increased with the increase of adsorption until it became varying between 6.33 and 1.38 (Table 4-12). The change in pH toward alkaline refers to the occupation of protons (H^+) some negative sites in palygorskite structure.

Table 4-12: Results of laboratory experiments of vanadium (V) sorption on palygorskite in ten solutions of various concentrations.

Sample number	Before experiment						After experiment							
	Initial conc. (ppm)	Total Vol (ml)	PH	TDS (mg/l)	EC (μ s/cm)	T $^{\circ}$ C	PH	TDS (mg/l)	EC (μ s/cm)	T $^{\circ}$ C	Final conc. (ppm)	Sorption (ppm)	Sorption (%)	Salinity (%)
1V	10	100	1.78	1469	2940	27	6.33	530	1176	26.3	1.39	8.61	86.1	0.4
2V	25	100	1.69	3672	7712	27	5.05	1020	2036	26.3	5.49	19.51	78.1	1.0
3V	50	100	1.28	7345	14543	27	4.02	1561	3119	26.3	19.6	30.4	60.8	1.8
4V	75	100	1.23	11017	21703	27	3.73	2287	4550	26.3	31	44	58.6	2.4
5V	100	100	1.13	14690	30990	27	3.1	2808	5560	26.3	45	55	55	3.0
6V	125	100	0.95	18362	36356	27	2.48	2995	6290	26.3	62	63	50.4	3.4
7V	150	100	0.89	22035	44062	27	1.63	5352	11400	26.3	76	74	49.3	6.4
8V	175	100	0.86	25707	50771	27	1.65	6091	12000	26.3	92	83	47.4	6.9
9V	200	100	0.79	29380	56997	27	1.4	7857	16500	26.3	109	91	45.5	9.8
10V	225	100	0.73	33052	65344	27	1.38	9622	19000	26.3	123	102	45.3	11.3

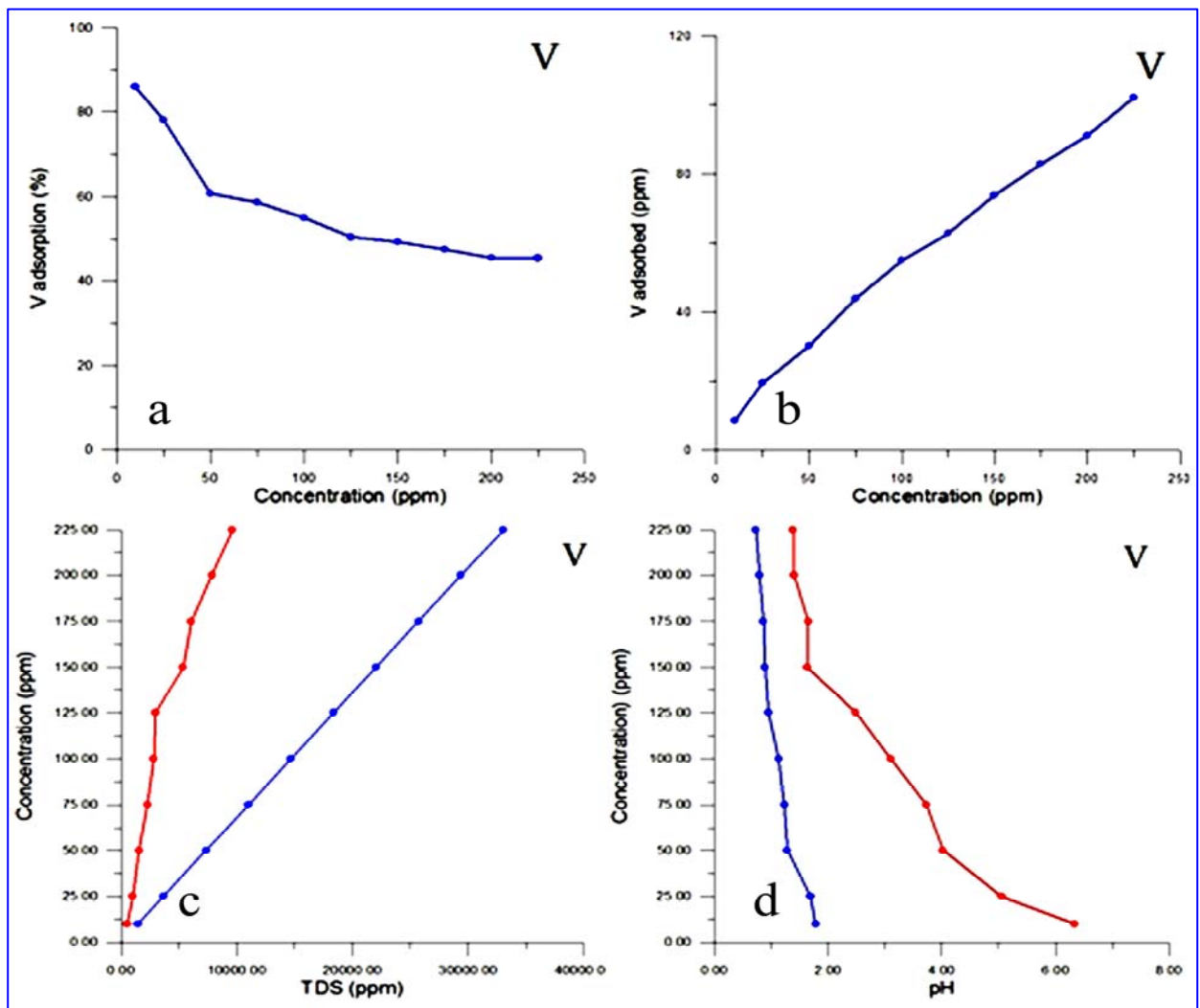


Figure 4-8: The effect of V adsorption on palygorskite; a: adsorbance (%) for ten initial solutions of different concentration, b: the effect of concentration on adsorption, c: TDS pattern for initial solutions (blue line) before experiment and final solutions (red line) after experiment, d: changes of pH before the experiment (blue line) and after the experiment (red line).

4-3-3-7 Zinc (Zn)

The experimental results of zinc treated with palygorskite for ten concentrations are listed in Table 4-13. The Zn concentrations in the initial solutions that have been treated with 1 gm palygorskite were reduced after the end of the experiment. The adsorption (%) of Zn at an initial concentration (10 ppm) was 94%; then decreased slightly with the increase Zn concentration (Figure 4-9a). The Zn adsorption (%) for the initial solutions of 25, 50, 75, 100, 125, 150, 175, 200, 225 ppm was 92, 82.4, 69.3, 66, 64, 59, 56, 55 and 50.2 respectively. Figure 4-9a clearly shows the status of decrease in adsorption efficiency with increase concentration due to the competition among ions of positive charge on the negative sites on palygorskite.

Table 4-13: Results of laboratory experiments of zinc (Zn) sorption on palygorskite in ten solutions of various concentrations.

Sample number	Before experiment						After experiment							
	Initial conc. (ppm)	Total Vol (ml)	PH	TDS (mg/l)	EC ($\mu\text{s/cm}$)	T $^{\circ}\text{C}$	PH	TDS (mg/l)	EC ($\mu\text{s/cm}$)	T $^{\circ}\text{C}$	Final conc. (ppm)	Sorption (mm)	Sorption (%)	Salinity (%)
1Zn	10	100	1.54	1200	2250	26.5	5.49	841	1864	26.7	3.29	9.4	94	0.8
2Zn	25	100	1.53	3004	6000	26.5	5.27	944	1888	26.7	8.61	23	92	0.9
3Zn	50	100	1.3	6005	11830	26.5	4.68	1570	3131	26.7	32.2	41.2	82.4	1.7
4Zn	75	100	1.15	9020	17769	26.5	4.06	2578	5080	26.7	69.7	52	69.3	2.7
5Zn	100	100	1.07	12034	23466	26.5	3.25	3145	6260	26.7	93.1	66	66	3.4
6Zn	125	100	0.75	15033	29465	26.5	4.16	3960	7720	26.7	112	80	64	4.3
7Zn	150	100	0.89	18038	34095	26.5	3.95	2949	8510	26.7	277	89	59	4.8
8Zn	175	100	0.83	21030	39745	26.5	2.87	5364	10460	26.7	176	98	56	6
9Zn	200	100	0.77	24021	47561	26.5	3.35	5495	10770	26.7	187	111	55	6.2
10Zn	225	100	0.71	27025	56752	26.5	2.73	6317	12500	26.7	207	113	50.2	7.2

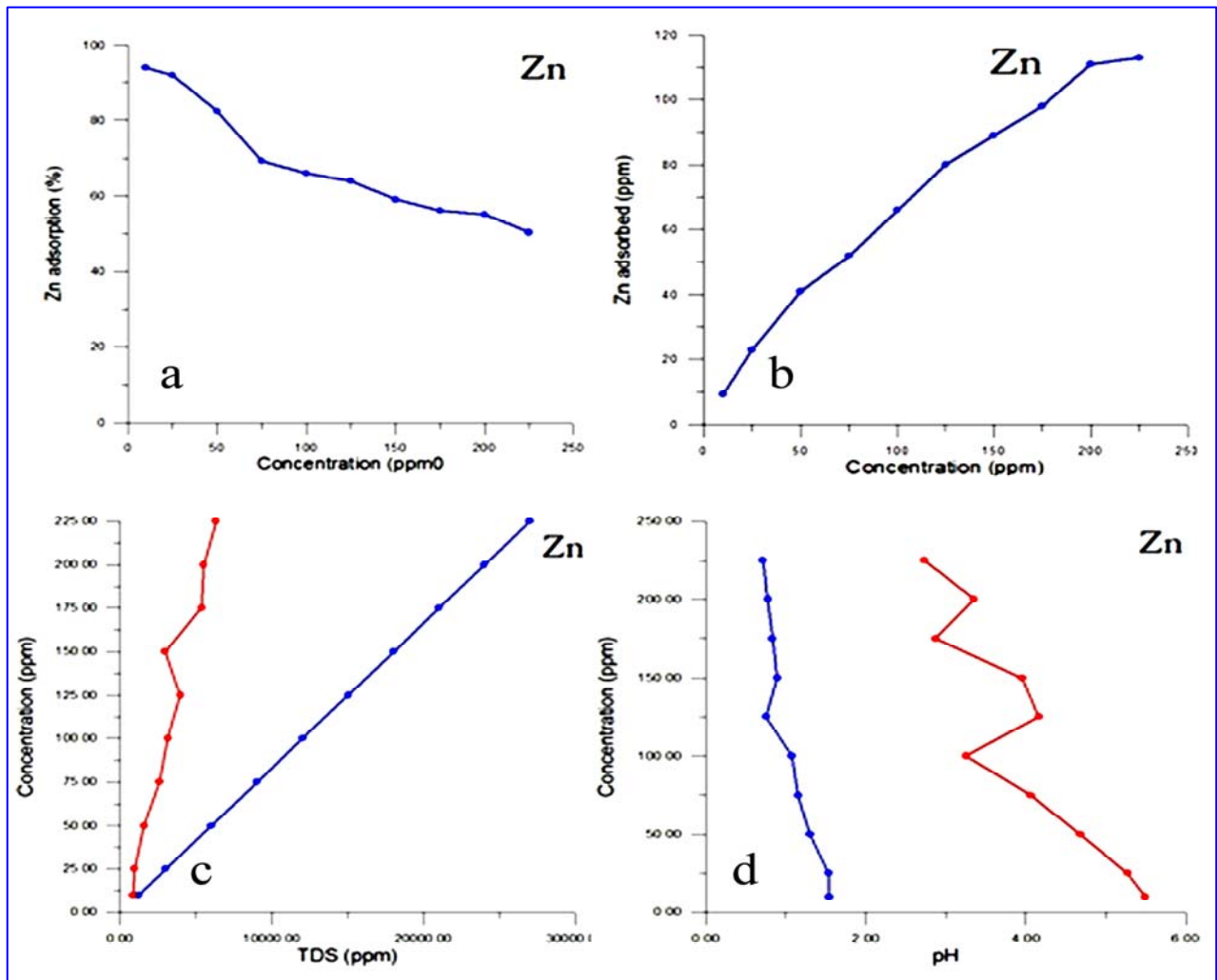


Figure 4-9: The effect of Zn adsorption on palygorskite; a: adsorbance (%) for ten initial solutions of different concentration, b: the effect of concentration on adsorption, c: TDS pattern for initial solutions (blue line) before experiment and final solutions (red line) after experiment, d: changes of pH before experiment (blue line) and after experiment (red line).

The Zn concentrations in the initial solutions (10, 25, 50, 75, 100, 125, 150, 175, 200, 225 ppm) are decreased after end the experiments to be 3.29, 8.61, 32.2, 69.7, 93.1, 112, 277, 176, 187, and 207 ppm respectively. The relationship between the Zn adsorbed and concentration of the solution is found to be clear positive linear (Figure 4-9b). The Total dissolved solid (TDS) is directly proportional to the increase in concentrations; Relationship between TDS and concentration of solutions before and after experiments shows how successful experiences in the processes of absorption on palygorskite (Figure 4-9c). TDS of initial solutions ranges from 1200 to 27025 ppm (Table 4-13) due to the Zn concentration in each solution. After the end of experiments; TDS clearly decreased to between 841 to 6317 ppm indicating adsorption process. For this set of experiments, pH (1.54-0.71) of the initial solutions increased with the increase of adsorption until it became varying between 6.33 5.495.49 and 2.73 (Table 4-13). The changing in the pH after the end of the experiment is evidence of absorption, the change towards alkaline proof link protons in the negative sites.

4-3-3-8 Copper (Cu)

The experimental results of Zinc treated with palygorskite for ten concentrations are listed in Table 4-14. The absorbency of copper increases in solutions of low concentration and weaken in highly concentrated solutions maintaining positive relationship. Palygorskite adsorb Cu from initial solution of concentration 10, 25, 50, and 75 ppm with adsorbance efficiency 99.9, 98.7, 76.8, 66.6% respectively (Table 4-12) and Figure 4-10a. But for solutions of higher concentration (100, 125, 150, 175, 200 and 225 ppm), palygorskite has become low efficient for adsorbing Cu (65.5, 64, 63, 61.1, 57.5, and 53.3 %) Table 4-14. Despite the decrease in absorption efficiency with high concentrations, but the relationship remains a positive correlation (Figure 4-10b).

TDS actually has a positive relationship with the Cu concentrations of the initial solutions. TDS in the initial solutions varies between 870-19575 ppm; then it decreases in the final solution (after experiments) ranging between 426 and 8525 ppm (Table 4-14). This relationship has changed in the final solutions, where Figure 4-10c shows significant decrease in the value of TDS referring to the changes happened in Cu concentrations in solution. This means that the effectiveness of the palygorskite to sorp Cu from solution,

Table 4-14: Results of laboratory experiments of copper (Cu) sorption on palygorskite in ten solutions of various concentrations.

Sample number	Before experiment						After experiment							
	Initial conc. (ppm)	Total Vol (ml)	PH	TDS (mg/l)	EC ($\mu\text{s/cm}$)	ToC	PH	TDS (mg/l)	EC ($\mu\text{s/cm}$)	ToC	Final conc. (ppm)	Sorption (ppm)	Sorption (%)	Salinity (‰)
1Cu	10	100	1.98	870	1739	26	6.62	426	899	26.5	0.01	9.99	99.9	0.2%
2Cu	25	100	1.58	2175	4025	26	5.74	900	1800	26.5	0.3	24.7	98.7	0.8%
3Cu	50	100	1.34	4350	8047	26	4.33	1451	2860	26.5	11.6	38.4	76.8	1.7%
4Cu	75	100	1.13	6525	11745	26	3.70	1990	3920	26.5	25	50	66.6	2.5%
5Cu	100	100	1.05	8700	16525	26	3.35	3008	6016	26.5	34.5	65.5	65.5	3.4%
6Cu	125	100	0.95	10875	20225	26	2.66	4000	7600	26.5	35	80	64	4.2%
7Cu	150	100	0.84	13050	24790	26	2.44	4864	9000	26.5	53	97	63	5%
8Cu	175	100	0.79	15225	28927	26	1.83	6170	11600	26.5	68	107	61.1	6.6%
9Cu	200	100	0.77	17400	32195	26	1.75	7388	13300	26.5	85	115	57.5	7.7%
10Cu	225	100	0.76	19575	27255	26	1.54	8525	16200	26.5	105	120	53.3	9.5%

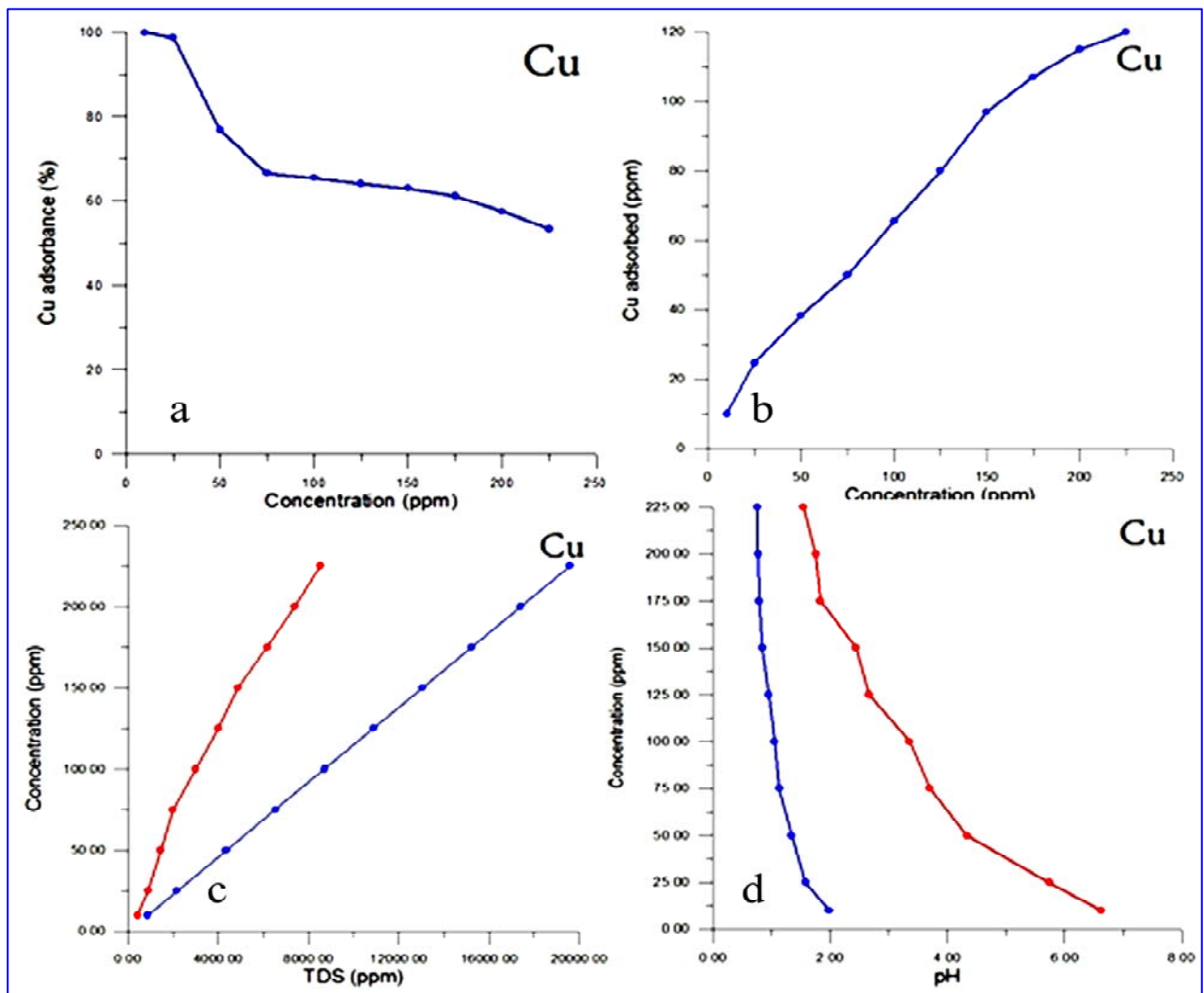


Figure 4-10: The effect of Zn adsorption on palygorskite; a: adsorbance (%) for ten initial solutions of different concentration, b: the effect of concentration on adsorption, c: TDS pattern for initial solutions (blue line) before experiment and final solutions (red line) after experiment, d: changes of pH before experiment (blue line) and after experiment (red line).

causing enrich Cu on the surfaces of palygorskite and the depletion of Cu in the remnant solution.

At the final solutions, pH changed to be ranged between 6.62-1.54, where, it was 1.98-0.76 at the initial solutions (Table 4-14). The changing in the pH is evidence of absorption, the change towards alkaline proof to link protons in the negative sites.

4-3-3-9 Iron (Fe)

The experimental results of Iron treated with palygorskite for ten concentrations are listed in Table 4-15. The Fe concentrations in the initial solutions that have been treated with 1 gm palygorskite were almost totally reduced after the end of the experiment. Iron followed a distinct behavior in absorption, where the sorption ability of palygorskite was very high at all concentrations. Adsorption (%) of palygorskite for the initial solutions (10, 25, 50, 75, 100, 125, 150, 175, 200 and 225 ppm) was very efficient (99.8, 99.92, 97.96, 99.97, 99.98, 99.59, 98.11, 99.54, 99.4 and 99.24%) respectively (Table 4-15 and Figure 4-11a). A positive relationship between initial concentrations and Fe adsorbed on palygorskite was revealed (Figure 4-11b).

TDS normally has a positive relationship with the Fe concentrations of the initial solutions. TDS in the initial solutions varies between 866-19485 ppm; then it decreased and found to be in the final solution as 490-6848 ppm (Table 4-13). This relationship has changed in the final solutions. Figure 4-11c presents a significant decrease in the value of TDS referring to the changes of Fe concentrations in the solutions. This means that the effectiveness of palygorskite to sorp Fe on the its surfaces (palygorskite) and depletion in the remnant solution.

At final solutions, pH changes between 6.56-2.06; where, it was 2.03-0.74 at the initial solutions (Table 4-15). The changing in the pH is evidence of absorption, the change towards alkaline proof to link protons in the negative sites.

Table 4-15: Results of laboratory experiments of iron (Fe) sorption on palygorskite in ten solutions of various concentrations.

Sample number	Before experiment						After experiment							
	Initial conc. (ppm)	Total Vol (ml)	PH	TDS (mg/l)	EC (μ s/cm)	ToC	PH	TDS (mg/l)	EC (μ s/cm)	ToC	Final conc. (ppm)	Sorption (ppm)	Sorption (%)	Salinity (‰)
1Fe	10	100	2.03	866	1735	25.9	6.56	490	973	27	0.02	9.98	99.8	0.3
2Fe	25	100	1.55	2156	4075	25.9	5.71	921	1852	27	0.02	24.98	99.92	0.9
3Fe	50	100	1.3	4330	8660	25.9	5.61	1370	2741	27	0.02	49.98	97.96	1.5
4Fe	75	100	1.2	6495	12275	25.9	4.86	1898	4600	27	0.02	74.98	99.97	2.4
5Fe	100	100	1.03	8660	16973	25.9	5.39	2864	5700	27	0.02	99.98	99.98	3.1
6Fe	125	100	0.85	10825	21325	25.9	4.66	3500	7000	27	0.05	124.95	99.95	3.8
7Fe	150	100	0.84	12990	25330	25.9	3.84	4100	8610	27	2.83	147.17	98.11	4.8
8Fe	175	100	0.83	15155	29855	25.9	2.01	5134	9700	27	0.8	174.2	99.54	5.5
9Fe	200	100	0.78	17320	33600	25.9	1.3	5986	11800	27	1.2	198.8	99.4	7.3
10Fe	225	100	0.74	19485	37995	25.9	2.06	6848	12670	27	1.70	223.3	99.24	10.5

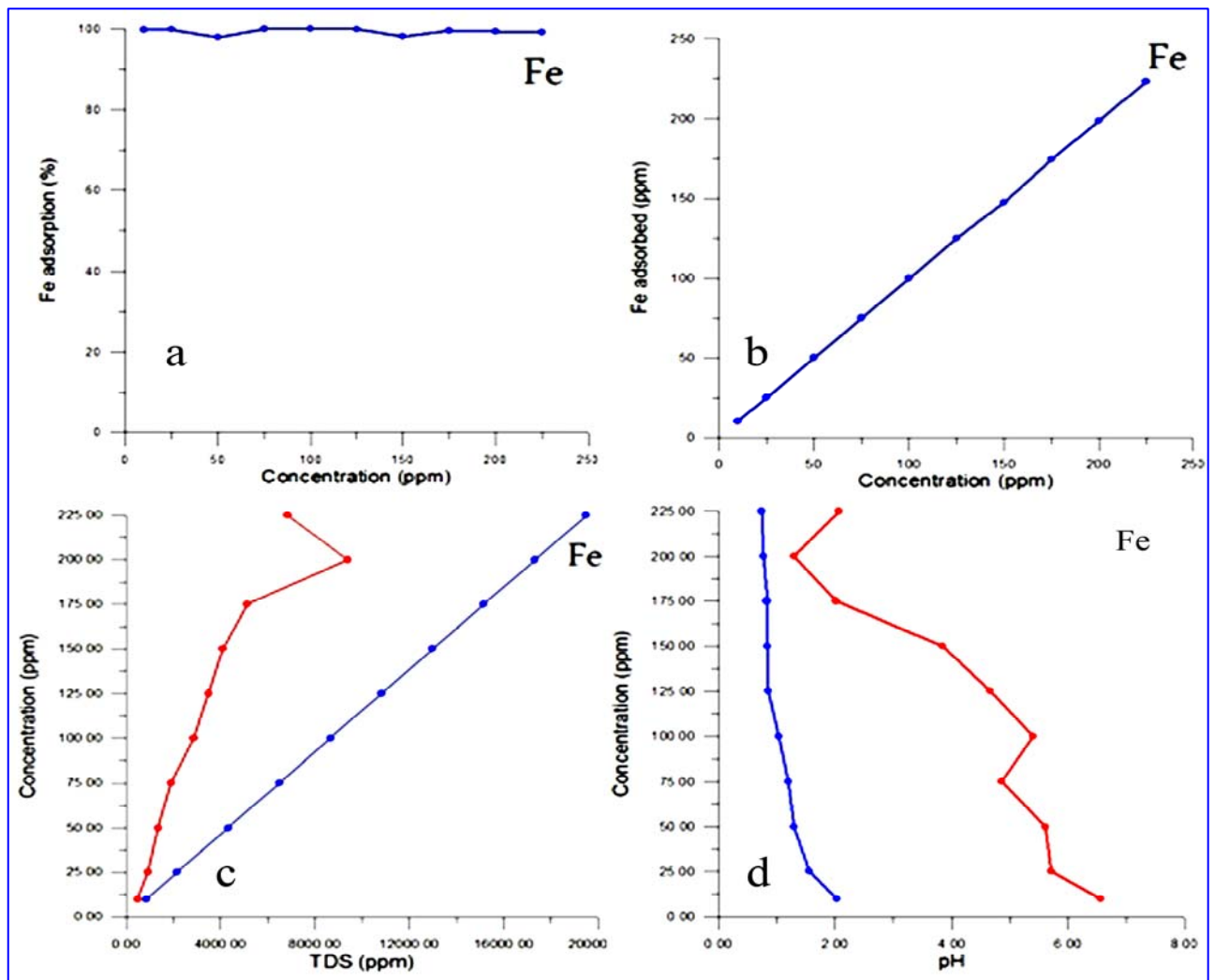


Figure 4-11: The effect of Fe adsorption on palygorskite; a: adsorbance (%) for ten initial solutions of different concentration, b: the effect of concentration on adsorption, c: TDS pattern for initial solutions (blue line) before experiment and final solutions (red line) after experiment, d: changes of pH before experiment (blue line) and after experiment (red line).

4-3-3-10 Manganese (Mn)

The experimental results of manganese treated with palygorskite for ten concentrations are listed in Table 4-16. The Mn concentration in the initial solutions (10, 25, 50, 75, 100, 125, 150, 175, 200, 225 ppm) that have been treated with 1 gm palygorskite became 0.3, 7, 17, 30, 41, 52, 72.1, 91, 112.6 and 134.5 ppm) in the final solution respectively. This indicates that the sorption amount was 9.7, 18, 33, 45, 59, 73, 77.9, 84, 87.4 and 90.5 and the sorption (%) was 77.8, 68.8, 68, 66.6, 67.6, 60, 54.8, 49.9, 44.3 and 39.6% respectively. There is a negative relationship between absorption and concentration (Figure 4-12a). The optimize sorption of Mn is 58.4% when the initial concentration was 125 ppm (Figure 4-12b).

The sorption efficiency at the high concentration seems to be decreased, where it recorded as 40.2% at initial solution of 225 ppm (Table 4-16). The decrease of sorption efficient at solutions of high concentrations can be attributed to the strong competition between cations on the negative sites on palygorskite.

Before the start of the experiment, TDS ranges between 964 and 21712 ppm; then after the end of the experiment, it clearly decreases verging between 410 and 6398 ppm (Table 4-16 and Figure 4-12c). This proves that the absorption process has happened. Basically, the electrical conductivity (EC) is positively correlated with TDS, and it also decreased during the end of the sorption experiment.

The hydrogen number (pH) was changed in the initial solutions from 1.94-0.65 toward alkaline ranging from 6.67 and 2.22 (Table 4-16 and Figure 4-12d). The change in pH toward alkaline is just referring to the occupation of protons (H^+) some negative sites in palygorskite structure.

Table 4-16: Results of laboratory experiments of manganese (Mn) sorption on palygorskite in ten solutions of various concentrations.

Sample number	Before experiment						After experiment							
	Initial conc. (ppm)	Total Vol (ml)	PH	TDS (mg/l)	EC ($\mu\text{s/cm}$)	ToC	PH	TDS (mg/l)	EC ($\mu\text{s/cm}$)	ToC	Final conc. (ppm)	Sorption (mm)	Sorption (%)	Salinity (‰)
1Mn	10	100	1.94	964	1935	27.1	6.67	410	890	27	0.3	9.7	97	0.2
2Mn	25	100	1.52	2410	4771	27.1	6.0	874	1754	27	7	18	72	0.8
3Mn	50	100	1.27	4825	9601	27.1	5.0	1325	2786	27	17	33	66	1.6
4Mn	75	100	1.11	7237	15197	27.1	4.24	2430	4830	27	30	45	60	2.5
5Mn	100	100	1.04	9650	19300	27.1	3.91	3052	5800	27	41	59	59	3.1
6Mn	125	100	0.96	12062	24124	27.1	3.88	2914	7500	27	52	73	58.4	4.2
7Mn	150	100	0.85	14475	28515	27.1	3.55	4444	8800	27	72.1	77.9	52	4.9
8Mn	175	100	0.75	16887	35463	27.1	2.37	5127	10100	27	91	84	48	5.7
9Mn	200	100	0.68	19300	38407	27.1	2.85	6000	11400	27	112.6	87.4	43.7	6.5
10Mn	225	100	0.65	21712	45595	27.1	2.22	6398	12700	27	134.5	90.5	40.2	7.3

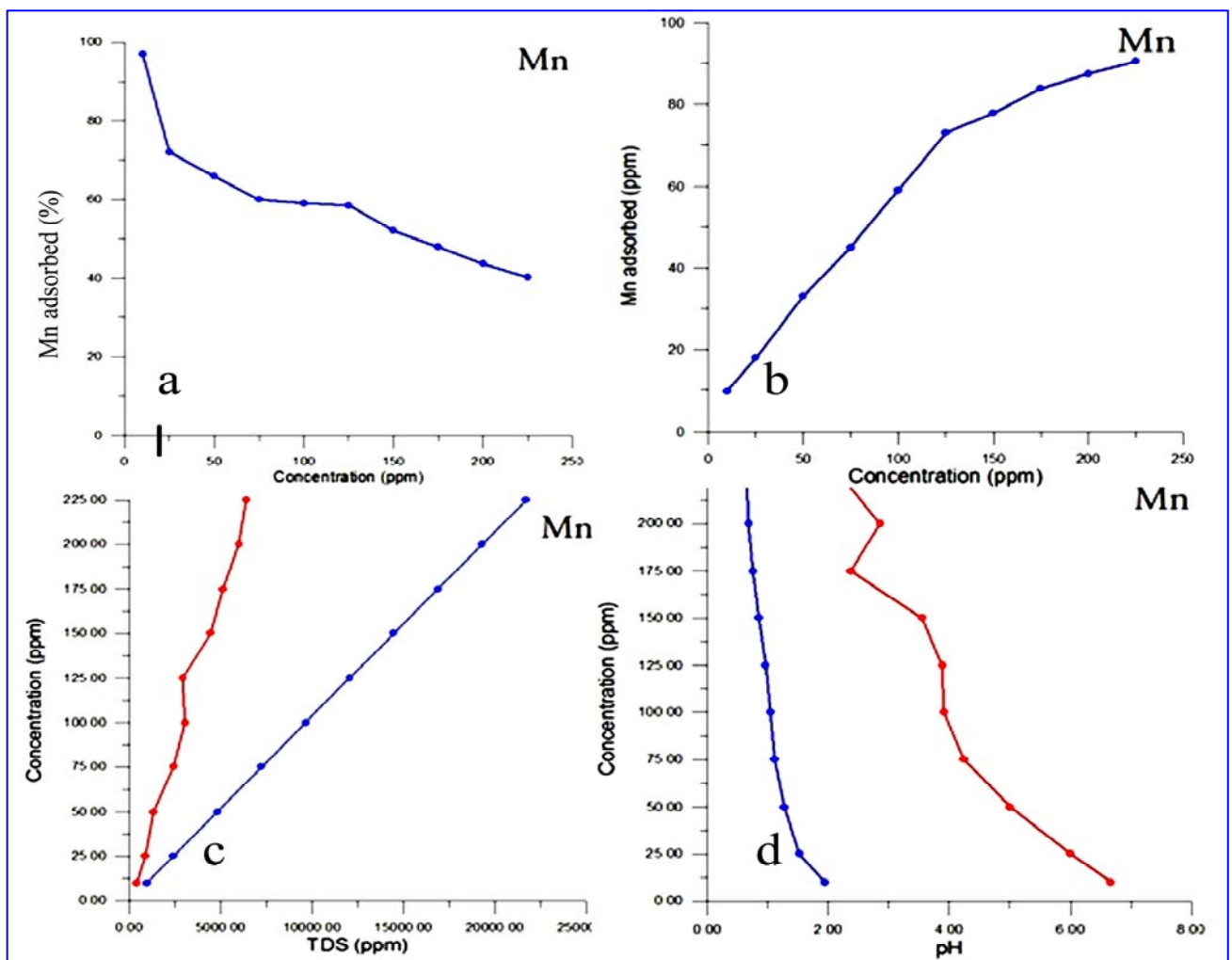


Figure 4-12: The effect of Mn adsorption on palygorskite; a: adsorbance (%) for ten initial solutions of different concentration, b: the effect of concentration on adsorption, c: TDS pattern for initial solutions (blue line) before experiment and final solutions (red line) after experiment, d: changes of pH before experiment (blue line) and after experiment (red line).

4-3-3-11 Boron (B)

The experimental results of boron treated with palygorskite for ten concentrations are listed in Table 4-17. The B concentrations in the initial solutions that have been treated with 1 gm palygorskite were slightly reduced in the final solution (after the end of the experiment). The B concentrations in the initial solutions (10, 25, 50, 75, 100, 125, 150, 175, 200, 225) ppm became (8.9, 24, 45, 71.2, 89.8, 119, 146, 170.2, 193.8 and 222) ppm in the final solution, respectively. This indicates that the sorption amount was very little such as 1.1, 1, 5, 3.8, 10.2, 6, 4, 4.8, 6.2, and 3 respectively. Accordingly, the sorption (%) on palygorskite was 11, 4, 10, 5, 10.2, 4.8, 2.66, 2.7, 3.1 and 1.3 respectively; it is very little and there is no clear trend (Figure 4-13a and b).

TDS values at the beginning of the experiments varied between 205-405 ppm, then it slightly decreased to 180-397 ppm (Table 4-17) in the final solution (after the end of experimental) indicating that the B adsorbed with very little amount (Figure 4-13).

At the final solutions, pH changed from 8 to 8.7; where, it was 5.45-5.76 at the initial solutions (Table 4-17). The changing of pH towards the alkaline refers to link protons in the negative sites on palygorskite and at the same time confirms the weak absorption of B on the surface of palygorskite.

Table 4-17: Results of laboratory experiments of boron (B) sorption on palygorskite in ten solutions of various concentrations, Nd=not determined.

Sample number	Before experiment						After experiment								
	Initial conc. (ppm)	Total Vol (ml)	PH	TDS (mg/l)	EC (μ s/cm)	ToC	PH	TDS (mg/l)	EC (μ s/cm)	ToC	Final conc. (ppm)	Sorption (ppm)	Sorption (%)	Salinity (‰)	
1B	10	100	5.45	205	328	27.1	8.0	180	291	26.5	8.9	1.1	11	Nd	
2B	25	100	6.02	220	356	27.1	7.65	217	345	26.5	24	1	4	Nd	
3B	50	100	6.06	245	398	27.1	7.6	220	350	26.5	45	5	10	Nd	
4B	75	100	5.87	264	448	27.1	7.50	250	410	26.5	71.2	3.8	5.0	Nd	
5B	100	100	5.86	280	461	27.1	7.4	249	401	26.5	89.8	10.2	10.2	Nd	
6B	125	100	5.82	302	515	27.1	7.3	294	483	26.5	119	6	4.8	Nd	
7B	150	100	5.91	330	567	27.1	7.34	320	520	26.5	146	4	2.66	Nd	
8B	175	100	5.82	351	585	27.1	7.0	332	537	26.5	170.2	4.8	2.7	Nd	
9B	200	100	5.84	375	650	27.1	7.01	356	602	26.5	193.8	6.2	3.1	Nd	
10B	225	100	5.76	405	680	27.1	7.08	397	635	26.5	222	3	1.3	Nd	

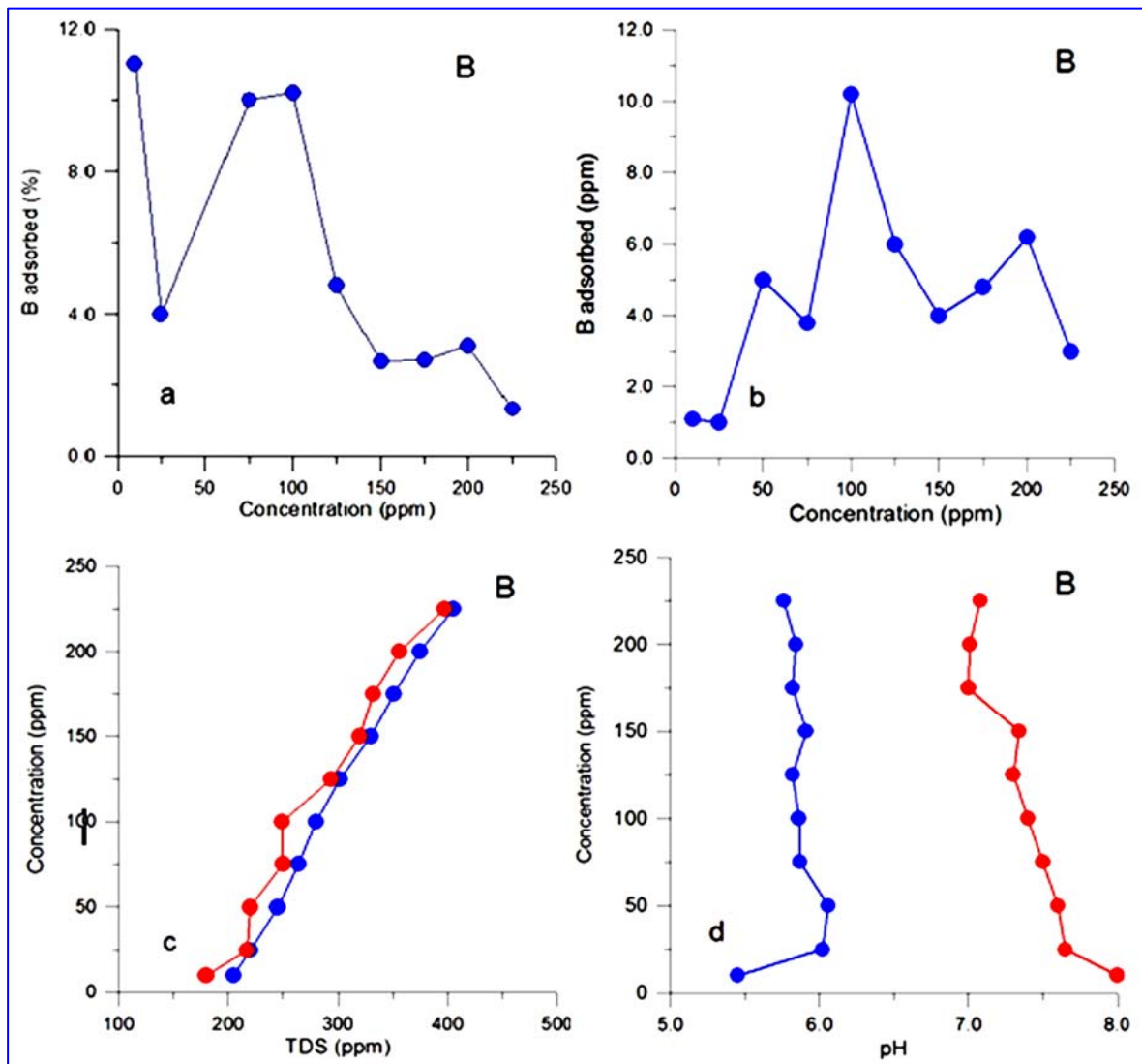


Figure 4-13: The effect of B adsorption on palygorskite; a: adsorbance (%) for ten initial solutions of different concentration, b: the effect of concentration on adsorption, c: TDS pattern for initial solutions (blue line) before experiment and final solutions (red line) after experiment, d: changes of pH before experiment (blue line) and after experiment (red line).

4-4 Sorption efficiency

There are three modes by which clay materials can exert adsorptive power on various molecules, from the liquid phase. These are: physical, exchange, and zeolitic action. Divalent Mg^{2+} , Fe^{2+} , Co^{2+} , Ni^{2+} , Zn^{2+} , Cu^{2+} readily substitute for each other (homovalent substitutions) because their ionic radii are contained between 0.83 \AA (Ni^{2+}) and 0.92 \AA (Fe^{2+}). This is also valid for trivalent Al^{3+} and Fe^{3+} . Trivalent (R^{3+}) can be replaced by divalent (R^{2+}) (heterovalent substitutions).

4-4-1 Cation exchange capacity (CEC) relationship with pH

The elongated grain gave palygorskite a good property of metal adsorption due to the increase of the surface area. Its characteristic high surface area ranges between 150- 360 m²/g . The CEC ranges between 30-50 meq/ 100g (Weiss et al., 1956). The CEC varies with pH conditions because H⁺ protons compete with other cations to fix the exchangeable sites (Meunier, 2005). As pH increases, the concentration of H⁺ declines; the competitive adsorption of heavy metals slows down, the solubility of heavy metals is reduced. However, acidic solution with a pH value of <4.5 releases Al³⁺ from palygorskite lattice. Notably, Al³⁺ in clay: generates adsorption sites, reducing the absorption of heavy metals from the soil (Wu-Chou et al., 2011). Palygorskite has high surface charges, and their CEC values are much higher than those of the same mass of non clay mineral. A low pH (acidic solution) can reduce negative charge, while a high pH (basic solution) increases the negative charge. Therefore, CEC increases as pH increases (Wu-Chou et al., 2011).

4-4-2 Effect of concentration

The effect of concentration on the uptake of aqueous Pb, Cd, Ni, Co, Cr, V, Cu, Zn, Mn, Fe, and B ions by palygorskite is investigated at the initial concentration of 10, 25, 50, 75, 100, 125, 150, 175, 200 and 225 ppm, while keeping the mixing time fixed at 1 hours. Moreover, the data are used to calculate percentage sorption using the equation:

$$\text{Sorption (\%)} = [(C_i - C_f) / (C_i)] \times 100$$

Where, C_i and C_f are the initial and final (equilibrium concentration) metal ion concentrations, respectively. The calculated values for all ions are given in Tables 4-7 to 4-17. For the initial concentrations of 10 ppm, the results indicate almost a 100% removal of ions Pb, Cd, Cr, Cu, Fe, and Mn by palygorskite (Figure 4-14). The percentage sorption decreases with further increase in the initial concentrations up to the initial concentration of 225 ppm. The range of sorption (%) for all ions is illustrated in Figure 4-14.

A negative relationship between concentration and sorption (%) was detected (Figure 4-15). The best absorption has been recorded with of Fe and Cr, where the sorption of Fe adsorbed on palygorskite from initial solutions of 10-225 is 99.9-99.24(%) respectively. In the same manner, and from same initial concentrations, Cr is adsorbed on palygorskite by 99.9-66.7 (Figure 4-14). Pb also responds and tends to be adsorbed on palygorskite particularly

for initial solutions of 10, 25, 125 ppm, where the sorption (%) is 99.5, 81.9 and 76.5% respectively. Boron appears to have weak strength of adsorption; this may be attributed to the low ionic potential. Consequently, the sorption (%) of metals on palygorskite almost shows a marked trend as follows:

Fe>Cr>Pb>Cd>Cu> Ni> Zn >Mn>V>Co>B (Figure 4-16).

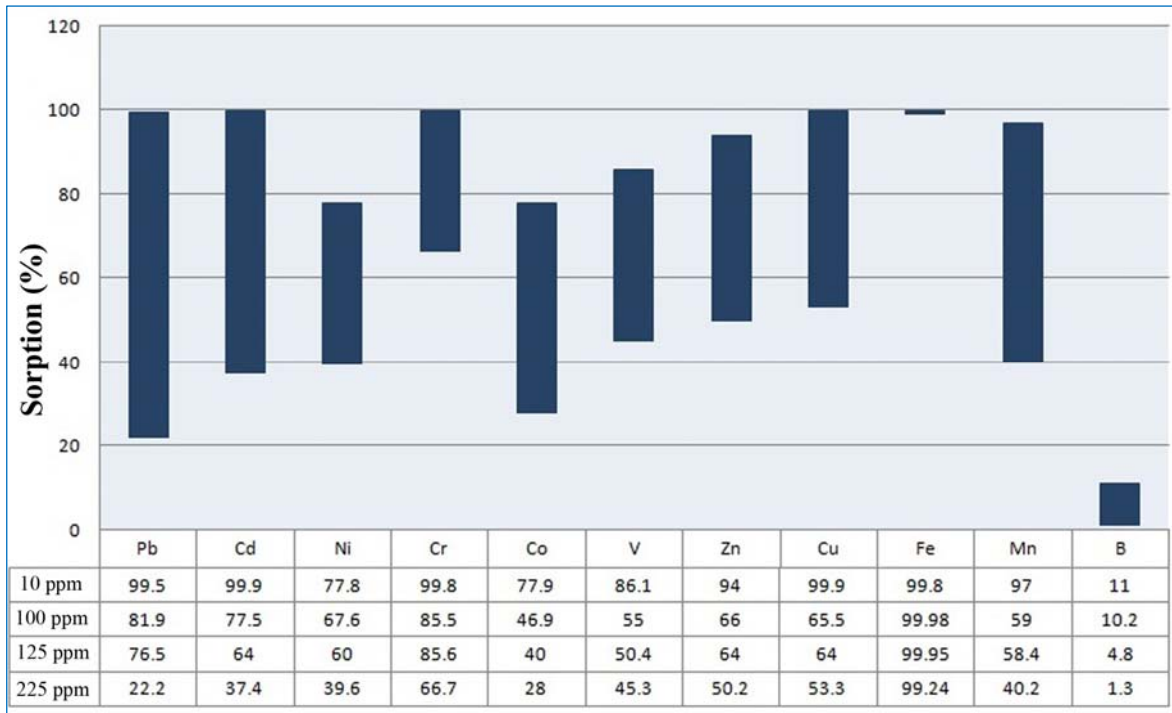


Figure 4-14: The range of sorption (%) for metals on palygorskite.

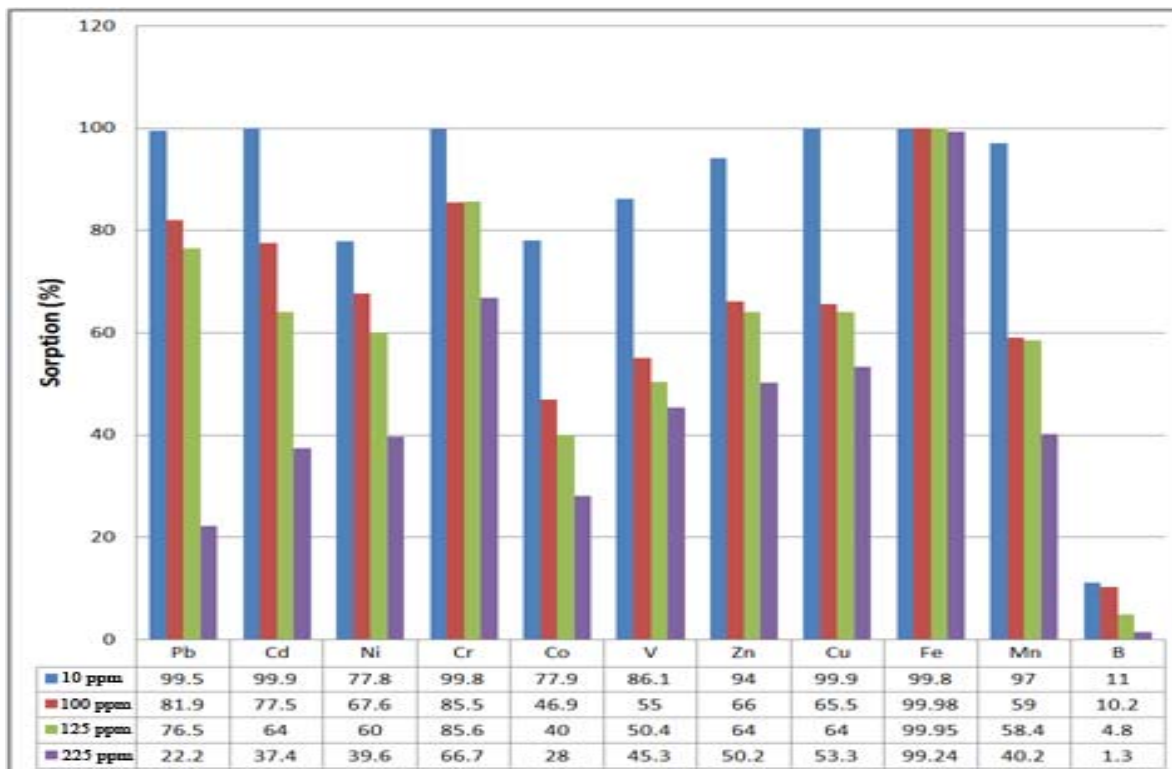


Figure 4-15: Negative relationship between the concentration of initial metals and sorption (%) on palygorskite.

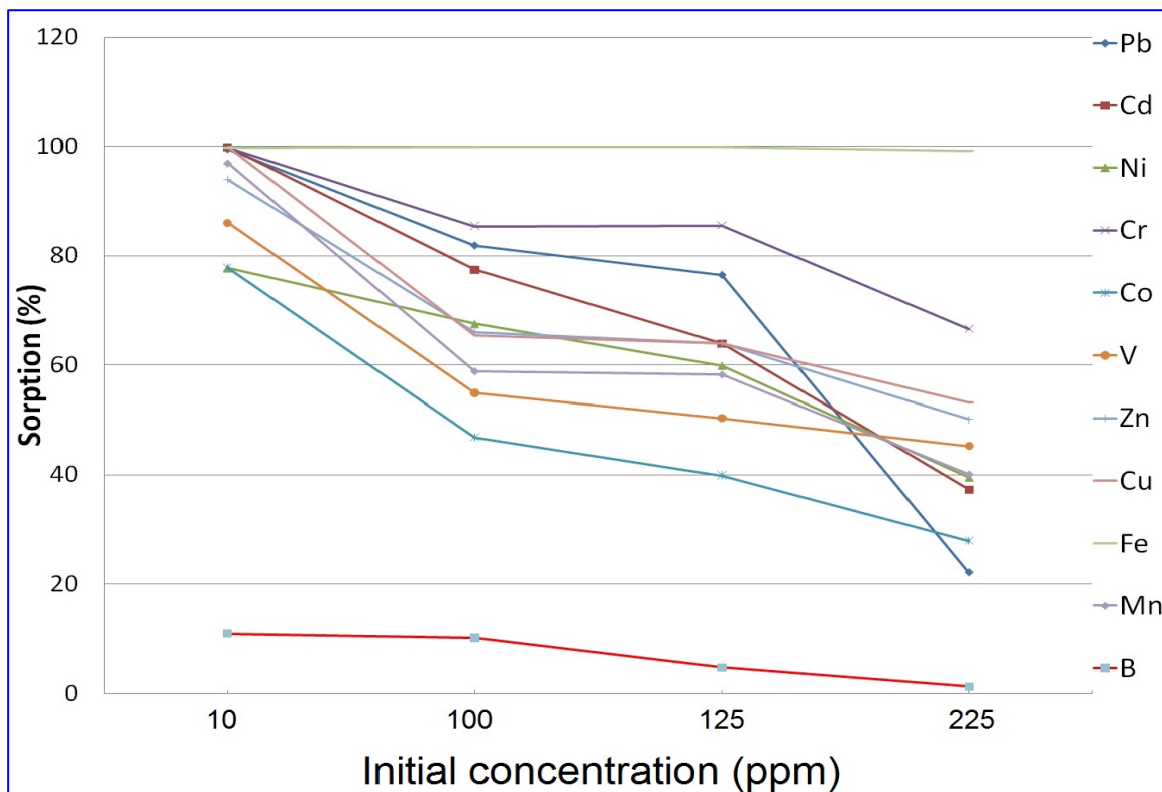


Figure 4-16: Distribution features of the metal sorption (%) on palygorskite.

4-4-3 Effect of pH

The effect of solution pH on M^{2+} (divalent cations) adsorption is determined for the pH range of 2.0 - 11.0 which would normally be found in an electro kinetic soil reclamation process (El-mofty and El-Shall, 2008).

The effect of pH on the sorption efficiency of palygorskite is studied through 110 experiments conducted on ten metals (lead (Pb), cadmium (Cd), nickel (Ni), chromium (Cr), cobalt (Co), vanadium (V), zinc (Zn), copper (Cu), iron (Fe), manganese (Mn), and boron (B)), with a variety of concentrations. Generally it is found that the pH is inversely proportional to the concentrations (Figures 4-3d to 4-13d). At low concentrations, the sorption ability of palygorskite seems to be higher than of its ability at high concentration, so to provide empty sites which contribute to the reception of cations. Significant amount of M^{2+} ions adsorption in the pH range of 2 – 7 was found. All the lab experiments revealed that the initial solutions have more acidity than final solutions. The tendency toward the alkaline occurs with the solutions of low concentration rather than the solutions of high concentration (Figures 4-3d to 4-13d) as no further cations competes the H^+

on the negative site on palygorskite. The experiments of heavy metal ion adsorbed on palygorskite reveal that the absorbability by palygorskite depends on pH and concentration. Since the pH is a measure of the concentration of the Hydrogen (and the Hydroxyl) ions, for an acidic solution, the lower the pH, the higher the H^+ concentration. Therefore, the availability of H^+ which exchange with metals competing on negative sites and hence more H^+ in the solution reduce the pH.

TDS and EC decreases with the trend of alkaline pH, so that more of the positively charged metal ions in the solution are absorbed on negative palygorskite surface and thus the adsorption of metals increases. This conclusion is similar to that of Naidu et al. (1994).

Adsorption of metals always decreases with an increase in ionic strength. This result can also be explained by the following fact. There is a silanol groups (Si-OH) on palygorskite particles as functional surface (Serna et al., 1977). This group (Si-OH) may act as Lewis basis in form (Si-O-) to bind one or two Lewis metal ions. Hence, when the concentration of metals increases, they can form more monodentate or bidentate complexes with Si-O-, and more H^+ came into solution resulting in the decrease of pH of the final solution. But this case is not observed.

The exchange of Ca^{2+} , Mg^{2+} , Al^{3+} and K^+ from palygorskite indicates that the adsorption mechanism of heavy metal ions is governed mainly by ion exchange mechanism. For this reason, the final Pb solution of 175 ppm was analyzed for Ca^{2+} , Mg^{2+} , Al^{3+} and K^+ (Table 4-18). The results listed in Table 4-18 refer to the case of ionic exchange between the palygorskite and the solution. Here we can conclude that the sorption has been got physically and chemically. The expulsion of these cations causes a decrease in positive charge on palygorskite which encourages adsorption of additional cations on surface surfaces.

Ca^{2+} , Na^+ and K^+ along with some of the Mg^{2+} , are probably present as exchangeable cations; however, in most samples these cations are more abundant than can be accounted for by the cation exchange values. Exchange values of 5-30 mequiv. /100 g seem to be most characteristic of the relatively pure samples (Weaver and Pollard, 1973).

The double-layer theory predicts qualitatively correctly that the affinity of the exchange of divalent ions is larger than monovalent ions and that this selectivity for ions of higher valence decreases with increasing ionic strength of the solution. However, according to the Gouty theory there should be no ionic selectivity of the exchange between different equally charged ions.

Table 4-18: Results of final Pb solution of 175 ppm.

Elements	ppm
Ca ²⁺	768
Mg ²⁺	339
Al ³⁺	4.84
K ⁺	1.1

4-4-4 Effect of ionic potential

Ionic potential is an ion's charge divided by its radius, and it is thus a measure of density of charge on the ion surface. Ionic potential gives a sense of how strongly or weakly the ion will be electrostatically attracted to ions of opposite charge, and to what extent the ion will repel other ions of like charge. The ionic potentials of chemical elements in this study are listed in Table 4-19, and it can be ordered from the highest to the lowest as:



The greater of ionic potential means greater of solubility. Consequently, the sorption of metals follow this rule in general, where we find that the sorption (%) of these metals in the initial solution of 50 ppm have ordered as:



The presence of some anomalies in some of elements is due to overlapping with other factors affecting absorption.

Table 4-19: Ionic potential of elements.

Elements	Atomic radius (°A)	Ionic Radius (°A)	Oxidation states	Ionic potential
Pb	1.81	1.19	2	1.68
Cd	1.71	0.97	2	2.06
Ni	1.62	0.69	2	2.89
Co	1.67	0.745	2	2.68
Cr	1.85	0.52	2	3.84
V	1.92	0.59	3	5.1
Fe	1.72	0.645	2	3.1
Mn	1.79	0.46	2	4.34
Zn	1.53	0.74	2	2.7
Cu	1.57	0.73	2	2.74
B	1.17	0.23	3	13

4-4-5 Effect of calcination

During calcination, the haystack structure of the clay becomes very porous. Pore volume is about 0.6 ml/g and pore diameter is about 200° A. The creation of this porous structure is believed to be more important to sorptive capability than the high surface area of palygorskite (McCarter et al., 1950). palygorskite can take up water to 200% of its own weight.

Palygorskite is a very important gel-forming clay. Compared to other clays, it gives stable suspensions of high viscosity at relatively low concentrations. Palygorskite is activated by heating, and therefore, it is subjected to calcinations at 200, 400, 600, 700, 800°C at 2 hours. Then 1 gm of clacinated palygorskite is treated with 100 ml of initial solution of 100ppm Pb to investigate how calcination influences the sorption. The results are listed in Table 4-20. The internal arrangement of the tetrahedral and octahedral layers of palygorskite is unique in that there are channels through its structure. These channels are filled with what is termed zeolitic water. When this water is driven off by heating, the surface area and thus the sorptivity is increased, chemical compounds that are of the size that will fit into these channels are readily absorbed. The sorption increases with increasing temperature until 600°C, which the maximum sorption (%) is recorded to be 93% (Table 4-20 and Figure 4-17). Thereafter, Sorption is declined to be 82% and 45% at 700°C and 800°C respectively. The results show that the channel of palygorskite is partial collapsed and the structure is not changed ultimately when thermally treated at 200, 400, 600, 700 °C. The structure of palygorskite gradually changes when the treating temperature is higher than 300°C and is damaged entirety till 800 °C (Zhang et al., 2011).

Table 4-20: Sorption (%) of 100 ppm Pb onto 1 gm of activated palygorskite.

Calcination °C	Sorption (%)
200	85
400	92
600	93
700	82
800	45

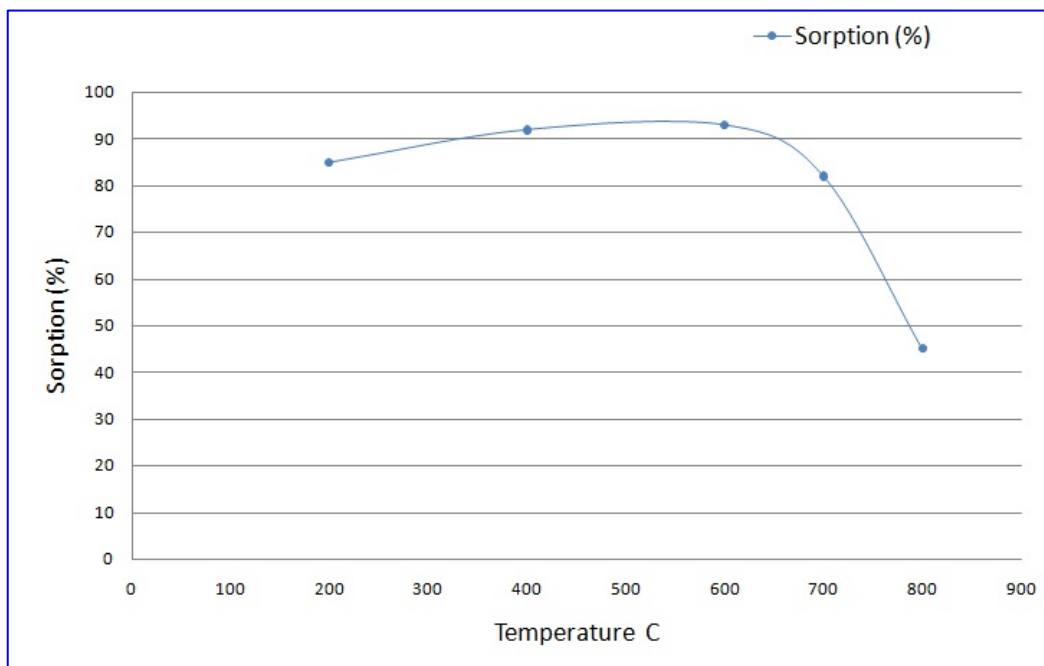


Figure 4-17: The influence of heating on palygorskite sorption.

4-5 Discussion

The palygorskite applications were divided into two broad categories, colloidal and non-colloidal (Haden, 1963). The elongated shape of palygorskite results in unique colloidal properties (Murray, 2007). An unusual needle-like shape is formed by cleavage parallel to the 110 planes along the Si-O-Si bonds holding the strips together. Consequently, it gives unusual colloidal and sorptive properties (Haden, 1963).

The extremely large surface area of palygorskite, approximately 167 m²/g, makes it very sorptive in its natural form (Murray, 2007). A large specific surface area and moderate cation exchange capacity (Galan, 1996) are beneficial for the adsorption of heavy metals from solution. The elongate particles vary in length from about 1 to 10 mm and are approximately 0.01 mm in diameter. This shape and size result in high surface area and high porosity when thermally activated (Christ, 1969).

One gram dose of palygorskite to 100ml solution at reaction time of 1h is determined as optimal conditions for a maximum removal of heavy metals by palygorskite. The sorption (%) increases proportionally to the time where the top sorption (%) can be seen at 1h.

The chemical composition of separated palygorskite is characterized by a high content of MgO (11.2%) indicating a high grade palygorskite. The

difference of valency between both ions in the tetrahedral sheet is Si^{4+} replaced by Al^{3+} produces a negative charge (0.42) which means positive charge deficiency. In the octahedral layer a homovalent (between Al^{3+} and Fe^{3+} or Mg^{2+} and Fe^{2+}) and Heterovalent substitutions (between Fe^{3+} , Fe^{2+} and Ti^{4+}) occur with an overall positive charge in this layer within the unit cell in 9.88. Three exchangeable cations (Ca, Na and K) in the interlayer have a net valence of 1.85. Divalent (R^{2+}) Mg^{2+} , Fe^{2+} , Co^{2+} , Ni^{2+} , Zn^{2+} , Cu^{2+} readily substitute for each other (homovalent substitutions) because their ionic radii are between 0.83 Å (Ni^{2+}) and 0.92 Å (Fe^{2+}), and also valid for trivalent (R^{3+}) Al^{3+} and Fe^{3+} that can be replaced by divalent (R^{2+}) as heterovalent substitutions.

Palygorskite exerts absorptive power on heavy metals from the liquid phase by three modes. These are: physical, ion exchange, and zeolitic action. The sorption (%) of metals on palygorskite almost shows a marked descending order as follows: $\text{Fe} > \text{Cr} > \text{Pb} > \text{Cd} > \text{Cu} > \text{Zn} > \text{Ni} > \text{Mn} > \text{V} > \text{Co} > \text{B}$. Boron appears to have weak strength of adsorption due to the low ionic potential. The ion with the greater radius will be the more strongly adsorbed (Brummer, 1986).

The presence of ions (Ca=768 ppm, Mg= 339 ppm, Al= 4.84 and K= 1.1 ppm) in the final Pb solution of 175 ppm refers to the case of ionic exchange between palygorskite and the solution and indicates that the sorption has been got physically and chemically.

CEC of palygorskite increases as pH increases. When pH increases, the concentration of H^+ declines; then the competitive adsorption of heavy metals slows down because the solubility of heavy metals is reduced. Further competition between the cations and H^+ on the negative site on palygorskite happened at the solutions of low concentration rather than the solutions of high concentration. This lead pH to be changed toward alkalinity. The decrease of TDS and EC values in the final solution is a function of the efficiency of palygorskite sorption, where TDS and EC decrease with the trend of alkaline pH.

Three forms of water in palygorskite are observed: a zeolitic water, bound water, and structural hydroxyls. Total water in palygorskite ranges from 18.6% to 22.3% (Caillire and Hknin, 1961). In the separated palygorskite, the water is 19.1%. Water is proportionally driven off by heating during calcination of palygorskite at 200, 400, 600, 700, 800°C at 2 hours. Calcination creates a porous structure, which is believed to be more important

to sorptive capability than the high surface area of palygorskite (Haden and Schwint, 1967). The sorption increases with increase temperature until reaching 600°C in which the maximum sorption (%) is recorded to be 93% due to the increase of surface area. Sorption declines to be 82% and 45% at 700°C and 800°C respectively due to the partial collapse and ultimate structure of the palygorskite, but it is damaged entirely at 800°C.

The decrease of sorption efficient at solutions of high concentrations may be attributed to the strong competition between cations on the negative sites on palygorskite. A negative surface charge is caused by substitutions of Al for Si in the Tetrahedral sheet and exchange of two-fold charged cations like Fe and Mg for Al in the octahedral sheets. Thus, the charge of the basal surface is always negative and independent on pH (Amman et al., 2005).

Chapter Five

Conclusions and Recommendations

5- Conclusions and Recommendations

5-1 Conclusions

The following conclusions are drawn from the present study:

- 1- Palygorskite appears as authigenic mineral formed from the transformation or alteration of smectite. Palygorskite is bedded within the Akashat and Digma Formations interstratified with dolomite, siliceous, calcareous clays and phosphatic zones. Occurrence of palygorskite with dolomite is interpreted as authigenic origin rather than detrital. Reaction of pore water rich in silicic acid with dolomite suggests the sepiolite is formed at first, then the sepiolite is transformed to palygorskite $(Mg,Al)_2Si_4O_{10}(OH)_4(H_2O)$ by getting Al from the surrounding area. The second model is the transformation of smectite to form palygorskite
- 2- Lithology suite of dolomite, cherty dolomite, Marly limestone, phosphatic sediments, siliceous minerals such as tridymite and cristabolite indicates shallow marine environment of inner platform. The porcellanite (opal-CT) with phosphatic facies occur in association with palygorskite provide a significant environmental evidence. Apatite in marl- phosphatic facies may indicate shallow to the deep inner platform. The phosphorite facies characterized by discontinuous extension of thick light gray color bed reflects a shallow water of inner platform. Porcellanite facies indicates open inner platform.
- 3- A strong competition between cations (heavy metals) on the negative sites on palygorskite occurs at a high concentrated solution causing decrease in sorption efficiency.
- 4- The decrease of TDS and EC values in the final solution is a function of the palygorskite sorption. TDS and EC decrease with the trend of alkaline pH, more of the positively charged metal ions in the solution are absorbed on the negative palygorskite surface and thus the adsorption of metals increases.
- 5- The ionic potential of chemical elements in this study can be ordered from the highest to the lowest as:



The greater the ionic potential the greater the solubility. Consequently, the sorption of metals follows this rule in general, where it is found that the sorption (%) of these metals in the initial solution of 50 ppm has the following ascending order:



The presence of any anomaly in some of the elements is due to overlapping of other factors affecting absorption. The best recorded sorption is of Fe and Cr, where Fe adsorbed on palygorskite from initial solutions of 10-225 is 99.9-99.24(%) respectively. The worst sorption of palygorskite is for boron (B).

- 6- The mass of adsorbant and time reaction are the control factors for sorping metals onto the palygorskite. The mass of adsorbent (palygorskite) affects on the sorption (%). The sorption (%) of Pb increases and the maximum removal is observed with 1 gm dose. With increasing palygorskite mass, the corresponding increase in adsorption (%) is less, because it becomes difficult for the cations to approach the adsorption sites due to overcrowding of clay mineral particles (palygorskite) termed as a kind of solid concentration effect. Accordingly, the solid-liquid ratio is determined to be 1 gm to 100 ml. The sorption (%) increases proportionally with the equilibrium time where the maximum sorption (%) can be seen at 60 minutes (1h). On this basis, the equilibrium time absorption and adsorption is determined to be 1h.
- 7- The basic mechanism governs the heavy metals adsorption characteristics of palygorskite at different pH is adsorption and ionic exchange. The hydrogen number (pH) was changed in the initial solutions towards alkaline trend referring to the occupation of protons (H^+) by some negative sites in palygorskite structure. Hydrogen also competes with heavy metals on negative sites in palygorskite.
- 8- The tendency toward the alkaline occurs with the solutions of low concentrations rather than the solutions of high concentrations because no further cations competes with the H^+ on the negative site in palygorskite.

- 9- The ability of palygorskite sorption (%) increases when thermally activated, where up to 93% occur at 600°C due to the driving off zeolitic water by heating, the surface area and thus the sorptivity is increased. Whilst, at 800°C sorption appears to decrease to a minimum due to the collapse of palygorskite structure.
- 10- Palygorskite can act physically and chemically as absorbent for Pb, Cd, Ni, Cr, Co, V, Cu, Zn, Fe and Mn, due to its high surface area. Therefore, it can be used as absorbent in the industry to adsorb hazardous waste in landfill. The absorbency of palygorskite prevents leaching in the landfill.

5-2 Recommendations

This study has found that the palygorskite is good absorbent material promising for liquid purification of pollutants, in particular heavy metals. Study of the reaction using palygorskite for the removal of heavy metals in waste-water is a fruitful scope of the present investigation. These investigations could be extended to try the removal of organic compounds from liquids. In addition, the adding of catalytic organic matter will be beneficial.

References

- Aba-Hussain, A., 1986: Geochemical, Petrographical and Mineralogical Study of Paleocene phosphate unit in Ga'ara-Akashat Area Ph.D. Thesis, University of Baghdad, 277p (in Arabic).
- Al-Ajeel, A. A., Hana, S.I., Al-Bassam, K.S. and Hussain, M., 1997: The use of Iraqi palygorskite- rich clays in de- coloring sun-flower oil. Proceedings of symposium, 24-25 March, College of Science, University of Baghdad. In: Al-Bassam, Kh. S., 2000 (Ed.), The Iraqi Palygorskite, Geology, Mineralogy, Geochemistry, Genesis and Industrial Uses. The State Company of Geological Survey and Mining, Baghdad, Iraq, pp: 203–210.
- Al-Baidari, A.P. ,1997: The use of Iraqi palygorskite- rich claystones from the Najaf-Razzaza area in pottery. Proceedings of symposium, 24-25 March, College of Science, University of Baghdad. In: Al-Bassam, Kh. S., 2000 (Ed.), The Iraqi Palygorskite, Geology, Mineralogy, Geochemistry, Genesis and Industrial Uses. The State Company of Geological Survey and Mining, Baghdad, Iraq, pp: 225-23.
- Al-Bassam, K. S., 2000: Distribution of Iraqi palygorskite in space and time. In: Kh. S. Al-Bassam, (Ed.), The Iraqi Palygorskite, Geology, Mineralogy, Geochemistry, Genesis and Industrial Uses. The State company of Geological Survey and Mining, Baghdad, Iraq, pp: 1–9.
- Al-Basam, K.S., 2007: Preface on Geology of the Iraqi Western Desert, Iraqi Bulletin of Geology and Mining. Special issue, No.1. pp: 1-4.
- Al-Bassam, K.S. and Karim, S.A., 1997: The Akashat Formation: A new name for the Paleocene Lithostratigraphic Unit in the Western Desert of Iraq. Iraqi Geol.Jour. Vol. 30, No.1, pp: 22 – 35.
- Al-Bassam, Kh.S., Jafar, M.R. and Al-Ajeel, A. 1997: The use of Iraqi palygorskite in the dehydration of hydraulic oil in electrical power stations. Proceedings of symposium, 24-25 March, College o Science, University of Baghdad. In: Al-Bassam, Kh. S., 2000 (Ed.), The Iraqi Palygorskite, Geology, Mineralogy, Geochemistry, Genesis and Industrial Uses. The State Company of Geological Survey and Mining, Baghdad, Iraq, pp: 197–202.
- Al-Bassam, K.S., Karim, S.A., Hassan, K.M., Saeed, L., Yakta, S., and Salman, M., 1990. Report on geological survey of the Upper

- Cretaceous – Lower Tertiary phosphorite bearing sequence, Western Desert, Iraq. GEOSURV, Int. Rep. No. 2008.
- Al-Haza'a, S.H., 2001: Basin Analysis of the Upper Cretaceous Sequence in the Western Desert, Iraq. Unpub. Ph. D. Thesis, Baghdad University.
- Al-Kadhimi, J., Sissakian, V. K., Fattah, A.S. and Deikran, D.B., 1996: Tectonic Map of Iraq, scale 1: 1 000 000, 2nd. ed., GEOSURV, Baghdad, Iraq.
- Al-Mubarak, M. and Amin, R., 1983. Report on the regional geological mapping of the eastern part of the Westren Desert and the western part of the western part of Southren Desert. GEOSURV , GEOSURV int. rep. no. 1380, 405p.
- Al-Naqib, K. M., 1960: Geology of the Arabian Peninsula, southeastern Iraq. U.S.G.S. professional paper No. 560-G, 54p.
- Al-Rawas, A. H. Sutherland, A. W. Hago, A. A Yousif, M. Al-Shihi, and B. Al-Shihi., 2001: A comparative quantitative study of an omani soil using X-ray diffraction technique. Journal of Geotechnical and Geological Engineering, 19, pp: 69-84.
- Al-Rawi, A.H., Jackson, M.I. and Hole, F.D. 1969: Mineralogy of some arid and semiarid soils of Iraq. Soil Science, 107, 480–486. American Mineralogists, 25, 405–411.
- Amman L., Bergaya F. and Lagaly G., 2005: Determination of the cation exchange capacity of clays with copper complexes revisited. Clay Minerals **40**, pp: 441-453.
- Anton, R. S. Al-Bassam. K. S. Al-Dulaimi. Sh. N. Musa, H. A., 1997: The use the Iraqi palygorskite (attapulgit) in oil well drilling. Proceedings of symposium, 24-25 March, College o Science, University of Baghdad. In: Al-Bassam, Kh. S., 2000 (Ed.), The Iraqi Palygorskite, Geology, Mineralogy, Geochemistry, Genesis and Industrial Uses. The State Company of Geological Survey and Mining, Baghdad, Iraq, pp: 179-190.
- Araujo Melo D.M., Ruiz, J.A.C., 2000: Preparation and characterization of terbium palygorskite clay as acid catalyst. Micropor Mesopor Mater, 38 (2–3), pp: 345–9.
- Aswad, Kh.J., Fat'hiy, D. A., and Thabit, K., 1997: Crystallochemical and thermodynamic characterization of Nineva palygorskite as microporous absorbent. Proceedings of symposium, 24-25 March, College o Science, University of Baghdad. In: Al-Bassam, Kh. S.,

- 2000 (Ed.), The Iraqi Palygorskite, Geology, Mineralogy, Geochemistry, Genesis and Industrial Uses. The State Company of Geological Survey and Mining, Baghdad, Iraq, pp: 211-224.
- Augsburger, M .S., Strasser,E .,P erino,E .,M ercader,R .c.,P edregosa, J.c., 1998: FTIR and M6ssbauer investigation of a substituted palygorskite: silicate with a channel structure. *Journal of Physical Chemical Solids* 59-2, pp: 175-180.
- Augusburger, M.S, Strasser, E, et al., 1998: FTIR and Mossbauer investigation of a substituted palygorskite: silicate with a channel structure. *J Phys Chem Solids*; 59(2), pp: 175–80.
- Bailey, S. W., 1980: Structure of layer silicates: in *Crystal Structures of Clay Minerals and Their X-ray Identification*, Brindley, G.W. and Brown, G.,eds., Mineralogical Society, London, pp: 2-123.
- Barchad, I., Ilalevy, I., Gold, H.A. and Hagin, J., 1956: Clay minerals in some limestone soils from Israel, *Soil Sci.*, 81, pp: 423-437.
- Bellen, R.c., Dunnington, H.V., Wetzel, R. and Morton, D. 1959. *Lexique Stratigraphique International*, pp. 1–333, Asie, Fasc 10a, Iraq, Paris.
- Bighamm, J. M., Jaynes, W, F., and Allen, B. L., 1980: Pedogenic degradation of sepiolite and palygorskite on the Texas High Plains: *Soil Sci. Soc. Amer. J.* 44, 159-167.
- Bignon, J., Sébastien, P., Gaudichet, A. and Jaurand, M. C.,1980: Biological effects of attapulgite. In: Wagner, J.C., ed., *Biological Effects of Mineral Fibres*, Vol. 1 (IARC Scientific Publications No. 30), Lyon, International Agency for Research on Cancer, pp: 163-181.
- Bish, D.L. and Guthrie, G.D., Jr., 1993: Mineralogy of clay and zeolite dusts (exclusive of 1: 1layer silicates). In: Guthrie, G.D., Jr and Mossman, B.T., eds, *Reviews in Mineralogy*, VoL. 28, *Realth Effects of Mineral Dusts*, Chelsea, MI, Book Crafters, pp. 139-184
- Bradley, W.P., 1940: The structural scheme of attapulgite. *American Mineralogist* 25, pp: 405-411.
- Brindley, G.W. and Brown, G., 1980: Crystal structures of clay minerals and their x-ray identification. pp. 1–495. Mineralogical Society; London.
- Brummer, G. W., 1986: *The Importance of Chemical Speciation in Environmental Processes*, Springer-Verlag, Berlin, pp: 169–192.
- Buday, T. and Jassim, S.Z., 1987: The regional geology of Iraq, tectonism, magmatism and metamorphism. pp. 1–352.

- Buday, T., 1980: The Regional Geology of Iraq. Stratigraphy and palaeogeography. pp. 1–445. State Organization for Mineral; Baghdad, Iraq.
- Buday, T., and Hak, J., 1980: Report on geological survey of the western part of the Western Desert, Iraq. GEOSURV, internal. rep. no. 1000. G., editor (1961) *The X-*, London, 544p.
- Caillire, S. and Hknin, S., 1961: Palygorskite. In: G. Brown (Icditor), *The X-Ray Meniification arid Crystal Structures of Clay Minerals*. London, London Mineral. Soc., London, pp. 343-353.
- Carretero, M.I., Gomes, C.S.F. and Tateo, F., 2006: Clays and human health. p. 717- 742. In F. Bergaya et al. (ed.) *Handbook of Clay Science*. Amsterdam, The Netherlands: Elsevier.
- Carroll, D., 1970: Clay minerals, a guide to their x-ray identification. Geological Society of America, Special Paper, 126: pp1–80.
- Chahi, A., Petit, S., Decarreau, A., 2002: Infrared evidence of dioctahedral-trioctahedral site occupancy in palygorskite. *Clays and Clay Minerals* 50 (3), pp: 306-313.
- Chamley, H., 1989: *Clay sedimentology*, Springer- Verlag; Berlin. 623p.
- Christ C L., 1969: Palygorskite; new X-ray data. *Am. Miner.*, 198p.
- Christ, C.L., Hathaway, J.C, Hostetler, P.B. and Shepard, A.O., 1969: Palygorskite: new X-ray data. *Am. Miner.*, 54,pp: 198-205.
- Coles, C.A., Yong, R.N., and joe, H., 2002: Aspects of kaolinite characterization and retention of Pb and C, *Applied Clay Science*, Vol. 22, pp:39-45.
- Connor, D.J., Sexton, B.A., Smart, R. 2003. *Surface Analysis Methods in Materials Science*, (Springer-Verlag, Germany), 205p.
- Dhannoun, H. Y. and Al-Dabbagh, S.M.A., 1988: Origin and geochemistry of palygorskite-bearing rocks (Middle Miocene) from NE Iraq. *Chem. Geol.*, 69: pp 87-93.
- El-Gabaly, M.M., 1962: the presence of attapulgitite in some soils of the western desert of Egypt. *Soil Science*, 93,387–390.
- El-mofty, S. E. and El-Shall, H., 2008: Adsorption mechanism of toxic metal ions by clay (attapulgitite). Twelfth International Water Technology Conference, IWTC12, Alexandria, Egypt, pp: 403-413.
- Esteoule-Choux, J., 1984: Palygorskite in the Tertiary deposits of the Armorican massif. In *Palygorskite-Sepiolite Occurences, Genesis and*

- Uses. Singer, A. and Galan, E., eds. Dev. In Sediment., 37, Amsterdam: Elsevier. pp:75-85.
- Farmer, V.C., 1974: The Infrared Spectra of Minerals, Mineralogical Society; London. 527p.
- Frost Ray L, Cash Gerg A, Kloprogge Theo J., 1998: Rocky Mountain leather', sepiolite and attapulgitite—an infrared emission spectroscopic study. *Vib Spectrosc*, 16(2), pp:173–84.
- Frost Ray L, Locos Oliver B, Ruan Huada, 2001: Near-infrared and mid-infrared spectroscopic study of sepiolites and palygorskites. *Vib Spectrosc*, 27(1), pp:1–13.
- Gadsden, J.A., 1975: Infrared spectra of minerals and related inorganic compounds. Butterworth, London, 277p.
- Galan, E. and carretero, I., 1999: A new approach to com positional limits for sepiolite and palygorskite. *Clays and Clay Minerals*, 47, 399–409.
- Galan, E., 1996: Properties and applications of palygorskite-sepiolite clays, *Clay minerals*, 31, pp: 443-453.
- Galan, E., and Castello, A., 1984: Sepiolite-Palygorskite in Spanish Tertiary Basins: General patterns in continental environments. In *Palygorskite-Sepiolite Occurences, Genesis and Uses*. Singer, A. and Galan, E., eds. Dev. In Sediment., 37, Amesterdam: Elsevier. Pp:87-124.
- Garg, V,K,, Gupta, R., Kumar R, Gupta ,R. K., 2004: Adsorption of chromium from aqueous solution on treated sawdust. *Bioresour. Technol.* 92, pp: 79–81.
- Geological Map of Iraq 1986. Series scale 1:1 000000. Directorate General of Geological survey and Mineral In- vestigation; Baghdad, Iraq.
- GEOSERV, 2009: State establishment of Geological Survey and Mining, Geological map of Saba'ebyer and Al-Rutba Quadrangles, Sheets NI-37-10 and NI-37-11, Scale 1:250 000.
- Giustetto, R. and Chiari, G., 2004: Crystal structure refinement of palygorskite from neutron powder diffraction. *European Journal of Mineralogy*, 16, pp 521–532.
- Grim, R.E., 1953: *Clay mineralogy*, Mc Graw-Hill; New York, 569p.
- Grim, R.E., 1962: *Applied clay mineralogy*. International Series in Earth Sciences. Mc Graw-Hill; New York.
- Grim, R.E., 1968. *Clay mineralogy*. McGraw Hill Book Company, 2nd edit., 569p.

- Haden Jr., and W. L., Schwint, I. A., 1967: Attapulgite – Its Properties and Applications,” *Industrial and Engineering Chemistry* 59 (9), 59p.
- Haden, W. L., 1963: Attapulgite, Properties and Uses, in *Proceedings of the 10th National Conference on Clays and Clay Minerals*, E. Ingerson, Ed., Pergamon Press, New York, P.284.
- Hagopian, D.H., 1979: Report on the regional geological mapping of Al-Tinif – Nahaidin Area. GEOSURV, int. rep. no. 983.
- Hassan, K.M., 1998: Paleocology and Stratigraphic Distribution of Cretaceous Molluses; Western Desert. Unpub. Ph. D. Thesis, Baghdad University.
- Hayashi, H., Otsuka, R. and Imai, N., 1969: Infrared study of sepiolite and palygorskite on heating. *American Mineralogists*, 54: 1613–1624.
- Hefne, J. A., Mekhemer, W. K., Alandis, N. M., Aldayel, O. A. and Alajyan, T., 2008: Kinetic and thermodynamic study of the adsorption of Pb (II) from aqueous solution to the natural and treated bentonite.
- Hofmann U. and Klemen R., 1950: Verlust der Austauschfähigkeit von Lithium-Ionen an Bentonit durch Erhitzung. *Zeitschrift für Anorganische und Allgemeine Chemie* 262, pp. 95-99.
- Hongxia, P. and Dajun. C., 2007: Preparation and characterization of waterborne polyurethane/attapulgite nanocomposites. *Eur. Polym. J.*,43(9), pp: 3766–72.
- Hower, J. and Mowatt, T.C., 1966: The mineralogy of illites and mixed-layer illite/montmorillonites. *Am Mineral* 51, pp: 825–854.
- Hu, Y., and Liu, X. 2003: Chemical composition and surface property of kaolins , *Minerals Engineering*, Vol.16, pp.1279-1284.
- Jassim, S.Z., Karim, S.A., Basi, M.A., Al-Mubarak, M. and Munir, J.,1984: Final report on the regional geological survey of Iraq, Vol. 3, Stratigraphy. GEOSURV, Int. Rep. no. 1447.
- Jeffers and Reynolds,1987: Expandable palygorskite from the Cretaceous-Tertiary boundary, Mankyshalk peninsula, U.S.S.R. *Clay and Clay Minerals*, vol.35, no.6, pp:473-476.
- Jones B. F. and Galan E., 1988: Sepiolite and Palygorskite in Hydrrous Phyllosilicates (exclusive of micas). Bailey S. W. (ed.), *Mineralogical Society of America* 19, BookCrafters Inc., Michigan, pp: 631-674.
- Jones, B. F., 1986: Clay mineral diagenesis in lacustrine sediments. In *studies in diagenesis*. USGS Bulletin, 1578, 291-300.

- Jones, B.F. and Gahin, E., 1988: Sepiolite and palygorskite. In: Bailey, S. W. (Ed.), *Hydrous Phyllosilicates (exclusive of micas)*. Mineralogical Society of America, pp. 631-674.
- Juma, N.H., Al-Bassam, Kh.S., Dawood, A.N., Nouri, I., Matti, N. and Rasheed, S.ch., 2000: the use of Iraqi palygorskite (attapulgitite) in decolorizing paraffin wax. *Proceedings of symposium, 24-25 March, College of Science, University of Baghdad*. In: Al-Bassam, Kh. S., 2000 (Ed.), *The Iraqi Palygorskite, Geology, Mineralogy, Geochemistry, Genesis and Industrial Uses*. The State Company of Geological Survey and Mining, Baghdad, Iraq, pp: 191–195.
- Kadum, M. A., 2009: *Geochemistry and Mineralogy of Palygorskite rich clays in Gercus Formation in Dohuk Governorate, North of Iraq*. M.Sc Thesis. University of Baghdad, College of Science. Department of Geology, 110p.
- Kannewischer, I., 2006: *Smectite clay adsorbents of aflatoxin B1 to amend animal feed*. M. Sc. Thesis, Texas A and M University. 86p.
- Karim, S.A. and Ctyroky, P., 1981: *Stratigraphy of the eastern and southern flanks of the Ga`ara High, Western Desert, Iraq*. GEOSURV, int. rep. no. 1185
- Karim, S.A. and Jassim, S.Z., 1985: *Biostratigraphy and environmental reconstruction of the Paleocene phosphorite sequence, Western Desert, Iraq*. GEOSURV, int. rep. no. 1538.
- Kas-Yonan, S. A., 1989: *Mineralogy, geochemistry and properties of palygorskite and associated rocks and clays of Safra member, Late Maastrichtian in Ga'ara, Akashat area*, M.Sc. thesis; Mosul University, pp: 1–167.
- Kaufhold S., 2001: *Untersuchungen zur Eignung von natürlich alterierten sowie mit Oxalsäure aktivierten Bentoniten als Bleicherde für Pflanzenöle*. Dissertation, Fakultät für Bergbau, Hüttenwesen und Geowissenschaften der Rheinisch-Westfälischen Technischen Hochschule Aachen, (Translated to English), 178p.
- Keller, W.D. , 1979: *Clays*. In: Grayson, M., ed., *Kirk-Othmer Encyclopedia of Chemical Technology*, Vol. 6, 3rd Ed., New York, John Wiley & Sons, 202 p.
- Lopez, G., Torres, R., and Gonzalez, G., 1996: *Mineral quantification in sepiolite – palygorskite deposits using X-ray diffraction and chemical data*. *Clay minerals*, 31, pp: 217-224.

- Loughnan, F.C., 1959: Further remarks on the occurrence of palygorskite at Red Banks Plains, Queensland. *Proc. R. Soc. Queensland*, 71, pp:43-50.
- Maxwell, J. A., 1968: *Rock and mineral analyses*. John Wiley and Sons. New York. 584p.
- McCarter, W. S. W., Krieger, K. A., and Heinemann, H., 1950: *Ind. Eng. Chem.* 42, 529p.
- McKeown, D.A., Post, J.E., Etz, E.S., 2002: Vibrational analysis of palygorskite and sepiolite. *Clays and Clay Minerals* 50-5, pp: 667-680.
- Mendelovici, E., 1973: Infrared study of attapulgite and HCl treated attapulgite. *Clays and Clay Minerals* 21,pp: 115-119.
- Mendelovici, E., Portillo, D., 1976: Organic derivatives of attapulgite: I. Infrared spectroscopy and X-ray diffraction studies. *Clays and Clay Minerals* 24,pp:177-182.
- Meunier, A., 2005: *Clays*. Springer Berlin Heidelberg New York, 465p.
- Mtinton, F.A. and Roy, R., 1958: New data on sepiolite and attapulgite. *Proc. Natl. Conf: Clays- Clay Miner. 5th-Natl. Acad. Sci. Natl. Res. Counc., Publ.*, 566: 136- 143.
- Murray, H., 2002: *Industrial clays case study*. Mining, Minerals and Sustainable Development (MMSD) publication, International Institute for Environment and Development, 64, 9 p.
- Murray, H. H., 2007: *Applied clay mineralogy, occurrences, processing and application of kaoline, bentonites, palygorskite-sepiolite and common clays*. Elsevier, *Developments in Clay Science*, 2. 180p.
- Naidu, R.; Bolan, N.S., Kookana, R.S., Tiller, K.G., 1994: Ionic-strength and pH effects on surface charge of Cd sorption characteristics of soils. *Journal of Soil Science*, v.45, pp: 419-429.
- Namecz, E., 1981: *Clay Minerals*, Akademiai Kiado, Budapest, 547p, (English translation).
- Noori M. H., 2007: *Geology of Iraqi Western Desert*. *Iraqi Bull. Geol. Min. Special Issue*, 2007: pp: 9– 27.
- Parthasarathy, G, Kunwar, A. C. and Srinivasan, R., 2001: *Eur. J. Mineral.* 13, 127p.
- Parthasarathy, G., Choudary, B. M., Sreedhar, B., Kunwar, A. C. and Srinivasan, R., 2003: *Am. Mineral.* 88, 1983.

- Pletsh, T., 2003: Authigenic palygorskite clay in deep-sea sediments-mineral deposits formed in ancient green- house oceans? *Z. Angew. Geol.* 2, pp: 22–29.
- Post, J.E. and Heaney, P.J., 2008: Synchrotron powder X-ray diffraction study of the structure and dehydration behavior of palygorskite. *American Mineralogist*, 93, pp: 667–675.
- Powers, R.W., Ramirez, L.F., Redmond, C.D. and Elberg, E.L., 1967: Sedimentary Geology of Saudi Arabia. In: *The Geology of Arabian Peninsula*. U.S.G.S. Professional Paper. No. 560-D, Washington, 177p.
- Pual, S., Dennis, P. and David, R., 2000: Purified attapulgite clay. U.S. Patent No. 6130179.
- Qaser, M.R., Al-Marsoomi, A.M., Ma'ala, Kh.A., Karim, S.M. Hassan, F.A., Basi, M.A., Al-Mukhtar, L.A., and Dawood, R.M., 1992: Final report on the detailed geological survey for Al-Hussainiyat area. GEOSURV, int. rep. no. 2089 (in Arabic).
- Qaser, M., Al-Marsoumi, A., Ma'ala, K. Karim, S., Ali, F., Bassi, M. Ezzildin, I., and Dawood, R., 1993: Final report on the detailed geological survey of North Rutbah area. GEOSURV, int. rep. no. 2196.
- Qassim, I., 1993: Mineralogy, Petrology and depositional environment of clays and siliceous rocks in Maastrichtian – Danian sequence in Westren Desert. Ph.D. thesis, University of Baghdad, 183p (in Arabic)
- Robert, J.P. and Dennis, C.P., 2002: Purified attapulgite. U.S. Patent No. 6444601
- Rytow, R., Serban C., S. Nir, and L. Margulies, 1999: Use of methylene blue and crystal violet for determination of exchangeable cations in montmorillonite. *Clay and Clay Minerals*, 39(5), pp: 551-555.
- Saikia, B.J., Parthasarathy, G. and Sarmah, N. C., 2008: Fourier transform infrared spectroscopic estimation of crystallinity in SiO₂ based rocks. *Bull. Mater. Sci., Indian Academy of Sciences*, Vol. 31, No. 5, October, 2008, pp. 775–779.
- Serna, C. J., Van Scoyoc, G. E., and Ahlrichs, J. L., 1977: Hydroxyl group and water in palygorskite: *Amer. Mineral.* 62, pp: 784-792.
- Shukla, S.S, Yu, L.J., Dorris, K.L., Shukla, A., Margrave, J. L., 2003: Adsorption of chromium from aqueous solutions by maple sawdust. *Journal of Hazardous Materials* .100 (1–3), pp: 53–63.

- Singer, A., 1984: Pedogenic palygorskite in the arid environment. In Palygorskite-Sepiolite Occurrences, Genesis and Uses. Singer, A. and Galan, E., eds. Dev. In Sediment., 37, Amsterdam: Elsevier. Pp 169-176.
- Singer, Arieh, 1989: Palygorskite and sepiolite group minerals, in Dixon, J.B., and Weed, S.B. (eds.), Minerals in soil environments, Soil Science Society of America, Madison, WI, 2nd Ed., pp: 829-872.
- Sissakian, V.K., 2000: Geological Map of Iraq, 3rd edition, scale 1: 1 000 000, GEOSURV, Baghdad, Iraq.
- Smyth, J.R., Ahrens, T.J., 1997” The crystal structure of calcite III, Geophysical Research Letters, Vol. 24, pp:1595-1598.
- Stanton, R. E., 1966: Rapid methods of trace elements for geochemical application, Edward Annold pub. London, 96p.
- Stevens R. E. ,1945: A system for calculating analyses of micas and related minerals to end members. U.S. Geol. Survey Bull. **950**, pp: 101-119.
- Suarez, M, Garcia-Romero, E., 2006: FTIR spectroscopic study of palygorskite: influence of the composition of the octahedral sheet. Appl Clay Sci, 31(1–2), pp:154–63.
- Suárez, M., García-Romero, E., Sánchez del Río, M., Martinetto, P., and Dooryhée, E., 2007: The effect of octahedral cations on the dimensions of the palygorskite cell. Clay Minerals, 42,pp: 287–297.
- Tamar Agha, M.Y. and Al-Janabi, S.A.F., 1997: Palygorskite in the Tayarat Formation (Upper Cretaceous), well KH 6 at Al-Ansab, Southern Desert of Iraq. Proceedings of symposium, 24-25 March, College o Science, University of Baghdad. In: Al-Bassam, Kh. S., 2000 (Ed.), The Iraqi Palygorskite, Geology, Mineralogy, Geochemistry, Genesis and Industrial Uses. The State Company of Geological Survey and Mining, Baghdad, Iraq, pp:11–34.
- Tamer-Agha, Al-Haza'a, S. H. and Al-Bassam, Kh. S., 1997: Palygorskite of the Zahra formation (Pliocene-Pleistocene) in the western and southern deserts of Iraq. Proceedings of symposium, 24-25 March, College o Science, University of Baghdad. In: Al-Bassam, Kh. S., 2000 (Ed.), The Iraqi Palygorskite, Geology, Mineralogy, Geochemistry, Genesis and Industrial Uses. The State Company of Geological Survey and Mining, Baghdad, Iraq, pp: 123-134.

- Torres-Ruiz, J., Lope-galindo, A., Gonzalez-Lopez, J. M., Delgado, A., 1994: Geochemistry of Spanish sepiolite: genetic considerations based on trace elements and isotopes. *Chem. Geol.* 112, pp: 221-245.
- Toyoda, K., Nakamura, Y. and Masuda, A., 1990: Rare Earth Elements of Pacific pelagic sediments. *Geochem. Cosmochem. Acta.* 54, pp:1093-1103.
- Weaver, C. H., and Pollard, L., 1973: *The Chemistry of Clay Minerals. Development in Sedimentology*, 15. Elsevier Scientific Publishing Company. Amsterdam, 213p.
- Weiss A., Mehler A., Koch G. and Hofmann U., 1956: Über das Anionenaustauschvermögen der Tonmineralien. *Zeitschrift für Anorganische und Allgemeine Chemie (Translated to English)*, **284**, pp. 247- 271.
- Wilson, M.J., 1994: *Clay Mineralogy: Spectroscopic and Chemical Determinative Methods*. Chapman and Hall, New York.
- Wu-Chou Yu , Jia-Twu Lee, Bing-Hung Tsai., 2011: Effects on Sunflower Growth Induced by Adding Different Soil Amendments to Cadmium-Contaminated Soil. *International Conference on Agricultural and Biosystems Engineering Advances in Biomedical Engineering Vols. 1-2*, pp: 74-79.
- Xu, B., Huang, W.M., Pei, Y.T., Chen, Z.G., Kraft, A., Reuben, R., De Hosson, Th.M. and Fu, Y.Q., 2009: Mechanical properties of attapulgite clay reinforced polyurethane shape-memory nanocomposites. *European Polymer Journal*, 45:1904–1911
- Yalcin, H. and Bozkaya, O., 1995: Sepiolite-palygorskite from the Hekimhan region (Turkey). *Clay and Clay Minerals*, Vol. 43, No. 6, pp:705-717.
- Zhang, X. L., Jiang, W. p. Wu, X. P., Shi, P.W., Yang, P. J., Jia, X. B. and Zhang, C. P., 2011: The Effect of Thermal Treatment on the Structure of Palygorskite Used for Flue Gas SO₂ Removal. *Advanced Materials Research, Volumes 356 – 360*, pp: 698-703.
- Zumwalde, R., 1976: *Industrial Hygiene Study*. Engelhard Minerals and Chemicals Corporation, Attapulgus, Georgia (NIOSH 00106935), Cincinnati, OH, National Institute for Occupational Safety and Health.

Appendices

Appendices

Table Ap-1: Certification of analyses issued by ALS group-Czech Republic.




CERTIFICATE OF ANALYSIS

Work Order	: PR1233010	Issue Date	: 17-AUG-2012
Client	: University of Baghdad College of Science Saad Muhi	Laboratory	: ALS Czech Republic, s.r.o.
Contact	: Saad Muhi	Contact	: Client Service
Address	: Al - Jadhiah PO box 47182 Baghdad Iraq 00954	Address	: Na Haise 336/9 Prague 9 - Vysocany Czech Republic 190 00
E-mail	: saadmuh@yahoo.com	E-mail	: customer.support@alsglobal.com
Telephone	: +964 1790 140 4370	Telephone	: +420 226 226 226
Facsimile	: ---	Facsimile	: +420 264 081 835
Project	: Standard solutions treated with polygonskite (Ph D- Seed)	Page	: 1 of 3
Order number	: ---	Date Samples Received	: 13-AUG-2012
C-O-C number	: ---	Quote number	: PR2012UNIBC-IQ0001
Site	: Seed - Iraq	Date of test	: 13-AUG-2012 - 16-AUG-2012
Sampled by	: client	QC Level	: ALS CR Standard Quality Control Schedule

General Comments

This report shall not be reproduced except in full, without prior written approval from the laboratory.
The laboratory declares that the test results relate only to the listed samples.

Responsible for accuracy

<u>Signature</u> Zdenek Jirak		<u>Position</u> Prague Laboratory Manager
----------------------------------	---	--

Testing Laboratory Accredited by CAJ





L 1163

ALS Czech Republic, s.r.o.
In name ALS Laboratory Group
Na Haise 336/9 Prague 9 - Vysocany Czech Republic 190 00
Tel: +420 226 226 226 Fax: +420 264 081 835

www.alsglobal.com

RIGHT SOLUTIONS RIGHT PARTNER

Appendices

Table Ap-2: Structure formula and charge equivalent of the separated palygorskite from the raw sample no 12D.

Oxides	%	Mole equiv.	Cation equiv.	Charge equiv.	Charge/44 charge	Cation/unit cell	Layers	Cation	Charge	Total charge
SiO ₂	52.3	0.871	0.871	3.48	31.45	7.86	Tetrahedral	Si ⁴⁺	7.86	8.0
Al ₂ O ₃	8.8	0.086	0.173	0.52	4.70	1.56		Al ³⁺	0.14	
Fe ₂ O ₃	3.1	0.019	0.038	0.12	1.05	0.35	Octahedral	Al ³⁺	1.42	4.15
MgO	10.2	0.255	0.255	0.51	4.61	2.3		Fe ²⁺	0.35	
CaO	5.2	0.093	0.093	0.19	1.68	0.84		Mg ²⁺	2.30	
K ₂ O	0.7	0.007	0.015	0.015	0.13	0.13		Ti ⁴⁺	0.08	
Na ₂ O	0.13	0.002	0.004	0.004	0.04	0.04	Interlayer	Ca ²⁺	0.84	1.01
TiO ₂	0.8	0.009	0.009	0.036	0.32	0.08		Na ⁺	0.04	
Total				4.867	44			K ⁺	0.13	



جمهورية العراق
وزارة التعليم العالي والبحث العلمي
جامعة بغداد - كلية العلوم
قسم علم الأرض

معدنية وجيوكيميائية وكفاءة الأمتصاص للباليجورسكايت في تكويني دكمة وعكاشات، غرب العراق

رسالة مقدمة الى

كلية العلوم - جامعة بغداد

وهي جزء من متطلبات نيل شهادة الدكتوراه فلسفة

في علم الأرض (الصخور والمعادن)

من

سعد محي توفيق

ماجستير علوم - جامعة كراتشي - باكستان

1989

باشراف

الاستاذ المساعد الدكتور صالح محمد عوض

2013م

1434هـ

المستخلص

درست الرواسب الغنية بمعدن الباليغورسكايت في تكويني دكمة (الماسرختي)، وعكاشات (الباليوسين) ضمن الصحراء الغربية، غرب العراق، من الناحية المعدنية والجيوكيميائية وبعض التطبيقات التقنية. شملت هذه التطبيقات فصل معدن الباليغورسكايت من العينة الخام، وإجراء مجموعة من التجارب المختبرية التي من شأنها أن تدل على قابلية الباليغورسكايت على إمتصاص وإدمصاص الفلزات الثقيلة من الاطوار السائلة. لتلبية هذا الغرض، تم أستعمال أسلوب جمع العينات الهادف لملاحقة وجمع الترسبات الغنية بمعدن الباليكورسكايت في 17 موقعا، حيث تم جمع بعض العينات من كل موقع واختبارها معدنيا لاختيار العينة المناسبة، ثم أخيرا، تم اختيار عينة ممثلة واحدة من كل موقع.

تم استخدام تقنيات الأشعة السينية الحادة والمجهر الالكتروني الماسح والأشعة تحت الحمراء جنبا الى جنب لدراسة معدنية العينات الخام (رسوبيات غنية بالباليغورسكايت)، والعينة المفصولة (الباليغورسكايت). كشفت الدراسة الحالية ترافق الباليغورسكايت مع الصخور السليكية، البورسيلينيات المسماة أوبال سي-تي والمتمثلة بالكرستبوليت والتريديمايت، مع كميات معتبرة للدولومايت والكاؤلينايت، وكمية قليلة من الكلسايت والكوارتز ضمن اللايمستون المارلي والاباتايت في تكوين دكمة ، بينما في تكوين عكاشات فإن الباليغورسكايت غالبا ما يترافق مع المونتموريلونيات والدولومايت واللايمستون المارلي، مع كمية قليلة من البورسيلينيات المتمثل بالابوال- سي تي (الكرستبوليت والتريديمايت) والكوارتز والجيرت. أن هذه السحنات تدل على بيئة بحرية ضحلة على الرصيف المفتوح.

إقترحت الدراسة الحالية نموذجين لنشأة الباليكورسكايت، النموذج الأول هو تفاعل ماء المسامات الغني بحامض السليسيك مع الدولومايت ليكون في بادئ الأمر السيبولوايت الذي لا يلبث الا ان يتحول الباليغورسكايت في نهاية المطاف وذلك بأخذ الالومينا من البيئة المحيطة، والنموذج الثاني هو تحول السمكايت الى الباليكورسكايت في بيئة غنية بالمغنيسيوم.

من الناحية الجيوكيميائية، فقد تم تحليل عينات من الرسوبيات الغنية بالباليغورسكايت، والالباليغورسكايت النقي المفصول من العينة الخام للأكاسيد SiO_2 و Al_2O_3 و MgO و Fe_2O_3 و TiO_2 و MnO و Na_2O و CaO و K_2O و P_2O_5 و LOI . تغير محتوى MgO من 0.61 الى 9.38 % ، علما ان جزء من هذا الاوكسيد يأتي من الدولومايت. في عينة الباليغورسكايت النقية، فقد دل المحتوى العالي للمغنيسيا مع الكمية المناسبة من مفقودات الحرق على نجاح عملية فصل الباليغورسكايت التي تم تعزيزها بالمجهر الالكتروني. تم حساب الصيغة التركيبية وتوزيع الشحنات على الطبقات الثمانية والرابعة والداخلية للباليغورسكايت المفصول.

من ناحية التطبيقات التقنية، خضع معدن الباليغورسكايت النقي (المفصول من العينة الخام) إلى مجموعة تجارب مختبرية التي أجريت لاختبار كفاءة الباليغورسكايت في إمتصاص الفلزات الثقيلة (الرصاص، الكاديوم، النيكل، الكروم، المولبت، الفناديوم، الزنك، النحاس ، الحديد والمنغنيز)، وكذلك البورون (B)، في تركيز 10، 25، 50، 75، 100، 125، 150، 175، 200 ، 225 ج.م. لكل عنصر. أجريت أكثر من 110 تجربة مختبرية بايلوب الوجبات، وفي درجة حرارة الغرفة. تم تحديد نسبة الصلب (palygorskite) إلى نسبة السائلة (المحلول الأولي) ليكون 1غم/100مل، وزمن التفاعل ليكون 1 ساعة .

كمية الأيونات المعير عنها بالاملاح الصلبة الكلية الذائبة، والايصالية الكهربائية في المحاليل النهائية (بعد انتهاء التفاعل) تتناقص باتجاه فلوية المحلول. حدث هذا الميل في التناقص في المحاليل واطئة التركيز أكثر منه في المحاليل عالية التركيز، بسبب عدم وجود المزيد من الايونات الموجبة تنافس البروتون (H^+) على المواقع السالبة الباليغورسكايت.

إزدادت قابلية الباليغورسكايت الامتصاصية (%) بعد تنشيطه بالحرارة، حيث وصلت الى 93% عند 600°م بسبب ازالة ماء الزيولايت، حيث المساحة السطحية تزداد وتبعا لذلك فالامتصاصية تزداد ايضا. أما في درجة حرارة 800°م فأن الامتصاصية انخفضت الى ادناها بسبب انهيار التركيب المعدني للباليغورسكايت.

لقد أعتبر الباليغورسكايت مستلم فعال للفلزات الثقيلة، بينما يلفظ الايونات Ca^{2+} و Mg^{2+} و Al^{3+} و K^{+} من المعدن الى المحلول دالا بذلك على إن ميكانيكية التبادل الايوني هي المسؤولة عن دمج الايونات الموجبة في تركيب الباليغورسكايت، ان طرد هذه الايونات الموجبة يسبب نقص في الشحنة الموجبة على الباليغورسكايت التي تشجع ايونات اضافية لتلتصق على على السطح. كفاءة الامتصاص لمعدن الباليغورسكايت تتباين حسب طبيعة العنصر، وقد حددت التجارب المختبرية الكثير من العلاقات والتي يمكن ان نرتب منها امتصاصية الباليغورسكايت (%) للمحاليل الأولية ذات التركيز 50 ج.م. على النحو الآتي:

